ADSORPTION STUDIES WITH THE FIELD-EMISSION AND FIELD-ION MICROSCOPE

A. A. HOLSCHER

ADSORPTION STUDIES WITH THE FIELD-EMISSION AND FIELD-ION MICROSCOPE

PROEFSCHRIFT

TER VERKRIJGING VAN DE GRAAD VAN DOCTOR IN DE WISKUNDE EN NATUURWETENSCHAPPEN AAN DE RIJKSUNIVERSITEIT TE LEIDEN OP GEZAG VAN DE RECTOR MAGNIFICUS DR K. A. H. HIDDING, HOOGLERAAR IN DE FACULTEIT DER GODGELEERDHEID, TEN OVERSTAAN VAN EEN COMMISSIE UIT DE SENAAT TE VERDEDIGEN OP WOENSDAG 31 MEI 1967 TE 16 UUR

DOOR

ANTON ALBERT HOLSCHER
GEBOREN TE 'S-GRAVENHAGE IN 1933

DRUCO DRUKKERIJBEDRIJVEN N.V. — LEIDEN

Promotor: Prof. Dr W. M. H. Sachtler

aan mijn ouders

aan Yvonne

CONTENTS

CHAPTER I

INTRODUCTION

I-1. CHEMISORPTION ON METALS

The study of the adsorption of gases on metals, though initiated some forty years ago, has developed particularly rapidly in the past decade. Recent advances are largely due to the growing appreciation that an understanding of the elementary processes taking place at the solid-gas interface is of vital importance to many branches of science and technology, such as heterogeneous catalysis, electron emission by metals, thin-film and ultra-high vacuum techniques. Conversely the cross-fertilization between ideas coming from these diverging fields of interest has significantly advanced the research into surface phenomena, not least as regards the development and perfection of experimental techniques.

The phenomenon of adsorption is usually divided into "chemisorption" and "physisorption", though no unambiguous criteria for making this distinction are available. Chemisorption is generally marked by a strong interaction between metal and adsorbate, and often involves the dissociation of molecules. Moreover, chemisorption is very specific for different gas-metal systems. Physisorption, on the contrary, is by definition never dissociative, the bonding being due to weak and non-specific attraction forces of the Van der Waals-London type. It therefore normally takes place at low temperature only, e.g. in the adsorption of rare gases or of molecules on a metal surface which is already covered with a chemisorption layer.

Of the two types of adsorption chemisorption is clearly the more important, but also the more complex. For its study numerous experimental methods have been developed[1], which can roughly be divided into two groups. The first group comprises methods based on the determination of the adsorption-induced changes in a physical property of the metal, such as the work function[2,3], the electrical conductivity[4,5,6], the magnetic moment[7,8], and the Hall constant[9]. The second category includes all those methods which permit the more direct measurement of thermodynamic quantities and kinetic parameters and/or give information about the surface bonds formed upon adsorption. The most important methods in this group are calorimetry[10,11], flash filament techniques[12,13], the measurement of sticking coefficients[14], isotope-exchange methods[15], infra-red spectroscopy[16,17] and low-energy electron diffraction (LEED)[18,19,20].

Before actually applying any of these techniques one has to prepare a clean metal surface. The most commonly used methods to do this are the heating of filaments or ribbons, the deposition of thin films by evaporation, the bombardment of surfaces with highly energetic electrons or ions, and the cleavage of crystals in situ[21]. If a high surface area is required, as for example in infra-red spectroscopy, use is made of metals finely dispersed on a support like silica[22]. In that case the surface is prepared and cleaned by chemical means.

Once prepared, the clean surface must be maintained free from contaminations during the time required to carry out the experiments. For that reason an ultra-high vacuum of about 10^{-10} Torr (1 Torr = 1 mm mercury) is essential. With commercially available apparatus it is nowadays almost a matter of routine to obtain and measure such low gas pressures[23].

Clearly it is impracticable to give a survey of all chemisorption studies reported to date. We will therefore limit ourselves to a short account of the principal views now being held about chemisorption on metals and the trends that can be observed in current research activities. These introductory notes will also provide an insight into the objectives of the study at hand.

In the past, attempts have been made to relate the chemisorptive properties of a metal to the properties characteristic of the metallic state and to describe the phenomena in terms of the electron band model[24,25]. This approach, however, has not turned out very successful. Chemisorption processes are essentially confined to the surface and in consequence more and more the viewpoint has been adopted that it is the local atomic and electronic configuration at the various surface sites rather than bulk properties which governs the adsorption behaviour[26,27].

Various experimental results have led to the conclusion that a chemisorption complex has to be regarded as a surface compound comprising the atoms of the adsorbate and the metal atoms in the surface, there being no fundamental difference between chemisorption bonds and bonds in ordinary chemical compounds. Firstly, investigations using the methods of the first group mentioned before have shown that chemisorption invariably causes a "demetallization" of the original metal surface, i.e. the metal atoms in the outer surface layer(s) no longer contribute to the collective properties of the metal owing to the formation of localized bonds with the adsorbate[28]. Secondly, there is the parallelism observed between the heats of adsorption of a number of diatomic molecules on transition metals and the heats of formation of the corresponding bulk compounds[28,29]. This evidently suggests that the stability of both chemisorption complexes and solid compounds is determined by the same "affinity rules".

The similarity between chemisorption complexes and metal compounds also shows up in the field of catalysis, where in many cases important connections exist between the mechanisms in corresponding homogeneous and heterogeneous systems[30]. The resemblance is even more striking when surface complexes are compared with coordination complexes having intermetallic bonds. Compounds of this type, containing a cluster of a few metal atoms[31], might in fact be considered the missing links between the one-centre metal complexes and the chemisorption structures on very small metal crystallites used in many heterogeneously catalysed processes.

Although at present it thus seems well established that the approach to chemisorption must be based upon concepts similar to those adopted in the treatment of solid compounds or coordination complexes, its study involves many specific problems. Whereas in ordinary chemistry investigations can be carried out either on pure material showing a three-dimensional periodicity

or on a large number of entities all having identical structure, this evidently cannot be done in the study of chemisorption complexes. On the one hand periodicity is restricted to two dimensions and often completely absent, on the other it is generally observed that chemisorption within one and the same gas-metal system leads to the formation of various structurally different complexes or different adsorbed states, as they are usually called.

Owing to the lack of symmetry and the non-uniformity observed in adsorption layers on metals, most techniques used in the structural analysis of solid compounds or of coordination complexes in homogeneous solution are unsuitable for investigations into chemisorption on metals. Moreover, the presence of bulk metal excludes the application of electron spin resonance techniques which in recent years have rendered signal service in the study of adsorption on ionic compounds[32].

What ways are to be followed to cope with the problems here sketched? Firstly, realizing that the environment of the surface metal atoms greatly differs for different crystal faces of a metal, we can expect that chemisorption proceeds differently for the various crystal faces of one and the same metal. To evaluate the dependence of chemisorption on surface structure and to remove at least part of the non-uniformity noted before, it is therefore most advantageous to study adsorption on substrates with a well-defined and uniform surface structure. Accordingly, an increasing number of investigations are at present concerned with adsorption on single crystal faces, whereas earlier efforts were almost exclusively made on metal wires or evaporated films, which normally expose various crystal faces of often unknown orientation.

Secondly, it seems necessary to develop and apply special experimental techniques which, as pendants to the techniques used in ordinary structure determinations, provide detailed information about the constitution of surface compounds. Such techniques are now becoming available. Indeed one of them, the low-energy electron diffraction technique, has gained a rapidly growing interest in the last few years. It has furnished ample evidence that chemisorption can lead to ordered surface structures in which the surface metal atoms have changed sites. Another new technique, which provides a really atomic view of a metal surface, is field-ion microscopy[33]. Its use and possibilities for research on chemisorption are described in the present study.

Summing up, we may state that the outstanding features of to-day's chemisorption research are the effort spent to control and define the surface structure of substrates and the endeavour to arrive at an atomic picture of chemisorption processes.

I-2. OUTLINE OF THE PRESENT STUDY

The work presented in this thesis consists of an experimental part and a more theoretical part.

The experimental part concerns a study of the adsorption of carbon monoxide and nitrogen on tungsten. Both adsorption systems have been extensively investigated before, but their complexity is still unresolved and

particularly the nature of the different binding states that can be distinguished has not been clarified satisfactorily. Most important in this respect is the question whether the positions of the surface atoms remain unchanged upon adsorption or whether these atoms seek new and more favourable sites in the chemisorption layer. The nitrogen-tungsten system is of special interest, because indications are that it shows face specificity. Following the line of thought of the previous section, we have aimed to investigate these problems by studying the adsorption on tungsten surfaces of exactly known structure and to do this in atomic detail. To this end use has been made of field-emission and field-ion microscope techniques.

Chapter II contains a review of the principles of these techniques. A survey is given of the phenomena of electron emission, desorption, evaporation and ionization as caused by very high electric fields and their utilization in the field-emission and the field-ion microscope. Also it is discussed how these instruments, which display the metal surface with a magnification of about one million and a resolution of 15 and 2 Å, respectively, can be employed in adsorption studies.

Chapter III describes the general procedures followed in the experiments together with the apparatus. These include the ultra-high vacuum equipment, the ion microscope and a special field-emission tube developed to study the individual crystal faces of a metal.

The experimental results are reported and discussed in Chapter IV. Some attention is also paid to the bearing which our results have on chemisorption phenomena in general. In addition, the potentialities and limiting factors of the experimental techniques are scrutinized.

The second part of this thesis, contained in Chapter V, is devoted to the theory of image formation in the field-ion microscope. This treatment was initiated because our experimental work gave rise to an interpretation of ion images different from the one which has so far been favoured in the literature. When thus considering the mechanism of image formation in detail, we discovered that many problems, particularly those related to surfaces covered with adsorbates, had not received any attention, while the treatment of several others turned out to be confusing and sometimes incorrect. As the usefulness of field-ion microscopy largely depends on the right interpretation of the images obtained, a critical review of this matter is included.

REFERENCES

1. D.O. Hayward and B.M.W. Trapnell, "Chemisorption", 2nd edition, Butterworth, London (1964).
2. R.V. Culver and F.C. Tompkins, Advan. Catalysis 11, 67 (1959).
3. A. Eberhagen, Fortschr. Phys. 8, 245 (1960).
4. R. Suhrmann, Advan. Catalysis 7, 303 (1955).
5. W.M.H. Sachtler and G.J.H. Dorgelo, Bull. soc. chim. Belges 67, 465 (1958).
6. J.W. Geus, H.T.L. Koks and P. Zwietering, J. Catalysis 2, 274 (1963).
7. P.W. Selwood, "Adsorption and Paramagnetism", Academic Press, New York (1962).
8. J.J. Broeder, L.L. van Reijen and A.R. Korswagen, J. Chim. Phys. 54, 37 (1957).
9. N. Hansen and W. Littman, Ber. der Bunsengesellsch. f. phys. Chemie 67, 970 (1963).
10. O. Beeck, Advan. Catalysis 2, 151 (1950).
11. D. Brennan, D.O. Hayward, B.M.W. Trapnell, Proc. Roy. Soc. (London) A256, 81 (1960).
12. J.A. Becker and C.D. Hartman, J. Phys. Chem. 57, 157 (1953).
13. G. Ehrlich, J. Appl. Phys. 32, 4 (1961).
14. D.O. Hayward, N. Taylor and F.C. Tompkins, Discussions Faraday Soc. 41, 75 (1966).
15. C. Kemball, Advan. Catalysis 11, 223 (1959).
16. N.G. Jaroslavski and A.N. Terenin, Dokl. Akad. Nauk SSSR 66, 885 (1949).
17. R.P. Eischens and W.A. Pliskin, Advan. Catalysis 10, 1 (1958).
18. H.E. Farnsworth, Advan. Catalysis 9, 493 (1957).
19. L.H. Germer, Advan. Catalysis 13, 191 (1962).
20. J.J. Lander in "Recent Progress in Solid State Chemistry", Vol. II, H. Reiss ed., Pergamon Press (1965).
21. R.W. Roberts, Brit. J. Appl. Phys. 14, 537 (1963).
22. G.C.A. Schuit and L.L. van Reijen, Advan. Catalysis 10, 242 (1958).
23. R.W. Roberts and Th.A. Vanderslice, "Ultra-high Vacuum and its Applications", Prentice-Hall Inc., Englewood Cliffs, N.Y. (1963).
24. G.M. Schwab, Angew. Chemie 67, 433 (1955).
25. D.A. Dowden and P.W. Reynolds, Discussions Faraday Soc. 8, 184 (1950).
26. W.M.H. Sachtler, Proceedings of the Third International Vacuum Congress, Pergamon Press, New York (1966), Vol. I, p. 41.
27. G.C.A. Schuit, Chem. Weekblad 62, 209 (1966).
28. W.M.H. Sachtler and L.L. van Reijen, J. Res. Inst. Cat. 10, 87 (1962).
29. K. Tanaka and K. Tamaru, Shokubai (Tokio) 4, 329 (1962).

30. J. Halpern, Proceedings of the Third International Congress on Catalysis, W.M.H. Sachtler, G.C.A. Schuit and P. Zwietering eds., North-Holland Publishing Co., Amsterdam (1965), Vol. I, p. 146.

31. See e.g. E.D. Braye, L.F. Dahl, W. Hübel and D.L. Wampler, J. Am. Chem. Soc. 84, 4633 (1962).

32. L.L. van Reijen, Thesis, Eindhoven (1964).

33. E.W. Müller, Advan. Electron. Electron Phys. 13, 83 (1960).

CHAPTER II

PRINCIPLES OF EXPERIMENTAL TECHNIQUES

II-1. INTRODUCTION AND SURVEY

The emission of electrons from a conductor into a vacuum under the influence of a high electric field (≈ 0.3 V/Å*) was first described by Wood[1] in 1897. However, a successful explanation of the phenomenon, which appeared to be independent of temperature up to several hundred degrees K, could only be given after the development of the quantum theory.

On the basis of the free-electron model of a metal Fowler and Nordheim[2] in 1928 derived an equation which related the emission-current density to the applied field strength and the work function of the metal. The physical picture underlying their theory is that of electrons tunnelling through the surface-potential barrier, which is narrowed by the applied field.

The study of field-emission phenomena received a great impetus from the development of the field-emission microscope by Müller[3,4] in 1937. Using a sharp metal tip as cathode and a fluorescent screen opposite to the tip as anode, he obtained a highly magnified electron image (resolution ≈ 20 Å) of the cathode surface, which was rounded off by surface migration at high temperatures. The various crystal faces of the metal showed up in a pattern of dark and bright spots reflecting the symmetry of the metal, the differences in emittancy being due to differences in work function.

Now that a well-defined cathode surface could be obtained it was possible to confirm the validity of the Fowler-Nordheim theory experimentally. Besides affording a closer insight into field emission from clean metal surfaces, the instrument rendered valuable services in the study of surface phenomena, such as adsorption, desorption and surface diffusion of gases on metals. The changes in the emission current brought about by these processes can be quantitatively measured and interpreted by means of the Fowler-Nordheim equation and observed visually from the fluorescent screen.

After 1950 in particular, when modern ultra-high vacuum techniques became available, numerous surface studies have been carried out with the field-emission microscope, which proved a unique tool for studying the specific behaviour of the various crystal faces of one and the same metal. A comprehensive account of techniques and experimental studies can be found in Gomer's book[5].

An important new element entered into field-emission microscopy when Müller[6] discovered that adsorbed layers could be torn off as positive ions by high fields (≈ 1 V/Å) of reversed polarity. At still higher fields even the atoms of the metal itself can be "evaporated" at low temperatures. These phenomena, called field desorption and field evaporation, respectively, can be utilized in techniques for cleaning metal tips and obtaining surfaces which are ideally ordered on an atomic scale.

---

* In field-emission and field-ionization work the unit V/Å is often used in preference to V/cm.

The effect of field desorption led Müller[7] to the more general idea of field ionization and subsequently to the development of the field-ion microscope in 1951. With this powerful instrument the metal surface is imaged by ions originating from a region very close to the surface. The resolution is about 2 Å, allowing individual atoms to be seen. The theory of field ionization, desorption and evaporation has mainly been developed by Müller[8], Gomer[5], Gomer and Swanson[9] and Brandon[10,11].

Till now the field-ion microscope has been used primarily in metallographic work[8,10,12] to study lattice defects, radiation damage and ordering in alloys. Adsorption studies with the field-ion microscope have only been made by Müller and co-workers[8,12] and Ehrlich[13].

Field emission and ionization have also found application outside the realm of microscopy. The fact that a field-emitted electron beam is almost monoenergetic and of a well-defined energy has enabled the present author to develop a method for measuring the work function of a metal film[14].

Inghram and Gomer[15] and particularly Beckey[16,17] have realized the value of field ionization in mass spectrometry. Compared with a conventional ion source, a field-ion source has the important advantage that fragmentation of molecules is almost completely suppressed.

The technical application of field emission in electronic devices has long been an object of extensive research. A major contribution in this field has been made by Dyke and collaborators[18,19]. By using pulsed fields they could substantially increase current densities. However, it seems that problems of emitter stability and contamination during operation are still serious impediments here[20].

II-2. FIELD-EMISSION MICROSCOPY

II-2.1. Theory of field emission

In the free electron model of a metal the conduction electrons are placed in the available levels according to Fermi-Dirac statistics. At 0 °K they will fill all the levels from the bottom of the band up to the highest filled level, the so-called Fermi level. At temperatures above 0 °K there will be some excitation of electrons; the Fermi level is then defined as the energy level which has a 50% probability of being filled. Below 1000 °K, however, this thermal excitation will be very small, because the Fermi level is several electron-volts above the bottom of the conduction band.

We first consider a metal with a uniform surface extending infinitely in vacuum with no electric field applied. The amount of work required to remove an electron from the Fermi level to charge-free infinity is called the work function φ of the metal surface. This quantity depends very much on the structure of the surface and will therefore in general differ markedly for the various crystal faces of one and the same metal*. For example, for

---

* In the case of a metal crystal of finite size, bounded by crystal faces with different structures, the work required to bring an electron from the interior to infinity must be independent of the way along which the electron is taken out. However, it can be shown that for such a real crystal the experimentally determined quantities may be interpreted as weighted averages of the true work functions of the individual crystal faces as defined above. The manner of weighting depends on the technique applied.

tungsten this difference may be as large as 1.7 eV. Average values of φ for different metals range from about 2 to 6 eV. It is the work function φ which plays the predominant role in the relations governing thermionic, photoelectric and field emission.

The potential barrier at the surface is not regarded as an abrupt potential step at the surface but a classical image potential is included. This image potential has its origin in the attractive forces which are exerted on a charged particle by an opposite charge induced in the conduction surface. Thus, for an electron with electric charge e at a distance x from an infinite planar surface the potential energy V(x) becomes

$$V(x) = -\frac{e^2}{4x} . \qquad (1)$$

This expression clearly does not hold at very short distances from the surface, for at $x \leq 0$ the potential energy V(x) of an electron should be equal to Vp, the potential energy of the electrons inside the metal. At $x = 0$ therefore a discontinuity is present. However, for slightly greater distances the classical image force seems to be a fairly good and useful approximation.

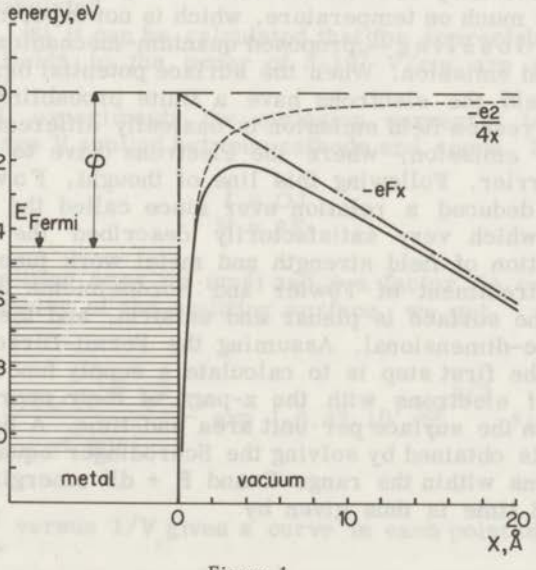

Figure 1

Potential-energy diagram for an electron near a metal surface with work function φ in the presence of an applied field of 0.3 V/Å;
-.-, without image potential
——, with image potential included

Now if an electric field of strength F is applied, the potential energy for $x > 0$ will be given by

$$V(x) = -\frac{e^2}{4x} - eFx \ . \qquad (2)$$

Fig. 1 shows the potential energy of an electron in the presence of an applied field, both with and without the image potential. It can be seen that the resultant potential barrier is smaller when the image effect is included. Also, the applied field lowers the barrier height, giving rise to the so-called Schottky saddle. The decrease of the effective work function can be calculated by setting the derivative of (2) equal to zero. The result is

$$\Delta\varphi = -(e^3F)^{1/2} \ . \qquad (3)$$

It was suggested by Schottky[21] that field emission might occur when the effective work function was reduced to zero by application of very strong fields. However, much higher fields would be required to produce this effect than are necessary in field emission. Moreover, the emission current would depend very much on temperature, which is not experimentally observed.

In 1926 Gossling[22] proposed quantum-mechanical tunnelling as the mechanism in field emission. When the surface potential barrier is narrowed by the applied field the electrons have a finite probability to penetrate the barrier. For this reason field emission is basically different from thermionic and photoelectric emission, where the electrons have to take up energy to pass over the barrier. Following this line of thought, Fowler and Nordheim[2] in 1928 deduced a relation ever since called the Fowler-Nordheim (F-N) equation, which very satisfactorily described the emission current density as a function of field strength and metal work function.

In the treatment of Fowler and Nordheim the temperature of the metal is 0 °K, the surface is planar and uniform, and the potential barrier is taken to be one-dimensional. Assuming the Fermi-Dirac energy distribution to be valid, the first step is to calculate a supply function N(E)dE, equal to the number of electrons with the x-part of their energy between E and E + dE incident on the surface per unit area and time. A barrier-penetration probability D(E) is obtained by solving the Schrödinger equation. The number P(E)dE of electrons within the range E and E + dE emerging from the metal per unit area and time is thus given by

$$P(E)dE = N(E)D(E)\ d(E) \ . \qquad (4)$$

The Fowler-Nordheim equation is then obtained by integration of this product over all E and multiplying by the electronic charge:

$$J = e \int_{V_p}^{\infty} P(E)\, dE \,, \tag{5}$$

where J is the electric current density.

In the original derivation the image potential was not included; this was done afterwards by Nordheim[23]. After some further refinements in the calculations, the equation acquired its present form[24]:

$$J = \frac{1.54 \cdot 10^{-6}\ F^2}{\varphi t^2(y)} \exp\left[-6.83 \cdot 10^7 \frac{\varphi}{F}^{3/2} \vartheta(y)\right], \tag{6}$$

where J = current density in A/cm^2
F = field strength in V/cm
φ = work function in eV and
t(y) and $\vartheta(y)$ functions of the variable $y = 3.79 \cdot 10^{-4} \frac{F}{\varphi}^{1/2}$
which have been tabulated.

With eq. (6) it can be calculated that for appreciable field emission ($J \approx 10^3$ A/cm^2) fields in the order of $3 \cdot 10^7$ V/cm are necessary when φ is about 4 to 5 eV.

In actual experiments the emission current I is measured as a function of the voltage V applied between cathode and anode. Substituting in (6)

$$I = OJ \tag{7}$$

and

$$V = \beta F \,, \tag{8}$$

where O is the emitting area (in cm^2) and β a factor (in cm) which depends mainly on the geometry of the emitting surface, we get

$$I = \frac{1.54 \cdot 10^{-6}\ V^2 \cdot O}{\varphi t^2(y) \beta^2} \exp\left[-6.83 \cdot 10^7 \frac{\beta\varphi}{V}^{3/2} \vartheta(y)\right] . \tag{9}$$

A plot of $\log I/V^2$ versus $1/V$ gives a curve in each point of which the slope is represented by*

$$m = \frac{d \log I/V^2}{d \frac{1}{V}} = -\ 2.96 \cdot 10^7\ \beta\varphi^{3/2}\ s(y) \,. \tag{10}$$

---

* Throughout this work log x means $^{10}\log x$.

As s(y) is a very slowly varying function of y, close to unity, the plot approaches a straight line.

At moderate temperatures, when T is less than the numerical value of $3.15 \cdot 10^{-5} \frac{F}{\varphi^{1/2}}$, the current density can be approximated by

$$J_T = J_0 \left[1 + \frac{1}{6} K^2 T^2\right] , \qquad (11)$$

where $K = 2.77 \cdot 10^4 \frac{\varphi}{F}^{1/2}$.

This, for example, gives $J_{300} = 1.03\ J_0$. At higher temperatures the so-called thermionic-field emission sets in. The whole temperature range has been treated by Murphy and Good[25]. In the present study field emission will be regarded as temperature-independent.

The validity of the model has been investigated by several workers. Dyke and Dolan[19] carried out a direct test of the dependence on field strength by the absolute measurement of F over a wide range of current densities. They found that the F-N equation is quantitatively obeyed within the experimental error (about 15 per cent). Proof that the current density depends on $\varphi^{3/2}$ comes from the work of Müller[26], who measured the relative work functions of various crystal faces of tungsten and found good agreement with thermionic determinations.

A more refined check of the F-N model is afforded by measurement of the energy distribution of field-emitted electrons. This was first achieved in an accurate way by Young and Müller[27]. The extremely narrow distributions of the total energy (0.14 eV at 77 °K) reflect the fact that the electrons are emitted mainly from energy levels near the Fermi level. The temperature dependence of the total energy distribution gives valuable proof of the validity of the free-electron approximation for evaluation of the supply function.

The structure of the surface potential barrier is still a point of discussion. A sensitive test of the applicability of the classical image potential would be a comparison of theoretical and experimental normal energy distributions. Owing to the attendant experimental problems, however, these energy distributions have not yet been determined with sufficient accuracy.

Cutler and co-workers[28,29] have proposed a corrected image-force potential leading to total energy distributions, which seems to be in slightly better agreement with the experimental ones as very recently reported by Van Oostrom[30]. The correction applied, however, only causes a deviation from the Fowler-Nordheim plot at fields above 0.5 V/Å. As space charge effects at these high fields give a similar deviation, it is difficult to decide from experiment between the classical and the corrected image potential. In general, it can be concluded that the F-N model with the classical one-dimensional image potential describes the experimental facts remarkably well.

II-2.2. The field-emission microscope

In 1937 Müller invented the field-emission microscope (FEM) which is still the principal application of field-electron emission. A schematic diagram of the instrument is presented in Fig. 2. The electron emitter is a fine metal wire, which has been etched to a very sharp tip. This metal tip is mounted in an evacuated glass bulb. The anode is formed by a conductive fluorescent screen, applied to the inner wall of the bulb opposite to the tip. The surface of the tip is cleaned by heating in vacuo, whereby it acquires a smooth and almost hemispherical shape. When a high voltage is applied between tip and screen an electron image is formed on the latter.

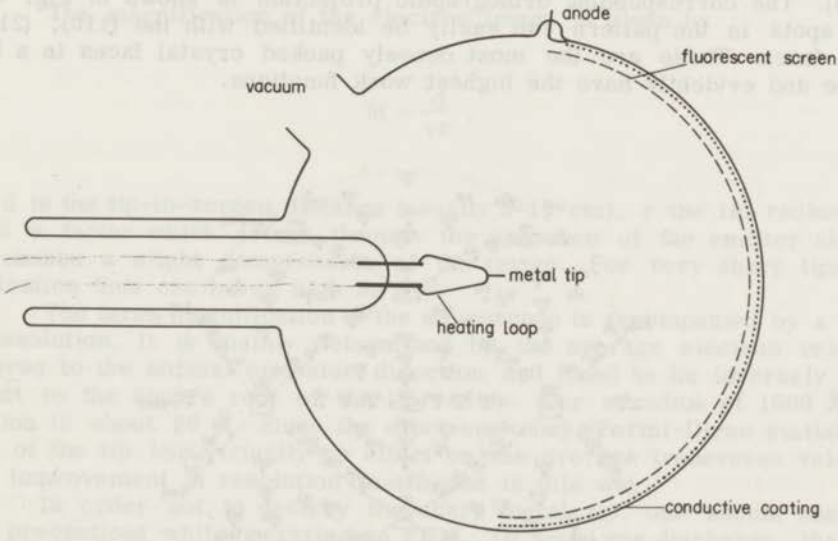

Figure 2

Schematic diagram of the field-emission microscope

The mechanism of image formation and the type of pattern obtained can be understood as follows. The electrons which have just tunnelled through the surface barrier possess little kinetic energy compared with the kinetic energy they subsequently acquire in the accelerating field between tip and anode screen. This acceleration mainly takes place very close to the tip in a region where the lines of force are orthogonal to the surface. Consequently, the electrons travel radially outwards from the tip to the screen, upon striking which they produce a highly magnified image of the surface of the tip. According to the Fowler-Nordheim equation (6) the emission current at constant field is governed by the work function φ. Therefore, if local variations in field strength can be neglected, the image obtained will be a map of the variation in work function over the surface.

Since the tip is usually small in size compared with the wire grains, it nearly always forms part of a single crystal. (Occasionally a grain boundary can be observed.) At the surface of this hemispherical crystal various crystal faces will be developed, differing in surface structure and consequently in work function. Crystal faces with a relatively low work function are therefore represented by a bright area on the screen, while dark areas correspond to faces with a high work function. The anisotropy in the emission will thus reflect the crystal symmetry.

Fig. 3 gives a pattern of a thermally cleaned tip of tungsten, which has a body-centred cubic (b.c.c.) lattice. Bearing in mind that cubic crystals have a four-fold axis of symmetry in the (100) direction and a three-fold axis in the (111) direction, we can conclude that the tip of Fig. 3 has the (110) direction in the axis (as is usually found with drawn tungsten wires). The corresponding orthographic projection is shown in Fig. 4. The dark spots in the pattern can easily be identified with the (110), (211) and (100) faces. These are the most densely packed crystal faces in a b.c.c. lattice and evidently have the highest work functions.

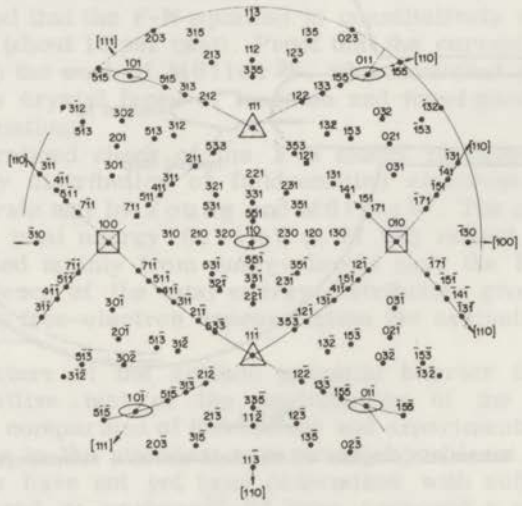

Figure 4

Orthographic projection of a cubic crystal, with the [110] direction in the axis

To visualize the atomic structure of crystal surfaces it is convenient to use marble models. Fig. 5 shows such a model of a portion of a spherical surface cut from a b.c.c. lattice. The different shades of black and white of the marbles indicate different degrees of "unsaturation" of the surface atoms. For example, atoms in the (110) face lack two nearest neighbours, atoms in the (100) face four.

The potential to be applied between emitter and screen to obtain the required high field of the order of ≈ 0.3 V/Å (see section II-2.1.) depends on the radius of curvature of the tip. It has been found[5] that a good approximation of the field at a metal tip with radius r and applied potential V is

$$F = \frac{V}{kr} , \tag{12}$$

where k ranges from 5 to 7 depending on tip shape and polar angle. According to eq. (12) potentials of about 300 to 3000 V are required for tips with radii ranging from 200 to 2000 Å.

The magnification of the electron image is given by

$$M = \frac{d}{\gamma r} , \tag{13}$$

where d is the tip-to-screen distance (usually 5-10 cm), r the tip radius and $\gamma \approx 1.5$ a factor which arises through the presence of the emitter shank, which causes a slight compression of the image. For very sharp tips the magnification thus can be as high as 10^6.

The large magnification of the microscope is accompanied by a very good resolution. It is mainly determined by the average electron velocity transverse to the normal emission direction and found to be inversely proportional to the square root of the tip radius. For a radius of 1000 Å the resolution is about 20 Å. Since the electrons obey Fermi-Dirac statistics, cooling of the tip has virtually no effect on the average transverse velocity and no improvement in resolution is effected in this way.

In order not to destroy the sharp metal tip, one should observe certain precautions while operating an FEM. To avoid gas discharge, the gas pressure in the microscope generally should not exceed 10^{-6} Torr. But even at this pressure emitter stability can be affected by ion bombardment, causing local field enhancement. The resultant increase in local emission may lead to vacuum arcing and destruction of the tip. The chance of ionizing gas molecules at these relatively high pressures can be reduced by limiting the total emitted current ($\leq 10^{-6}$ A). Vacuum arcing may also result from resistive heating due to extremely high current densities. In normal operation the latter should not exceed about 10^5 A/cm^2. Heating of a tip is limited to temperatures at which blunting by surface diffusion becomes appreciable. Surface diffusion will be enhanced by an applied field, leading to facet growth and edge formation, the so-called "build-up".

II-2.3. Application to adsorption

Generally the adsorption of gas on a metal surface drastically changes the charge distribution at the surface, thus inducing a change in the work function φ[31,32].

$$\Delta\varphi = \varphi_{cov} - \varphi_{cl} , \tag{14}$$

where the subscripts cl and cov refer to the clean and covered surface, respectively. Very often the term "surface potential" is used, being defined by

$$\text{s.p.} = - \frac{\Delta\varphi}{e} . \tag{15}$$

If the adsorbed layer is visualized as consisting of N adsorbed particles per unit area with a dipole moment μ associated with the surface bond formed, then the surface potential is given by[33]

$$\text{s.p.} = 4\pi N\mu , \tag{16}$$

the surface potential being positive when the dipole moments point outwards with their positive ends.

As can be seen from the F-N equation (9) field emission is very sensitive to changes in the work function of the emitting surface, which renders the FEM particularly well suited for studying adsorption phenomena. This has so far been its most important application. An important advantage of the FEM over other techniques for measuring the change in work function is the possibility of simultaneously observing various crystal faces of one and the same metal and studying their specific properties with regard to adsorption. Moreover, it is possible, before any adsorption experiment is started, to check the cleanliness of the surface by visual observation of the emission pattern. By studying changes in the pattern upon adsorption we can draw significant, if qualitative, conclusions.

A quantitative determination of the changes induced by adsorption is provided by the application of the F-N equation (9). When F-N plots are measured for clean and covered surfaces a comparison of the respective slopes (eq. (10)) gives

$$\varphi_{cov} = \left(\frac{m_{cov}}{m_{cl}}\right)^{2/3} \varphi_{cl} \left(\frac{\beta_{cl}}{\beta_{cov}}\right)^{2/3} \left(\frac{s(y)_{cl}}{s(y)_{cov}}\right)^{2/3} . \tag{17}$$

If we take into account that the geometric factor β presumably does not change upon adsorption and that the last factor of (17) is very close to unity, eq. (17) yields

$$\varphi_{cov} = \left(\frac{m_{cov}}{m_{cl}}\right)^{2/3} \varphi_{cl} . \tag{18}$$

Strictly speaking eq. (10) can only be applied when φ and F are uniform over the emitting surface region. These conditions obviously are not fulfilled for the case where the total current emitted by the tip is measured in the FEM. However, it can be shown theoretically[34] and experimentally that for the general case of a non-uniform surface the total emission current as a function of the applied voltage can still be described by an F-N equation of the form

$$I = AV^2 \exp\left(-\frac{B\bar{\varphi}}{V}\right)^{3/2} . \qquad (19)$$

Here $\bar{\varphi}$ is an average work function, which is heavily weighted in favour of the low-work-function areas, because these areas contribute most to the emission current.

Following the procedure outlined above (see (18)) in adsorption experiments, we obtain a value of the change in average work function. However, such a value has only significance when the relative emission anisotropy is unchanged upon adsorption, otherwise the regions which determine the average work function (and the F-N plot) are not the same before and after adsorption. But even if the emission anisotropy remains unaltered the information provided by the measurement of F-N plots for the total surface is of limited value. The averaging obscures the specific changes on the various crystal faces and no information at all is gained from areas which do not contribute to the total current.

The inaccuracies and indefiniteness inherent in the determination of average values can be avoided with the FEM, which, if properly modified, allows the measurement of work functions of individual crystal faces, including the weakly emitting ones. These so-called "probe-hole" techniques are described in section III-3.

Methods have been used by which only the F-N plot for the clean surface is determined and the changes in work function are derived from the measurement of the current at constant voltage or from the voltages required for constant emission. In such a procedure the pre-exponential factor A of the F-N equation (19) is assumed to remain constant upon adsorption. Very often, however, large changes in A are observed, rendering the measurement of F-N plots mandatory. The possible reasons for the changes in A will be discussed in connection with our experimental results (see Chapter IV).

The measurement of the emission current from clean and covered surfaces is not only used to characterize the adsorption complex by its surface potential according to eq. (16). It also permits the determination of the activation energies of processes taking place at the surface, like rearrangements, diffusion and desorption, by following these processes and the concomitant emission changes in the course of time and at different temperatures. If the adsorption step requires no activation energy, then the activation energy for desorption is equal to the heat of adsorption. From the latter the strength of the metal-adsorbate bond can be derived. In this way numerous studies with the FEM have furnished valuable information about adsorption systems. It should be noted that nearly all studies so far reported have been concerned with measuring average values on thermally cleaned metal surfaces. A more detailed account of these experiments is given by Gomer[5], who has also reviewed other applications of field emission and the FEM.

II-3. FIELD-ION MICROSCOPY

II-3.1. Theory of field ionization, desorption and evaporation

In the course of field-emission experiments Müller[6] observed that adsorbed layers of electropositive metals on tungsten could be desorbed under the influence of high fields of reversed polarity. It then occurred to him to use this effect deliberately for imaging the surface by admitting hydrogen at low pressure and applying a positive potential to the metal tip. The first pictures so obtained were consequently interpreted as resulting from the impact of desorbing protons on the fluorescent screen. Soon, however, it was shown[15] by a mass-spectrometric analysis of the ion energies that the ions originated mainly in a region close to the tip surface, and not necessarily at the surface. These facts could be satisfactorily explained by the theory of field ionization which was then developed[15,35].

The mechanism of field ionization of a free atom or molecule (henceforth called particle) is analogous to that of field emission from a metal. An electron tunnels through a potential barrier, which is narrowed by a high electric field, the barrier width at a given field strength now being determined by the ionization energy I of the particle. As the value of the ionization energy for simple gases in most cases exceeds the work function of metals, the field strength required for field ionization is generally much higher (roughly by a factor of ten) than that required for field emission, and even then the current density is much less.

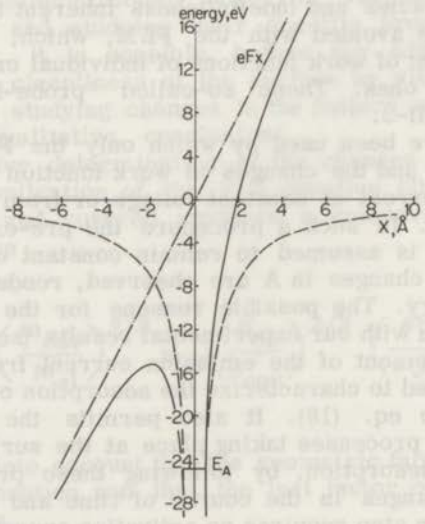

Figure 6

Potential-energy diagram for an electron in a helium atom as a function of the distance x from the nucleus;

-- , the Coulomb potential energy $\frac{Ze^2}{x}$ (with Z taken equal to one)

——, the potential energy when an external field of 4 V/Å is applied

E_A , the energy level of the electron in the atom

Fig. 6 shows the effect of a high electric field on the potential energy of an electron in a particle (in this case a helium atom) in free space. By solving the Schrödinger equation a barrier penetration coefficient D can be calculated. For a one-dimensional barrier D is given by[8]

$$D \approx \exp\left[-\int_{x_1}^{x_2}\left\{\frac{8m}{\dagger h^2}(V-E)\right\}^{1/2} dx\right], \tag{20}$$

where m is the mass of the electron, $\dagger h$ Planck's constant h divided by 2π, V the potential energy and E the total energy of the electron. As can be seen from eq. (20) D is very sensitive to changes in size of the barrier, which ranges from x_1 to x_2.

The probability per unit time of a particle being ionized is found by multiplying D by the frequency ν_e with which the electron inside the particle arrives at the barrier (ν_e is of the order of 10^{16} s^{-1}). A characteristic time for ionization or a mean lifetime τ of the particle is then defined by

$$\tau = \frac{1}{\nu_e D}. \tag{21}$$

When the potential barrier is approximated by a triangle of height I and base $\frac{I}{eF}$ the following expression is obtained for τ:

$$\tau \approx 10^{-16} \exp\left(0.68\,\frac{I}{F}^{3/2}\right), \tag{22}$$

with τ in seconds, I in eV and F in V/Å. The exponential part of eq. (22) closely resembles the one in the F-N equation (6) for field emission.

Figure 7 shows the energy diagram for the case where the particle is close to a metal surface, but no bonding takes place. Again a helium atom is chosen as example. Two things should be noted. Firstly, owing to the presence of the metal and image-potential terms, the potential barrier is much smaller than it is in free space at the same values of F and I. Consequently, τ will decrease sharply when the particle approaches the metal surface. Secondly, the electron can only tunnel into a vacant energy level in the conduction band of the metal. Since at low temperatures nearly all levels below the Fermi level are filled the ionization probability will drop sharply ($\tau \longrightarrow \infty$) when the energy level in the particle falls below the Fermi level. It can easily be seen that this will happen at a distance from the surface less than

$$x_c \approx \frac{I - \varphi}{eF}. \tag{23}$$

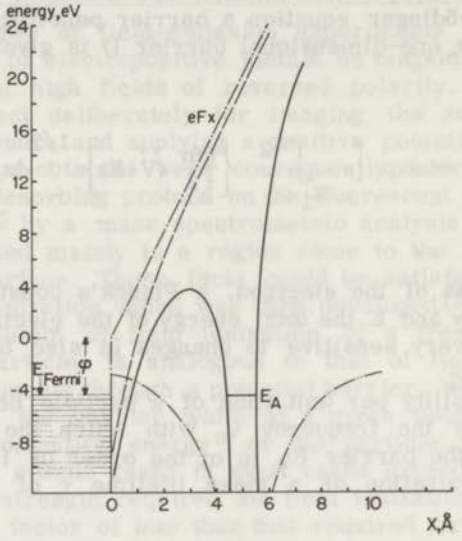

Figure 7

Potential-energy diagram for an electron in a helium atom (I = 24.5 eV) at a distance of 5 Å from a metal surface with φ = 4.50 eV in the presence of an applied field of 4 V/Å;
-.- , the applied potential
--- , the superposition of image and applied potential
-..-, the Coulomb potential
——, the total resultant potential

When calculating τ as a function of x with eq. (20) and (21), we obtain the potential energy V by superposition of the potential of the electron in the particle, the applied potential Fx and the image potential arising from the interaction of the electron and the image-charge distribution induced in the metal by the electron and the ion. Again, the integration is carried out over the width of the barrier.

As is explained in the following section the optimum conditions in the ion microscope are such that ionization only takes place near the minimum distance x_c. In that case τ can be approximated[5,10] by

$$\tau = 10^{-16} \exp \left\{ 0.68 \frac{I - \varphi}{F} \left(I - 7.6\ F^{1/2} \right)^{1/2} \right\} . \qquad (24)$$

The total amount of ions produced by field ionization obviously depends on the supply of particles to the zone where ionization can take place. In actual field-ionization experiments the applied field is highly inhomogeneous.

Consequently, the gas particles are attracted by polarization forces to the high-field region near the tip surface. For this reason the gas concentration close to the tip as well as the rate of arrival at the surface exceed the value calculated for the case where no field is applied. Attempts have been made to treat the gas supply which is a complicated function of field and temperatures in detailed kinetic models. In the author's opinion, however, these models require some corrections. The topic will be dealt with in more detail in Chapter V.

So far we have discussed the ionization of free particles and found as a prerequisite for tunnelling that the energy level of the electron in the particle should be raised by the field to or above the Fermi level in the metal. Tunnelling then occurs in a characteristic time τ, which is determined by the size of the potential barrier seen by the electron. The supply of the particles to the ionization zone at the critical distance x_c can, in principle, be described by gas kinetics if allowance is made for the effects of the inhomogeneous electric field.

We will now consider the phenomenon of field desorption, in which a particle bonded to the metal surface is removed as an ion. This effect can, at least qualitatively, be explained by an analogous model. In this case an electron may tunnel from the metal-adsorbate bond into the metal when in the presence of a high field the bonding level is raised to the Fermi level by vibrational excitation, so that the adsorbed particle spends a certain time beyond a critical distance x_c.

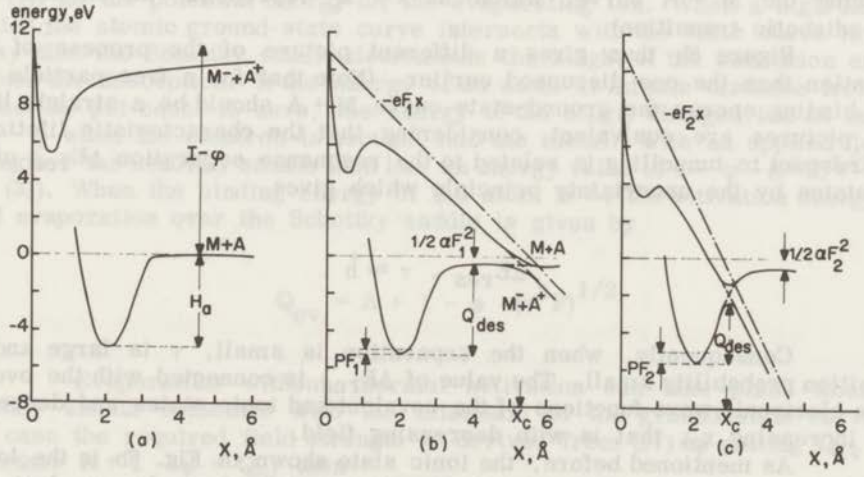

Figure 8

Potential-energy diagram illustrating field desorption of an adsorbate A with ionization energy I adsorbed on a metal M with work function φ; H_a, heat of adsorption; Q_{des}, the activation energy for desorption; P, bond dipole moment; α, polarizability of A; (a) with field F = 0; (b) with F_1 = 2 V/Å; (c) with F_2 = 4 V/Å

As was pointed out by Gomer[36], field desorption and its relation to field ionization can be treated most illustratively in terms of potential-energy diagrams of the metal-adsorbate system. We will here discuss the case of a covalent chemisorption of an atom A with ionization energy I on a metal with work function φ. The lower curve of Fig. 8a represents the potential energy of the neutral state M + A as a function of the distance x of the atom from the surface. H_a is the heat of adsorption. The upper curve gives the potential energy of an ionic state $M^- + A^+$. There exists a whole set of such states depending on the energy level in the metal into which the electron from A goes. When the electron is accommodated in the lowest available level, i.e. the Fermi level, the energy separation between the two states for large values of x is equal to $I - \varphi$.

When a field of moderate strength F_1 is applied the potential energy situation as shown in Fig. 8b is obtained. The $M^- + A^+$ curve is greatly deformed, while M + A is only slightly displaced owing to the polarization energy $\frac{1}{2}\alpha F^2$ of the atom, with polarizability α, and the field-dipole interaction PF, where P is the bond dipole moment. The two curves intersect at x_c. Normally the degeneracy implied by the crossed potential curves is absent, so that the curves will separate and give rise to the new states indicated by the solid lines. Vibrational desorption with an activation energy Q_{des} which is almost equal to the zero field value H_a leads in the first instance to desorption of a neutral atom. However, when the atom moves away from the surface it can be ionized at x_c, whereupon the system follows the lower curve (adiabatic transition). If the time spent in the transition region is short compared with the characteristic time τ the chance that electronic rearrangement (tunnelling) occurs is small. The system then keeps following the M + A curve, which at $x > x_c$ represents an excited state (non-adiabatic transition).

Figure 8b thus gives a different picture of the process of field ionization than the one discussed earlier. (Note that for a free particle with zero binding energy the ground-state curve M + A should be a straight line.) Both pictures are equivalent, considering that the characteristic lifetime τ with respect to tunnelling is related to the resonance separation ΔE_{res} of the two states by the uncertainty principle which gives

$$\Delta E_{res} \cdot \tau \approx \hbar . \qquad (25)$$

Consequently, when the separation is small, τ is large and the transition probability small. The value of ΔE_{res} is connected with the overlap of the electronic wave functions of the covalent and ionic states and decreases with increasing x_c, that is with decreasing field.

As mentioned before, the ionic state shown in Fig. 8b is the lowest of a whole set of such states. An electronic transition from the covalent state to an ionic state at a given field is therefore also possible at $x > x_c$. The probability of such a transition will, however, be smaller owing to a decrease in ΔE_{res} at larger values of x. These considerations are in complete accordance with those of the preceding discussion on the mechanism of field ionization.

The potential-energy situation for the case where a much higher field is applied is represented in Fig. 8c. The critical distance x_c now lies within the attractive part of the ground-state curve. Vibrational excitation might thus lead to ionic desorption over a potential barrier which is reduced vis-à-vis the zero field value H_a. In view of the large resonance separation between the states at small x_c it can be assumed that a particle which has the required energy to pass over the barrier will indeed make the electronic transition. The activation energy Q_{des} depends on the field strength and can therefore be made very small. It is readily seen that Q_{des} may be approximated by

$$Q_{des} = V(x_c) + H_a \ , \tag{26}$$

where $V(x_c)$ is the (negative) potential energy of the field-free covalent state at x_c ($V(x) = 0$ for $x \longrightarrow \infty$).

Gomer and Swanson[9] have extended the theory of field desorption by quantum-mechanical calculations and have also treated other types of adsorption system with a relative position of ionic and covalent potential-energy curves differing from the one for covalent chemisorption with a large value of $I - \varphi$ as discussed above.

Closely related to field desorption is the process of field evaporation, i.e. the removal of surface atoms of the metal itself as ions. Müller[37] has treated field evaporation by assuming a Schottky image potential (see eq. (1)) as the potential energy for the evaporating ion. When a high field is applied the atomic ground-state curve intersects with the ionic curve in such a way that the Schottky saddle determines the height of the activation energy barrier for desorption. If the energy of an atom at infinite distance from the surface is put equal to zero, the energy of the singly charged ion at infinity is $I - \varphi$ when the electron is brought into the metal. With an applied field of strength F the Schottky saddle then has an energy value of $I - \varphi - (e^3F)^{1/2}$ (cf. eq. (3)). When the binding energy of the atom is Λ, the activation energy for field evaporation over the Schottky saddle is given by

$$Q_{ev} = \Lambda + I - \varphi - (e^3F)^{1/2} \tag{27}$$

Evaporation without thermal activation can take place when the Schottky saddle coincides with the minimum of the ground-state curve. In that case the required field strength is derived from (27) by putting $Q_{ev} = 0$; if further $\Lambda + I - \varphi = Q_o$, then

$$F_{ev} = \frac{Q_o^2}{e^3} \ . \tag{28}$$

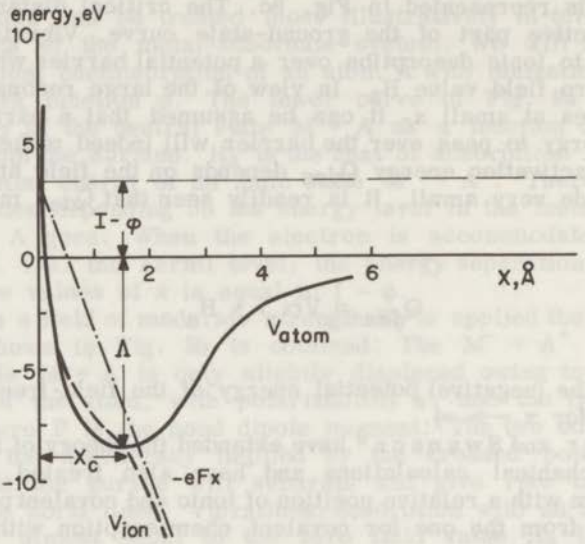

Figure 9

Potential-energy diagram for field evaporation; values of parameters are those of tungsten: heat of sublimation $\Lambda = 8.7$ eV, ionization energy $I = 7.9$ eV and work function $\varphi = 4.50$ eV

Brandon[10] has argued that a simple image potential is not adequate to describe the potential of the ion because the Schottky saddle is located within 1 Å from the surface. He therefore proposed to add a repulsion term, so that the potential energy of the ion should then become

$$V_{ion}(x) = I - \varphi - \frac{e^2}{4x} - eFx + \frac{A}{x^n} , \qquad (29)$$

where A and n are constants. Non-activated field evaporation occurs when the ionic curve intersects the atom potential curve at its minimum as is shown in Fig. 9; then

$$V_{ion} = V_{atom} = -\Lambda . \qquad (30)$$

Combining (29) and (30), we get

$$F_{ev}\, e\, x_c = Q_o - \left(\frac{e^2}{4x_c} - \frac{A}{x_c^n} \right) . \qquad (31)$$

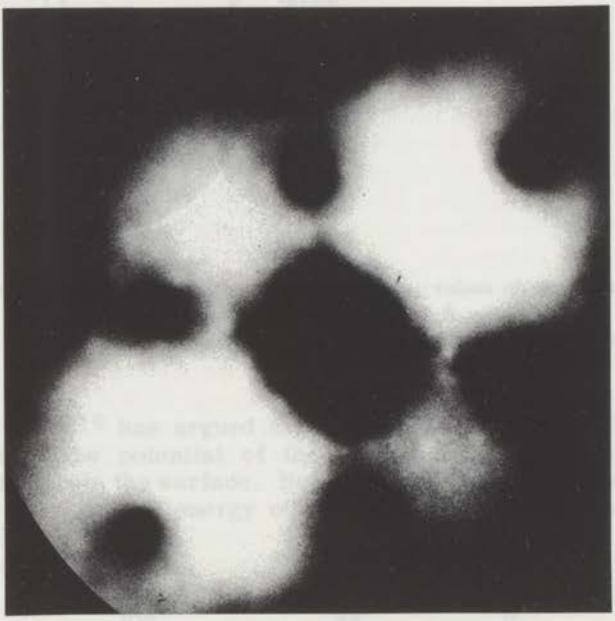

Figure 3

Field-emission pattern of a clean thermally annealed tungsten surface

100
111
111
110

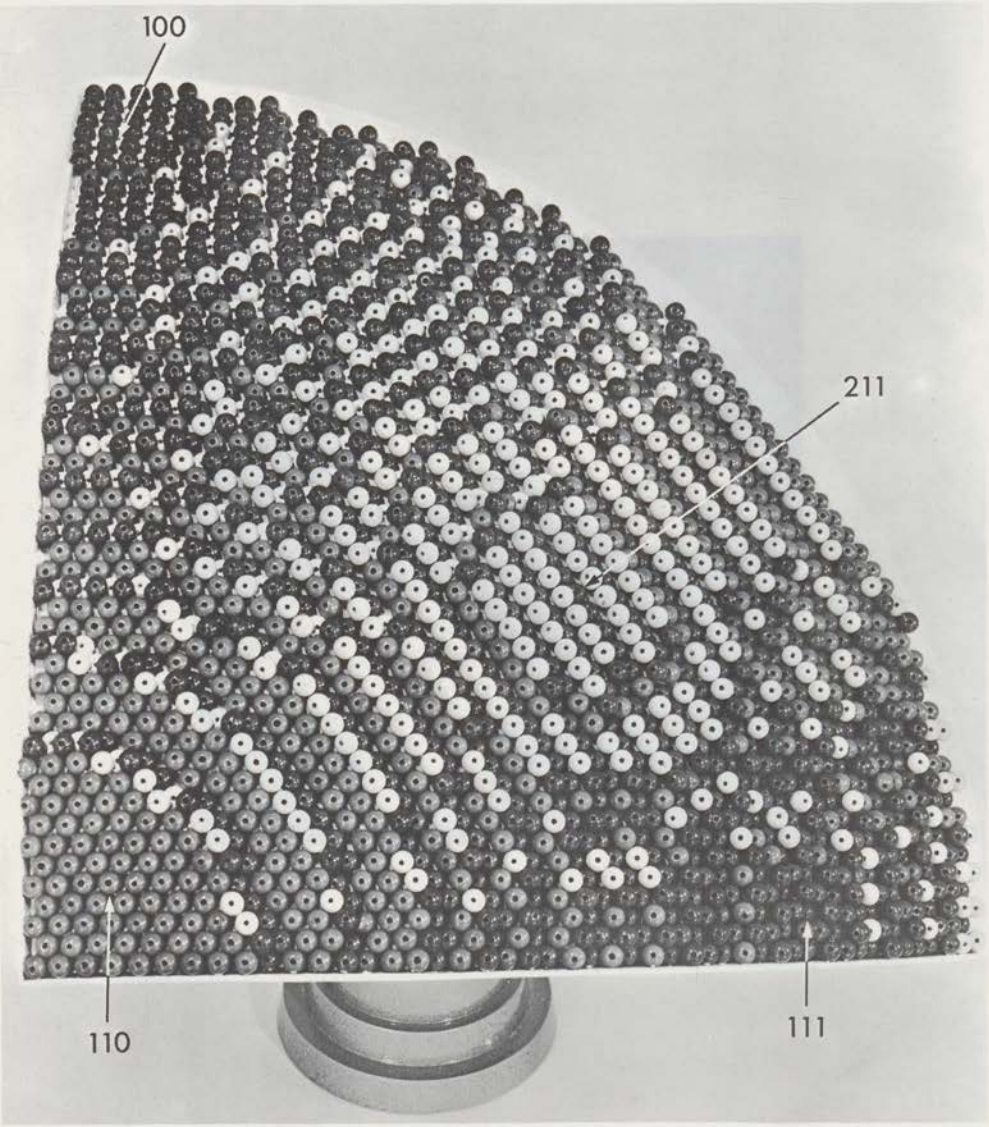

Figure 5

Marble model of a b.c.c. lattice

Figure 10

Helium-ion image of an ordered tungsten surface, field-evaporated at 20 °K and 13.6 kV; image at 20 °K and 10.5 kV

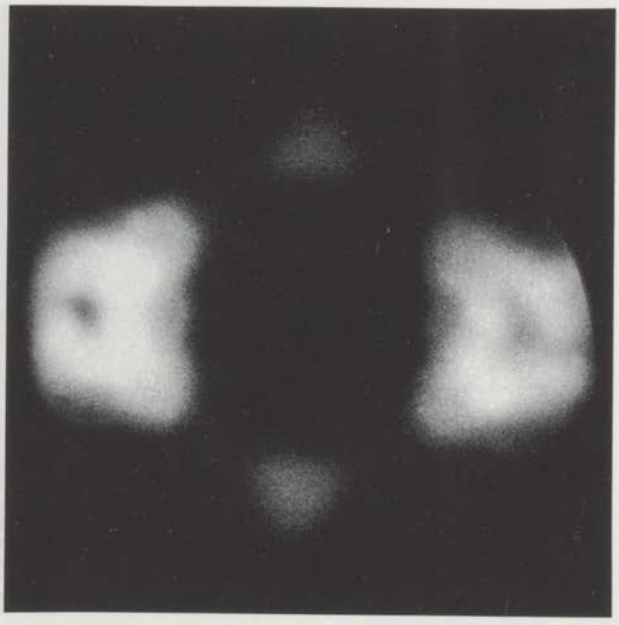

Figure 12

Field-emission pattern of an ordered tungsten surface

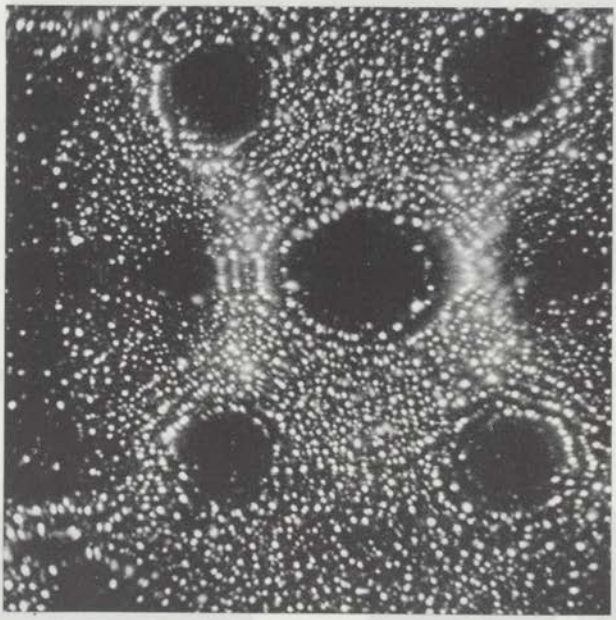

Figure 13

Helium-ion image of a thermally annealed tungsten surface at 20 °K and 16.5 kV

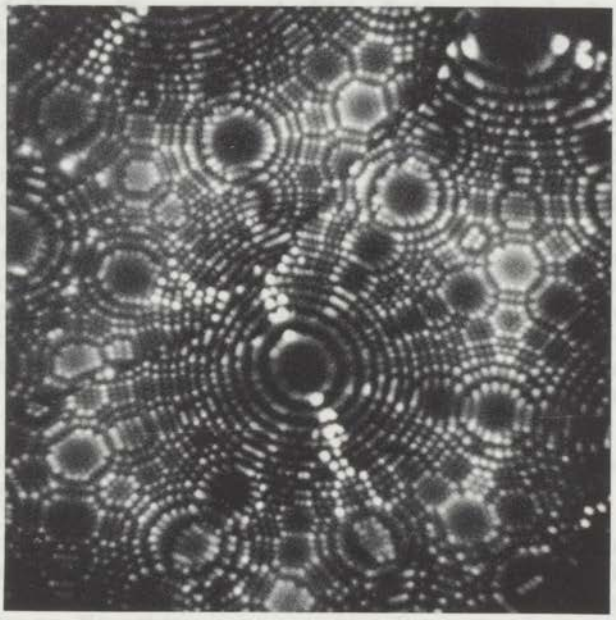

Figure 14

Helium-ion image of a tungsten surface showing a grain boundary, running from middle left to upper right; image at 63 °K and 7.8 kV

a

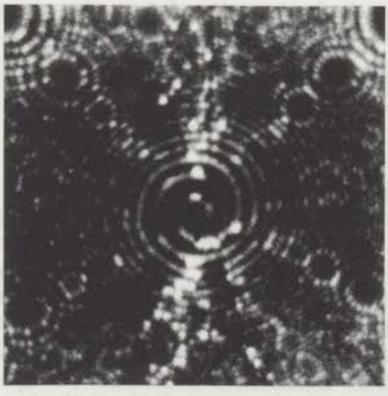

b

Figure 15

Helium-ion images of tungsten (110) face and surrounding lattice steps showing a dislocation;

(a) image taken at 63 °K and 11.8 kV

(b) after field evaporation of (a), image at 63 °K and 12.3 kV

In the band model of a metal non-activated-field evaporation can be understood as follows. The extremely high field pushes back the conduction electrons into the metal by raising the electron energy levels at the surface. When the lowest conduction level at the surface coincides with the highest filled level inside the metal, the electrons are completely drained out of the surface region, while the positive metal ions are torn away by the field.

Equation (31) gives a linear dependence of F_{ev} on Q_o, resulting in a range of evaporation fields for the various metals of about 2 to 7 V/Å. This seems in slightly better agreement with experimental findings than the larger range of F_{ev} predicted by eq. (28).

Equations (28) and (31) have been extended by including energy terms which account for the difference in polarizability of the atom and the ion, and the penetration of the field into the metal. Moreover, for most metals it proves to be energetically favourable that the evaporating ions are not singly but doubly charged. This has in fact been verified experimentally in some cases. Brandon[11] has discussed these points in detail.

At present there are many discrepancies between the experimental observations and the theories outlined in this section. This hardly seems surprising. In the theory of field emission it is a fairly good approximation to regard the metal surface as a smooth uniform plane, because the effects of the actual non-uniformness on an atomic scale have levelled out over a distance small compared with the width of the potential barrier seen by the tunnelling electron. For this reason a one-dimensional theory can give an adequate description of field-electron emission, at least from clean surfaces.

The processes of field ionization, field desorption and a fortiori of field evaporation, however, take place within such extremely short distances from the surface that the discreteness of the surface structure, i.e. the specific atomic configuration in any one point, can no longer be ignored and three-dimensional theories are needed. However, as long as a detailed theory about the electronic structure of metal surfaces is not available, the one-dimensional models discussed above remain useful for a qualitative description of the phenomena observed.

II-3.2. The field-ion microscope

The field-ion microscope (FIM), developed by Müller after his first experiments with hydrogen, is at present operated primarily with helium as imaging gas, though some progress has been made with the use of neon[38]. Its construction is in principle the same as that of the field-emission microscope (Fig. 2); the two differ only in the way the tube is operated. Into the evacuated microscope tube pure helium gas is introduced at a pressure of about 10^{-3} Torr. The metal is then brought to a high positive potential (5-20 kV, depending on the radius) relative to the fluorescent conductive screen, so that field ionization of the helium atoms can take place. The ions are radially accelerated on their way to the screen, where they produce a faint but highly detailed image of the surface, provided that the field ionization mainly takes place close to the surface. When the tip has been field-evaporated and cooled to 20 °K a picture as shown in Fig. 10 is obtained.

It represents the image of a tungsten tip with a radius of about 400 Å. Every bright spot is the image of a locus of relatively high ionization probability for the helium atoms and evidently corresponds with an individual atom in the metal surface. The latter is indeed almost perfectly ordered by the low-temperature field evaporation in all regions except in the (100) face. The resolution is remarkable, and distances of a few Ångströms are readily resolved.

Obviously, by no means all surface atoms are imaged. Only the most protruding and less well coordinated atoms act as discrete ionization centres. This can be understood if, by analogy with macroscopic electrostatics, we visualize the potential lines as following the atomic contours of the surface (Fig. 11). The field anisotropies will then be much larger in the atomically rough areas (e.g. the (111) faces of a b.c.c. lattice, and lattice steps at the edges of faces) than in the smooth areas (e.g. the (110) face). Since the ionization probability is extremely sensitive to variations in field strength it will exhibit a correspondingly marked anisotropy just before the rough areas. It is this anisotropy in ionization probability which is imaged.

When the voltage is raised the ionization probability will increase and ionization will also occur between protruding atoms and to a less extent at a larger distance from the surface as well, so that the effect of the discrete atomic structure fades out. This means that the structure of the image gets lost, i.e. the resolution goes down, up to a point where the pattern on the screen is completely diffuse.

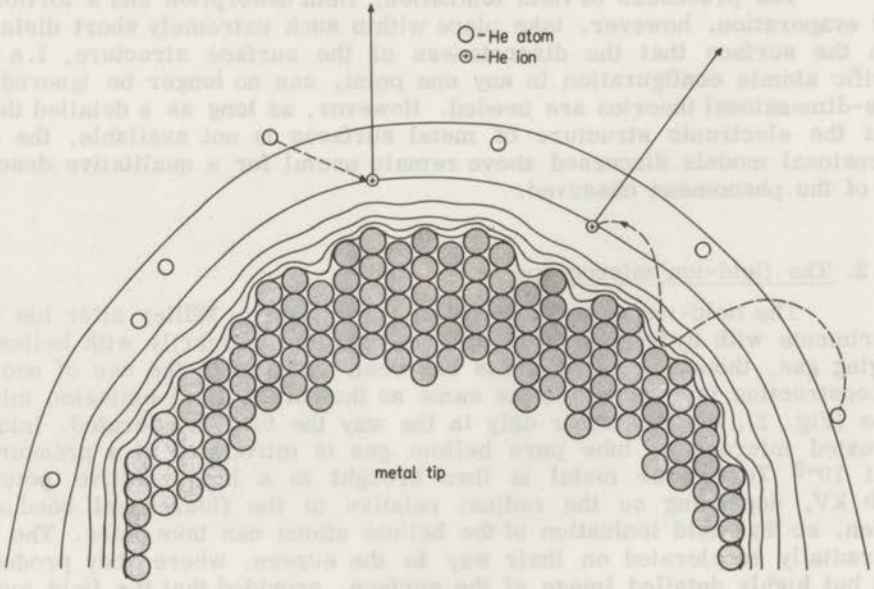

Figure 11

Schematic representation of the field ionization process showing the equipotentials near the tip surface

When the voltage is lowered the image gradually disappears, since the field becomes too low for ionization. It is thus possible to indicate a "best-image voltage" and a "best-image field". The latter is for helium about 4.5 V/Å; with I = 24.5 eV and φ = 4.5 eV, and applying eq. (23), the critical distance $x_c \approx 4.5$ Å. By determining the energy distribution of the ions with a retarding-potential technique Tsong and Müller[39] have proved that the ions indeed originate at about 4 Å from the surface. The narrow energy distribution indicates that the ionization zone is extremely thin (about 0.2 Å).

The second factor which determines the resolution is the transverse velocity of the ions. The velocity can be lowered by cooling the tip in order that the helium atoms accommodate and lose at least part of their kinetic energy before they become ionized. Here we meet with a fundamental difference between the FEM and the FIM as regards the effect of cooling on the resolution, owing to the different statistics the image-forming particles obey in each case.

The magnification is again given by formula (13); with a typical tip-to-screen distance of 10 cm and the usually very sharp tips (200-500 Å) the magnification lies in the range of 10^7-10^6. The intensity of the ion images is extremely low and perfect dark adaptation is needed before the detailed structure can be observed. The intensity sharply increases with the radius, because the total current (of the order of 10^{-9} A) goes up with a power of the radius between 2.5 and 3.0 and the brightness of the screen rises about linearly with the applied voltage, i.e. with the radius. The intensity can be increased further by raising the helium pressure, but beyond about $3 \cdot 10^{-3}$ Torr the scattering of the ions on their way to the screen becomes appreciable, resulting in a decrease in resolution.

Although it might be concluded from the foregoing that the mechanism of image formation is qualitatively understood, many experimental observations remain unexplained or are even at variance with present theory. Some of these will be discussed in Chapter V.

The structure of the surface represented in Fig. 10 is typical of a tip which is field-evaporated at low temperature (20 °K) and results from a complex balance of various effects. In the preceding discussion on field evaporation (section II-3.1.) no attention has been paid to the dependence of field evaporation on the particular configuration at the evaporation site. However, the activation energy Q of eq. (26) may vary from one surface atom to another. Such variations can be attributed to differences in (a) the binding energy Λ of the atoms, (b) the polarization and field-penetration terms and (c) the effective field strength at the evaporation site. The orientation dependence of the work function arises from differences in the structure of the electric double layer and is therefore accounted for by (b). At a given applied field the effective field strength at a site is determined by two field enhancement factors: one, f_1, is related to the local radius of curvature, the other, f_2, to the specific lattice geometry (lattice step height).

Field evaporation of a metal tip prepared by electrolytical etching will proceed most easily for regions and sites where Q is low. Thus in the first stages sharply curved regions (high f_1) will be flattened and protruding atoms (low Λ and high f_2) removed. From the smoothened surface evaporation now proceeds preferentially from edges of lattice planes where the atoms are

most weakly bonded. The binding energy at these evaporation sites is nearly constant for the various surface regions, but the lattice step is markedly higher (larger f_2) for the close-packed planes than for the less densely packed planes. In the former areas field evaporation will therefore be enhanced, resulting in an increase in local radius (smaller f_1). The value of Q, however, does not necessarily become uniform for all sites for two reasons. Firstly, the surface density of evaporation sites is lower in the close-packed regions. To have an equal evaporation rate for a close-packed region and a rough region we therefore need a lower value of Q for the former. Secondly, for a stable tip geometry it is required that the evaporation rate per unit area is a maximum at the apex of the tip, falling off towards the shanks. If a close-packed region is at the apex (as the (110) face with tungsten tips), then we have another reason why Q should be lower for these regions.

If a balance of all factors (including surface polarization) is struck a so-called field-evaporated "end form" is obtained. This end form is marked by the development of many high-index planes, which can be observed in particular at tips with a relatively large radius of curvature ($\approx$ 1000 Å). The occurrence of the array of bright dots along the [100] zone, the so-called "zone decoration", is attributed by Müller[40] to stabilization owing to the polarization by the field penetrating over a protruding atom. The polarization binding energy on the sites in question then compensates the smaller degree of coordination by nearest neighbours.

II-3.3. Applications

The very high resolution and magnification of the field-ion microscope make it an ideal tool for examining the lattice structure of metal surfaces in atomic detail. The application of the instrument in metallographic studies has been pioneered by Müller and co-workers at Pennsylvania State University and by a group at the University of Cambridge, England.

The difference between a thermally annealed surface and a field-evaporated surface, already noticeable in the electron-emission patterns (cf. Fig. 3 and Fig. 12), shows up most clearly in the ion micrographs of the two types of surface (Fig. 10 and Fig. 13). The thermally annealed tip invariably exhibits large low-index planes, while the other regions are marked by a severe frozen-in disorder.

It has also become possible to study lattice defects, grain boundaries, the effect of a bombardment with high-energy particles and the like, on an atomic scale. For example, Fig. 14 shows a grain boundary in tungsten and Fig. 15 a dislocation on the (110) face, due to the presence of a low-angle grain boundary. A review of the metallurgical applications can be found in the literature[8,10,12].

So far field desorption, field evaporation and the field-ion microscope have found only a few applications in adsorption studies. Field desorption can be used to clean metal tips without heating them. This is of special advantage with low-melting metals and alloys which can only be cleaned thermally by applying temperatures close to the melting point, so that severe blunting occurs. Gomer[36] has pointed out that field-desorption measurements can be used to determine the shape of the ground-state curve in covalent binding. Swanson and Gomer[41] have applied the technique to carbon

monoxide on tungsten and found fair agreement with the theory. Müller[42] has observed corrosion of tungsten and platinum surfaces after adsorption of oxygen at room temperature. Mulson and Müller[43] have found corrosion of tungsten and iridium upon field desorption of adsorbed nitrogen and carbon monoxide. Nakamura and Müller[44] have studied the oxidation of tantalum.

A study of oxygen adsorption on field-evaporated tungsten with field emission was reported by George and Steer[45]. They used the ion microscope mainly to characterize the structure of initially clean surfaces and concluded that the field-emission results are independent of initial surface order. After adsorption at 20 °K on a field-evaporated surface and removal of the oxygen by field desorption they obtained an ion image of a surface littered with out-of-place atoms.

Far more extensive studies with the ion microscope were made by Ehrlich and Hudda[46] with the system nitrogen on tungsten and by Ehrlich[47] with carbon monoxide on tungsten. They concluded that the metal surface is only negligibly disturbed by the adsorption and that individual adsorbed nitrogen atoms and carbon-monoxide molecules can be seen.

In the adsorption studies especially we touch upon the limitations of the ion-microscope technique, at least in its present form. Under the conditions of imaging the stability of the adsorbate proves to be reduced by a combined effect of field and image gas. Ehrlich and Hudda[48] observed promoted field desorption of hydrogen from tungsten. While they trace it to the impact of slow electrons from the ionization process, Nishikawa and Müller[38] attribute the effect to the impact of image gas atoms which have acquired a polarization energy $\frac{1}{2}\alpha F^2$ (about 0.15 eV for helium).

If under image conditions the metal itself evaporates, no stable images can be obtained at the field strength required for helium-ion microscopy. This, in fact, is the case with the lower-melting metals like gold, copper and iron, and with most alloys. In principle use can be made of other image gases of which neon seems to be the most promising. However, as the image intensity goes down with increasing mass of the ion, neon-ion microscopy calls for artificial intensification of the image. Internal and external intensifying methods can be distinguished. The former category includes the dynamic gas supply system[49], post-acceleration of the ions[50,51], and the conversion into an electron image by the emission of secondary electrons from a grid[52]. Besides having manifest disadvantages, these systems do not yield magnification factors higher than about 100. Much higher gains are obtained by external image intensification with commercially available photoelectronic tubes[53].

REFERENCES

1. R.W. Wood, Phys. Rev. 5, 1 (1897).

2. R.H. Fowler and L. Nordheim, Proc. Roy. Soc. (London) A119, 173 (1928).

3. E.W. Müller, Z. Phys. 106, 541 (1937).

4. E.W. Müller, A. Phys. 108, 668 (1938).

5. R. Gomer, "Field Emission and Field Ionization", Harvard University Press, Cambridge, Massachusetts (1961).

6. E.W. Müller, Naturwissenschaften 29, 533 (1941).

7. E.W. Müller, Z. Physik 136, 131 (1951).

8. E.W. Müller, Advan. Electron. Electron Phys. 13, 83 (1960).

9. R. Gomer and L. Swanson, J. Chem. Phys. 38, 1613 (1963).

10. D.G. Brandon, Brit. J. Appl. Phys. 14, 474 (1963).

11. D.G. Brandon, Surface Science 3, 1 (1965).

12. E.W. Müller, Science 149, 591 (1965).

13. G. Ehrlich, Advan. Catalysis 14, 255 (1963).

14. A.A. Holscher, Surface Science 4, 89 (1966).

15. M. Inghram and R. Gomer, Z. Naturforsch. 10a, 863 (1955).

16. H.D. Beckey, Z. Naturforsch. 14a, 712 (1959).

17. H.D. Beckey, Bull. soc. chim. Belges 73, 326 (1964).

18. W.P. Dyke, J.P. Barbour, J.K. Trolan and E.E. Martin, Phys. Rev. 98, 263A (1955).

19. W.P. Dyke and W.W. Dolan, Advan. Electron. Electron Phys. 8, 89 (1956).

20. A.G.J. van Oostrom, J. Appl. Phys. 33, 2917 (1962).

21. W. Schottky, Z. Phys. 14, 63 (1923).

22. B.S. Gossling, Phil. Mag. 1, 609 (1926).

23. L. Nordheim, Proc. Roy. Soc. (London) A121, 626 (1928).

24. R.H. Good and E.W. Müller in "Handbuch der Physik", Springer, Berlin (1956), 2nd ed., Vol. 21, p. 176.

25. E.L. Murphy and R.H. Good, Phys. Rev. 162, 1464 (1956).

26. E.W. Müller, J. Appl. Phys. 26, 732 (1955).

27. R.D. Young and E.W. Müller, Phys. Rev. 113, 115 (1959).

28. P.H. Cutler and J.J. Gibbons, Phys. Rev. 111, 399 (1958).

29. P.H. Cutler and D. Nagy, Surface Science 3, 71 (1965).

30. A.G.J. van Oostrom, Thesis, Amsterdam (1965).

31. R.V. Culver and F.C. Tompkins, Advan. Cat. 11, 67 (1959).

32. A. Eberhagen, Fortschr. Phys. 8, 245 (1960).

33. J.C.P. Mignolet, Bull. soc. chim. Belges 64, 122 (1955).

34. R. Klein, J. Chem. Phys. 31, 1306 (1959).

35. E.W. Müller and K. Bahadur, Phys. Rev. 102, 624 (1956).

36. R. Gomer, J. Chem. Phys. 31, 341 (1959).

37. E.W. Müller, Phys. Rev. 102, 618 (1956).

38. O. Nishikawa and E.W. Müller, J. Appl. Phys. 35, 2806 (1964).

39. T.T. Tsong and E.W. Müller, J. Chem. Phys. 41, 3279 (1964).

40. E.W. Müller, Surface Science 2, 484 (1964).

41. L. Swanson and R. Gomer, J. Chem. Phys. 39, 2813 (1963).

42. E.W. Müller in "Structure and Properties of thin Films", C.A. Neugebauer, J.D. Newkirk, D.A. Vermilyea eds., Wiley, New York (1959).

43. J.F. Mulson and E.W. Müller, J. Chem. Phys. 38, 2615 (1963).

44. S. Nakamura and E.W. Müller, J. Appl. Phys. 36, 3634 (1965).

45. T.H. George and P.M. Steer, J. Chem. Phys. 37, 1935 (1962).

46. G. Ehrlich and F.G. Hudda, J. Chem. Phys. 33, 1253 (1960) and 36, 3233 (1962).

47. G. Ehrlich, Trans. N.Y. Acad. Sci. 101, 722 (1963).

48. G. Ehrlich and F.G. Hudda, Phil. Mag. 8, 1587 (1963).

49. B.J. Waclawski and E.W. Müller, J. Appl. Phys. 32, 1472 (1961).

50. D.G. Brandon, S. Ranganathan and D.S. Whitmell, Brit. J. Appl. Phys. 15, 55 (1964).

51. V.G. Weizer, J. Appl. Phys. 36, 2090 (1965).

52. D.G. Brandon, J. Sci. Instr. 43, 708 (1966).

53. S.B. McLane, E.W. Müller and O. Nishikawa, Rev. Sci. Instr. 35, 1297 (1964).

CHAPTER III

EXPERIMENTAL PROCEDURES

III-1. ULTRA-HIGH VACUUM TECHNIQUES

For a fundamental study of gas adsorption it is essential to start the experiment with a perfectly clean surface and with the residual gases in the system at such a low pressure that in the course of the actual runs adsorption of these gases is negligible. From gas kinetics it can be calculated that at a pressure of 10^{-6} Torr a surface is covered in a few seconds with a monolayer of adsorbate when about half the number of molecules that collide with the surface stick to it. In order that reliable evidence may be collected, the partial pressures of all reactive residual gases must therefore be in the order of 10^{-10} Torr or less. The attainment of such low pressures nowadays presents no serious problems, if care is taken that the apparatus only consists of materials which have a low degassing rate and are capable of withstanding a bake-out temperature of 400 °C.

As general ultra-high vacuum techniques are known from the literature[1] we will confine ourselves to a description of the vacuum system and procedures developed for the present study.

In our field-emission measurements and the ion-microscope work we used a vacuum installation of essentially the same set-up, which is schematically shown in Fig. 16. It consists of an ultra-high vacuum part with a sputter ion pump and a fore-vacuum line with an oil-diffusion pump, backed by a two-stage rotary oil pump. The ion pump is mounted in a working table, which has a surface of Sindanyo board, a heat-resistant material. The ultra-high vacuum part of the system is above the table and separated from the fore-line by two bakeable all-metal valves A_1 and A_2. Between the oil diffusion pump and A_2 there is a cold trap. The pressure in the fore-line is measured with a Penning gauge.

The gases to be used in the experiments were introduced from a gas storage system via the dosing valves A_4, A_5, A_6, respectively, A_3 and a magnetically operated ball-joint valve. The last is only effective, however, at pressures below 10^{-4} Torr. The ion pump can be shut off by valve A_7. The pressure in the ultra-high vacuum part is measured with a Bayard-Alpert type ionization gauge.

The system above the table can be baked out at 400 °C by enclosing it in portable ovens. The connecting tubes between valves A_4, A_5 and A_6, and the gas ampoules are to be degassed with heating tape. Bake-out of the ion pump with its magnet in position is limited to a temperature of 300 °C and this was also effected with heating tape.

The evacuation of the above apparatus took place as follows. After the system had been evacuated by the rotary pump and subsequently by the oil-diffusion pump to a pressure of about 10^{-4} Torr, the trap being cooled with liquid nitrogen, the ion pump was switched on and valve A_1 closed. All other valves were in open position. Generally the pressure fell rapidly into the 10^{-7} Torr range. After preliminary outgassing of the ionization gauge, the heating tapes were turned on and the ovens placed in position. The tem-

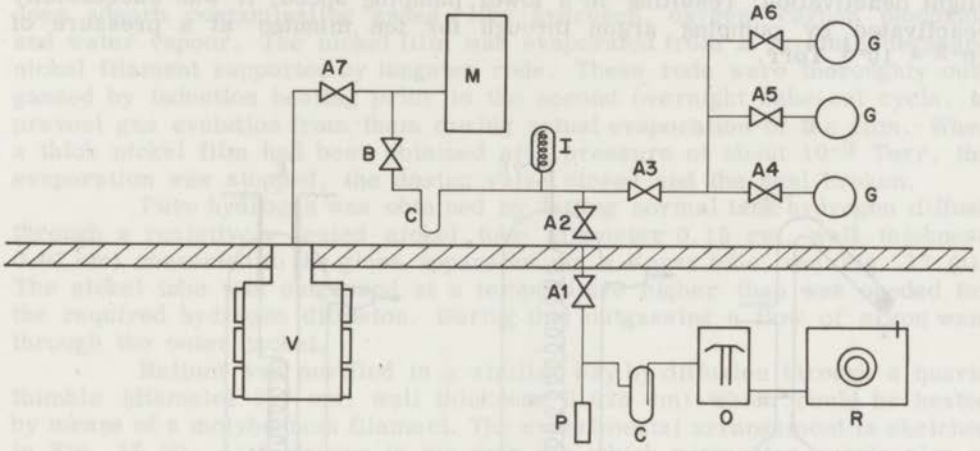

Figure 16

Schematic representation of vacuum apparatus

T - working table; V - 75 l/s VacIon pump;
O - 10 l/s oil-diffusion pump; R - 2-stage rotary pump;
M - microscope tube; C - cold trap; P - Penning gauge;
I - ionization gauge; A 1, 2, 3, 4, 5, 6 - bakeable UHV valves
Granville Phillips type C; A 7 - ditto type L;
B - magnetically operated ball-joint valve;
G - gas supply (storage flasks or diffusion thimbles)

perature was raised to 400 °C very slowly, in order that the pressure should not exceed 10^{-5} Torr. After an overnight bake-out the pressure had normally dropped to about $3 \cdot 10^{-8}$ Torr, while the system was still at 400 °C. The ovens were then removed and the ion gauge was subjected to a prolonged outgassing. After a second overnight bake-out, cooling down the entire system to room temperature and closing valve A_2 resulted in a pressure of about $3 \cdot 10^{-10}$ Torr.

Once a seal of a gas-storage flask (Fig. 17) is broken in the course of the experiments, the corresponding dosing valve can no longer be baked out without introducing contaminations into the pure gas. When it was necessary to replace a metal tip in the microscope tube, valve A_3 was therefore closed before exposing the main system to air. A_3 was not opened again before the pressure had been reduced to 10^{-7} Torr by another evacuation. In this way we avoided exposure of the dosing valves to atmospheric pressure and repeated bake-outs.

When only a metal tip had been replaced and the previously baked-out system was exposed to air just for a short time one bake-out cycle (valves A_4, A_5 and A_6 left out) was normally sufficient. We found it particularly advantageous to keep the ion pump under vacuum by closing valve A_7 before letting in dry air via the fore-line.

After a long period of action the ion pump sometimes showed a slight deactivation, resulting in a lower pumping speed; it was successfully reactivated by pumping argon through for ten minutes at a pressure of 10^{-5} - 10^{-4} Torr.

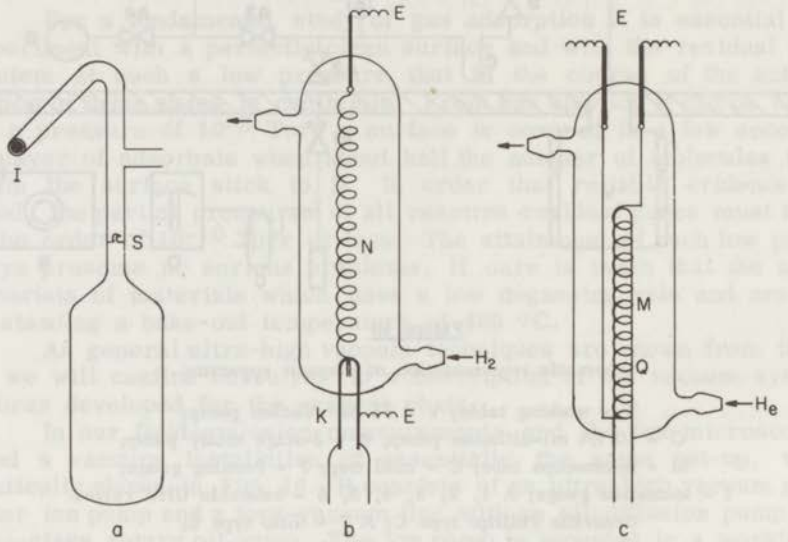

Figure 17

(a) Gas-storage flask;
S - glass seal; I - iron ball in glass envelope

(b) Diffusion leak - hydrogen purifier;
N - nickel tube; K - Kovar tube; E - electrical lead

(c) Diffusion leak - helium purifier;
Q - quartz tube; M - molybdenum filament

In the ion microscope studies the fore-vacuum line was also used to remove the main part of the helium after the ion pictures had been taken. To diminish the backflow of contaminants into the ultra-high vacuum part of the system during helium pumping the fore-line was also baked out with heating tape. The ultimate vacuum then obtained by the oil-diffusion pump was about 10^{-6} Torr.

The gases used in this study were all of high purity. Nitrogen and carbon monoxide were purchased in 1 l·atm flasks provided with a break seal as shown in Fig. 17 (a). According to the specification the impurity content was less than 0.01%. The seals were broken by means of an iron ball contained in a glass envelope and manipulated with a magnet. The nitrogen was further purified by storage over a nickel film evaporated on the walls of a

glass bulb which was inserted in the connection between the flask and the dosing valve. Nickel does not adsorb nitrogen at room temperature, but it does adsorb contaminating gases, like hydrogen, oxygen, carbon monoxide and water vapour. The nickel film was evaporated from a carefully degassed nickel filament supported by tungsten rods. These rods were thoroughly outgassed by induction heating prior to the second overnight bake-out cycle, to prevent gas evolution from them during actual evaporation of the film. When a thick nickel film had been obtained at a pressure of about 10^{-9} Torr, the evaporation was stopped, the dosing valve closed and the seal broken.

Pure hydrogen was obtained by letting normal tank hydrogen diffuse through a resistively heated nickel tube (diameter 0.15 cm, wall thickness 0.01 cm) connected to the glass apparatus via a Kovar tube; see Fig. 17 (b). The nickel tube was outgassed at a temperature higher than was needed for the required hydrogen diffusion. During this outgassing a flow of argon went through the outer jacket.

Helium was purified in a similar way by diffusion through a quartz thimble (diameter 0.7 cm, wall thickness 0.025 cm) which could be heated by means of a molybdenum filament. The experimental arrangement is sketched in Fig. 17 (c). As hydrogen is the only gas which permeates quartz also at an appreciable rate, tank helium with a low hydrogen content (less than 0.01%) was used. In some of the ion microscope experiments we employed pure helium from commercially available 1 l·atm flasks, which showed no differences compared with the helium purified by diffusion.

III-2. FIELD-ION MICROSCOPY

The ion-microscope tube is diagrammatically represented in Fig. 18. Compared with a conventional field-emission microscope it has as special features a flat conductive fluorescent screen (for the preparation of these screens see Appendix 1) with a large diameter (11 cm) and a double Dewar. The outer Dewar is normally filled with liquid nitrogen and shields an inner Dewar, which during imaging is filled with some suitable coolant, e.g. liquid nitrogen (77 ^{o}K) or liquid hydrogen (20 ^{o}K). It is also possible to obtain solid nitrogen (63 ^{o}K) by pumping off the liquid nitrogen with a rotary oil pump.

The tip assembly (see Fig. 19 and Appendix 2) is mounted on tungsten rods, which are led through the inner Dewar and connected to silver wires which provide for the electrical contacts. The distance from the tip to the screen is about 9 cm.

A polished stainless steel cylinder, closely fitting about the lower end of the Dewar and kept at the same potential as the screen, serves two purposes. Firstly, it prevents spurious electron emission from the conductive coating during field desorption and helium-ion experiments. Secondly, it effectively helps in accommodating the helium atoms before they are ionized at the tip surface, thus improving the intensity as well as the resolution of the ion image.

External electrical contact with the conductive coating is made via a Kovar tube sealed with a glass bead, and contact with the cylinder via a platinum wire and a tungsten rod sealed in the top of the Dewar assembly. For renewal of a metal tip the tube has to be opened a few centimetres below this lead-in, so that the inner Dewar can be taken out. After insertion of the new tip the tube is sealed again.

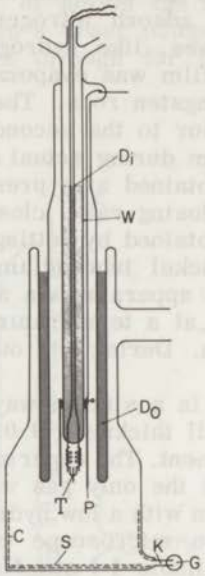

Figure 18

Field-ion microscope

S - fluorescent screen; C - conductive coating; D_i - inner Dewar; D_o - outer Dewar; T - tip assembly; P - polished cylinder; K - Kovar tube; W - platinum wire; G - glass bead

In carrying out the experiments with the ion microscope we generally followed a strict routine to be sure that the experiments took place under comparable conditions. Occasional deviations from the standard procedures will be explicitly mentioned.

After completion of the evacuation procedure (see section III-1.) the metal tip was first cleaned by field desorption and field evaporation at 300 ^{o}K by applying a high positive potential to the tip, with the screen and the cylinder on earth potential. We always started at 2.5 kV and increased this value with steps of 0.1 kV. After each voltage increment the possible effect was checked by reversing the polarity. When electron emission commenced, the evaporation process was carefully continued and checked by visual observation of the electron image. The voltage required to give a constant emission current (0.5 μA) normally first dropped, the surface getting cleaner, and then rose again when actual field evaporation took place and the radius of curvature increased. At this stage the process was stopped and the tip degassed by heating to about 1000 ^{o}K for some thirty minutes. After this heat treatment which had no measurable influence on the radius of the tip, field evaporation was resumed until again a clean field-evaporated surface was obtained. In most cases a final field evaporation was carried out at temperatures equal to

or below 77 ^{o}K. Ion images of the surfaces so prepared invariably showed a perfect atomic order. Accordingly, we omitted imaging of the clean surface whenever this was inconvenient.

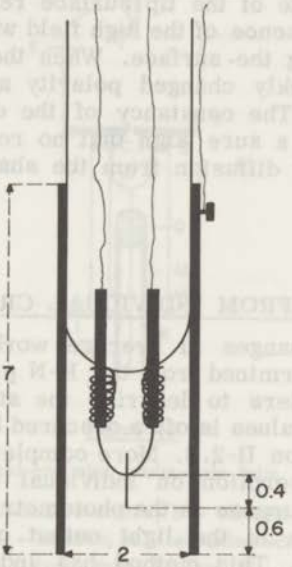

Figure 19

Tip assembly;
dimensions are in cm

In adsorption experiments the requisite amount of gas was dosed onto the metal tip by manipulating valves A_4, A_5 and A_6, respectively, the ball-joint shutter and valve A_7. Clearly the microscope tube shown in Fig. 18 is equally well suited for field-emission studies as long as we are interested in average values derived from the F-N plot (see section II-2.3.) for the total surface. In fact, a given state of adsorption was characterized by a comparison of the F-N data, i.e. the average work function $\bar{\varphi}$ and the pre-exponential factor A of eq. (19) for the clean and the covered surface. F-N plots of covered surfaces were taken after reduction of the pressure to about $5 \cdot 10^{-9}$ Torr.

Before helium was introduced into the microscope tube, valve A_7 was closed and the required image voltage applied to the tip to prevent any contaminant in the helium from being adsorbed. The ion pictures were taken at a helium pressure of about $2 \cdot 10^{-3}$ Torr (for details of the photographic procedures see Appendix 3). After imaging the main part of the helium was removed via the fore-line by opening valves A_1 and A_2. When a pressure of

10^{-5} Torr was reached (in about five minutes) valve A_2 was closed. Then valve A_7 was opened and the ion pump quickly restored a vacuum of less than 10^{-9} Torr.

In those experiments where the electron emission was to be measured after taking an ion picture, we kept the tip at the high voltage required for image formation when pumping off the helium. Under these conditions the adsorption state of the tip surface remains unaltered, adsorption being prevented by the presence of the high field which ionizes all the reactive gas molecules approaching the surface. When the pressure was again in the 10^{-9} Torr range we quickly changed polarity and determined the electron-emission characteristic. The constancy of the emission current at a given voltage was found to be a sure sign that no readsorption took place either from the gas phase or by diffusion from the shanks of the tip.

III-3. FIELD EMISSION FROM INDIVIDUAL CRYSTAL FACES

Although the changes in average work function and in the pre-exponential factor as determined from the F-N plot for the total surface can still be used as parameters to describe the state of adsorption, the exact meaning of the measured values is often obscured by the averaging procedure, as was pointed out in section II-2.3. More complete and significant information is obtained when the adsorption on individual crystal faces is studied. An obvious method for this purpose is the photometric measurement of the local adsorption-induced change in the light output of the fluorescent screen at constant emission voltage. This method has indeed been used[2,3], but must be regarded as unreliable for two reasons. Firstly, as stated in section II-2.3., the interpretation of the experimental data requires the assumption that the pre-exponential factor A does not change upon adsorption. Secondly, scattering of secondary electrons and reflections take place in the screen and consequently the dark areas might become brighter than corresponds with the actual emission current in these areas.

A reliable method for measuring work functions and changes in work function is the determination of the F-N plots for individual crystal faces. To this end a small hole is made in the fluorescent screen and an electron collector placed behind. Two techniques are available to direct the emission current from the desired crystal face into the hole, viz. mechanical adjustment of the metal tip and magnetic deflection of the electron beam. These so-called "probe-hole" techniques, proposed by Müller[4] and Smirnov and Shuppe[5], respectively, have until recently[6,7] been applied only for the measurement of work functions of clean surfaces[8,9] and not in adsorption studies.

For our investigation we chose a modified version of Müller's technique and constructed a measuring tube which is shown schematically in Fig. 20. In the centre of the fluorescent screen (diameter 5.5 cm) is a conical hole (upper diameter 0.2 cm, lower diameter 0.4 cm), which serves as a diaphragm to the electrons emitted by the metal tip. A platinum wire sealed in the conductive coating and spot-welded to a tungsten rod provides for the external electric contact with the screen. The distance from tip to screen is about 4.5 cm.

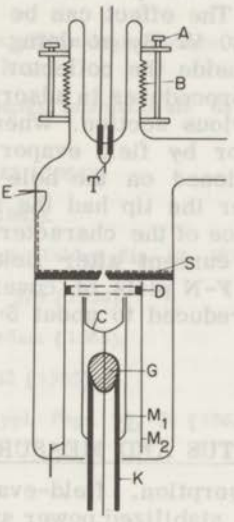

Figure 20

Field-emission probe-hole tube

S - fluorescent conductive screen; E - electric lead to screen; T - tip assembly; B - bellows; A - adjusting screw; C - collector; G - glass bead; K - Kovar tube; M_1 and M_2 - molybdenum foil cylinders; D - double grid

The tip assembly (see Appendix 2 and Fig. 19) is mounted on tungsten rods which are led through a cooling finger. The latter can be positioned by means of stainless steel bellows and adjusting screws, thus allowing the electron image of a selected single crystal face to be centred on the hole. The electrons of this specific face only are collected by a collector made of molybdenum foil and spot-welded to a Kovar rod. This rod is led through a glass bead sealing a Kovar tube to ensure the required high electrical insulation of the collector relative to earth (about 10^{14} ohm). The screen of the coaxial cable of the current-measuring circuit is directly connected to the Kovar tube and a molybdenum foil cylinder which shields the collector from stray fields. A double metal grid inserted in another molybdenum cylinder serves as a second shield. The grids, 0.3 cm apart and with meshes of 0.01 cm^2, are made of tungsten wire (diameter 0.004 cm) wound on a tantalum ring. In experiments employing field-desorption and field-evaporation techniques a stainless steel cylinder enclosed the cooling finger, just as in the ion microscope.

For measuring the small emission currents from single faces with the probe-hole technique it is preferable to keep the fluorescent screen and the cylinder on the high positive potential and the tip on a low negative potential (-70 V) relative to the collector being on earth potential. This mini-

mizes the risk of collecting secondary electrons which might be released from the cylinder or the screen. The effect can be further minimized by keeping the double grid on about -20 V. By so doing we also prevented secondary electrons which originated inside the collector from escaping.

The experimental procedures in adsorption experiments were similar to those described in the previous section. When a clean surface was obtained either by thermal heating or by field evaporation the image of the crystal face to be studied was positioned on the hole by manipulating the adjusting screws. To establish whether the tip had the field-evaporated end form, we used as criteria the appearance of the characteristic pattern of such a tip and the decrease in probe-hole current after field evaporation at successively higher voltages. Normally, F-N plots of covered surfaces were taken after the gas pressure had been reduced to about $5 \cdot 10^{-9}$ Torr.

III-4. ELECTRIC APPARATUS AND MEASUREMENTS

For the field-desorption, field-evaporation and ion-microscope experiments a 0-50 kV d.c. stabilized power supply was available. By means of a voltage divider the applied voltage could be regulated continuously over three ranges: 0-10, 0-20 and 0-50 kV, respectively. Measurement of the potential drop over a small portion of the resistance separating the output terminal of the voltage divider from earth made it possible to determine the applied voltages with an accuracy of about 1%.

An ultra-high-stability 0-5 kV d.c. power supply (drift less than 0.005%/hour; regulation 0.001%) was used in the electron-emission experiments. The output voltage (either negative or positive) could be regulated in steps of 10 V, while a fine regulation provided for intermediate values. The calibration accuracy of the dial setting was checked and found to be better than 0.2%. For this reason no separate voltage measurements were carried out during experiments, the sum of the dial settings being taken as the output voltage.

Stabilized low-voltage supplies were used for all other necessary voltages.

Emission currents from the total surface as well as the probe-hole currents were measured with vibrating-reed electrometers, and the outputs of the latter displayed on a recorder. The accuracy of the current measurements was estimated at about 2%. The emission current was recorded by stepwise varying the voltage over a range of about 10% above the minimum applied voltage. The probe-hole currents were invariably kept in the range 10^{-10} - 10^{-14} A, while the F-N plots for the total surface as measured with the ion microscope tube were determined in the range 10^{-8} - 10^{-7} A.

The experimental data were processed on a computer to calculate slopes and values of log A of the F-N plots. The accuracy of the results, although differing slightly in the various experiments, was normally better than 0.4% for the derived work functions and better than 1% for the values of log A. For the average work function of the clean tungsten surface we assumed a value of 4.50 eV for both thermally cleaned and field-evaporated tips[9].

REFERENCES

1. R.W. Roberts and Th.A. Vanderslice, "Ultra-high Vacuum and its Applications", Prentice-Hall Inc., Englewood Cliffs, N.Y. (1963).

2. J.A. Becker, Actes du 2-ième Congrès Internationale de Catalyse, Editions Technip, Paris (1961), Part 2, p. 1777.

3. T. Oguri, J. Phys. Soc. Japan 19, 83 (1964).

4. E.W. Müller, Z. Physik 120, 261 (1943).

5. B.G. Smirnov and G.N. Shuppe, Zhur. Tekhn. Fiz. 22, 973 (1952).

6. A.A. Holscher, J. Chem. Phys. 41, 579 (1964).

7. A.G.J. van Oostrom, Thesis, Amsterdam (1965).

8. E.W. Müller, J. Appl. Phys. 26, 732 (1955).

9. R.D. Young and E.W. Müller, J. Appl. Phys. 33, 91 (1962).

CHAPTER IV

RESULTS FOR CARBON MONOXIDE AND NITROGEN ON TUNGSTEN

IV-1. INTRODUCTION

In this Chapter results are presented of studies into the adsorption of carbon monoxide and nitrogen on tungsten with the field-emission and field-ionization techniques described in Chapter II and III. Although the systems in question have been extensively investigated before with a variety of experimental techniques, they are still imperfectly understood, and the nitrogen-tungsten system has even given rise to controversial results. In addition to the adsorption on clean tungsten, we carried out some experiments on the adsorption of carbon monoxide on tungsten precovered with hydrogen. Mixed adsorption systems of this type seem particularly interesting as their understanding is the first step to that of more complicated catalytic systems.

The experimental findings are first discussed separately for each of the systems investigated and compared with previous work by other authors; a brief introductory survey of this work precedes the presentation of the results. Then follows a more general discussion of those aspects which the systems have in common. Attention is paid to the possibilities provided by the experimental techniques applied in this work as well as to their limitations.

As observations made with the field-ion microscope are purely visual, the conclusions are based on a comparison of photographs of ion images. In the reproduction of these photographs, however, we had to restrict ourselves to those necessary for illustrating the most important points only.

IV-2. CARBON MONOXIDE ON TUNGSTEN

Studies with flash-filament desorption, field-emission microscope and electron-impact desorption techniques have shown that in the adsorption of carbon monoxide on tungsten at least three different adsorption "states" can be distinguished, differing in bond strength, bond dipole moment and electron desorption cross-section. A comprehensive survey of this work is given in articles by Swanson and Gomer[1], Gomer[2] and Ehrlich[3,4]. Briefly, the most important aspects are the following.

At low temperature mainly a weakly bonded "virgin" state with a negative surface potential (increase of the work function) is formed. Heating such a virgin layer to 300 ^{o}K and above leads to partial desorption and the formation of a more tightly bound β-state with a negative surface potential and a low electron desorption cross-section. Readsorption does not restore the virgin layer but leads to a state with a positive surface potential, relatively low bond strength and a high electron desorption cross-section. Formation of this α-state is only possible when the β-state is present.

The irreversible conversion of the virgin layer into a β-layer is understood as a rebonding of the adsorbed species. This rebonding has been regarded as taking place in the adsorbate layer only, either by a change in the type of bonding or by a more favourable filling of adsorption sites[1]. As carbon monoxide on tungsten becomes mobile only at about 600 °K, the observed effects cannot be due to a redistribution by surface diffusion over large distances.

The possibility of a rearrangement of the tungsten atoms in the surface layer accompanying the rebonding has not so far been taken into account. We have investigated this point in some detail by studying the adsorption on ideally ordered surfaces, using the ion microscope in combination with field-emission data.

A pronounced specificity of the various crystal faces of tungsten towards carbon-monoxide adsorption seems to be absent. This might be concluded from the field-emission patterns which indicate little change in emission anisotropy upon adsorption. In accordance herewith the average change in work function as determined from field emission agrees very well with values determined with other techniques. For this reason the probe-hole technique has not been applied to the carbon monoxide-tungsten system.

IV-2.1. Field-emission microscopy

Carbon monoxide was adsorbed on tungsten at 300 °K and 77 °K. The results obtained at saturated surfaces are summarized in the following scheme. The data are averages of several experiments.

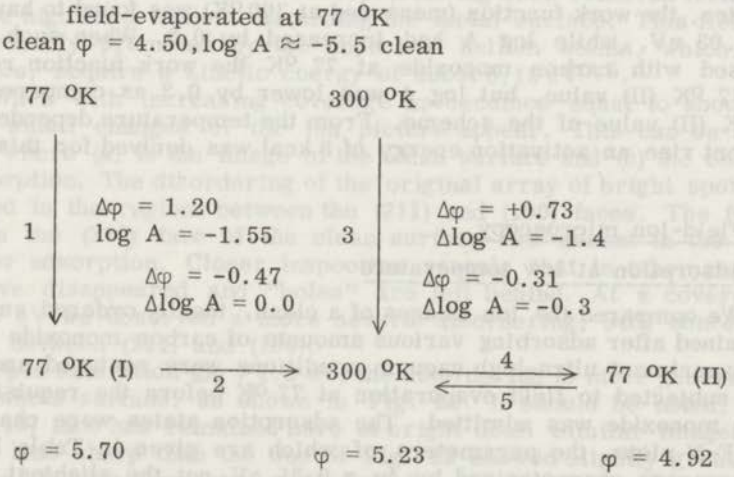

where $\Delta \log A = \log A_{final} - \log A_{initial}$

and $\Delta\varphi = \varphi_{final} - \varphi_{initial}$ (eV).

Some of these results need commenting on.

(i) The adsorption state* at 77 °K depends on the way it is obtained. Direct adsorption at 77 °K (step 1) leads to a large increase in φ, while adsorption at 300 °K and subsequent saturation at 77 °K (steps 3 and 4) give a much smaller increase in φ. The same result can be obtained by temporary heating of the 77 °K (I) state to 300 °K (steps 2 and 4). Obviously, the attainment of the stable 77 °K (II) state involves an activated process, which has the effect of decreasing φ. Step 4 was found to be completely reversible (step 5).

(ii) The work function and electron pattern for the 300 °K state are the same, no matter whether this state is reached directly (step 3) or via the 77 °K (I) state (steps 1 and 2). This also holds for the stable 77 °K (II) state, which can be obtained via the 300 °K state.
Although there is a slight difference in the drop in log A for the two routes, it seems that previous adsorption at lower temperatures has not much influence on the 300 °K state.

(iii) Adsorption, whether at 300 °K or at 77 °K, causes a large decrease in the pre-exponential factor A. In contrast to this, relatively small, if any, changes in A occur upon heating of the 77 °K (I) state to 300 °K and redosing at 77 °K.
Although the 300 °K state is independent of the way it was reached, it is not quite a true equilibrium. We observed that the emission current at 300 °K rose slowly with time, even in the absence of gaseous carbon monoxide. No current rise was noticed at 77 °K. The rise could be accelerated by temporarily heating the tip to 330 °K. After heating for five minutes, the work function (measured at 300 °K) was found to have dropped by 0.03 eV, while log A had increased by 0.3. When such a tip was redosed with carbon monoxide at 77 °K the work function returned to the 77 °K (II) value, but log A was lower by 0.3 as compared with the 77 °K (II) value of the scheme. From the temperature dependence of the current rise an activation energy of 8 kcal was derived for this process.

IV-2.2. Field-ion microscopy

(a) Adsorption at low temperature

We compared the ion images of a clean, ideally ordered surface with those obtained after adsorbing various amounts of carbon monoxide at 77 °K. In each experiment ultra-high vacuum conditions were restored and the surface was subjected to field evaporation at 77 °K before the requisite amount of carbon monoxide was admitted. The adsorption states were characterized by their F-N plots, the parameters of which are given in Table I. Up to a surface coverage characterized by $\Delta\varphi = 0.35$ eV not the slightest difference was observed between ion images taken before and after adsorption of carbon monoxide. To be sure that the procedure of imaging the clean surface before

---

* The word "state" is used here to describe the adsorption situation as a whole, in contrast with its use in a more specified sense, e.g. the α-state, where it denotes one particular type of the various adsorbed species.

Table I

Fowler-Nordheim data and observed changes in ion images after adsorption of increasing amounts of carbon monoxide at 77 °K on a field-evaporated tungsten surface

φ, (eV)	$\Delta \log A = \log A_{covered} - \log A_{clean}$	Change in ion image compared with image of clean surface
4.59	-0.40	no change at all
4.61	-0.24	" " " "
4.85	-0.43	" " " "
5.03	-0.55	very slight disordering between (211) and (100) see Fig. 21
5.15	-1.27	increased disordering, also around (111)
5.70	-1.52	generally spread disordering see Fig. 22

adsorption took place did not influence the results, we also carried out experiments in which an ion image was made after adsorption only. The images so obtained never differed from those taken directly from clean surfaces. Evidently, under these conditions the adsorbed carbon monoxide molecules are not observed in the ion microscope, having been removed from the surface by the high field without disturbing the metal surface. This field desorption is probably promoted by the impact of helium atoms, which, owing to polarization, acquire a kinetic energy of about 0.15 eV[5,6].

When with increasing coverage $\Delta\varphi$ becomes equal to about 0.5 eV, the first small changes of the ion picture appear. This can be seen from Fig. 21, where (a) is the image of the clean surface and (b) the one obtained after adsorption. The disordering of the original array of bright spots is most pronounced in the regions between the (211) and (100) faces. The four atoms visible on the (310) face of the clean surface are absent in the ion image taken after adsorption. Closer inspection reveals that in other regions also atoms have disappeared and "holes" are left behind. At a coverage where $\Delta\varphi$ = 0.65 eV we observed a more severe disordering, still concentrated in the areas between (211) and (100).

Upon saturation ($\Delta\varphi$ = 1.2 eV) the disordering is more generally spread over the whole surface, as shown in Fig. 22. It should be noted, however, that the (110) face has remained bare of bright dots. Similar images obtained from tips less sharp than the one of Fig. 22 showed slightly greater effects of disorder, but the symmetry of the tungsten pattern always remained clearly recognizable.

How are these changes to be interpreted? The new dots obviously do not represent carbon monoxide molecules on an otherwise undisturbed surface as there is no reason why such molecules would not have shown up at lower

coverage. On the contrary, one expects in this case field desorption to proceed more easily at high coverage than at low coverage, because the heat of adsorption decreases with increasing coverage. We therefore propose to identify the changes with a disordering of the tungsten surface itself. The following model can then be set up to fit the experimental observations. With increasing coverage, metal atoms move out of their original lattice sites into more favourable positions where they are more completely surrounded by adsorbed carbon monoxide molecules. Imaging of such a rearranged surface in the ion microscope will result in a complete or partial field desorption of the adsorbed complexes (including both carbon monoxide molecules as such and tungsten-carbon monoxide complexes), leaving behind the remnants of a disordered surface structure.

That the rearrangement and hence the observed changes depend on the degree of coverage and on the atomic structure of the adsorbing surface can be understood for two reasons. First, it is reasonable that the rearranged structure is thermodynamically more stable only above a certain minimum coverage. Secondly, rearrangement of surface atoms will be an activated process. It is conceivable that the activation energy decreases with increasing coverage owing to the weakening of the intermetallic bonds upon formation of the chemisorption bonds[7]. Moreover, it is to be expected that the activation energy required for rearrangement is different for the various crystal faces and smallest for the atomically rough areas, as e.g. (411) and (611). These are, in fact, the regions where the first changes are observed. A further verification of this interpretation is provided by experiments reported under (b) and (c) below.

(b) Adsorption at room temperature

Fig. 23 shows a surface which had been saturated at 300 ^{o}K ($\Delta\varphi \approx 0.73$ eV, $\Delta \log A \approx -1.4$). Now the symmetric pattern of the clean surface (not shown) is completely replaced by a random array of dots all over the surface. The disorder is far greater than that observed after (direct) adsorption at 77 ^{o}K (Fig. 22). Note that after adsorption at 300 ^{o}K bright dots are also present on the (110) face. A similar pattern is obtained after adsorption at 77 ^{o}K followed by heating to 300 ^{o}K and redosing at 77 ^{o}K ($\Delta\varphi = 0.42$ eV, $\Delta \log A = -1.7$). These experiments prove that the disordering as observed in the ion picture of Fig. 23 involves an irreversible activated process. This is exactly what can be expected when metal atoms participating in a chemisorption layer have to rearrange in order to attain a more stable configuration. The occurrence of an activated process in going from the low-temperature state 77 ^{o}K (I) to the 300 ^{o}K state was already inferred from field-emission experiments alone. The ion-microscope studies have now revealed the nature of this process.

Dosing experiments similar to those reported under (a) showed that the disorder increased with increasing coverage. Although a completely unchanged pattern was never obtained after adsorption at 300 ^{o}K, the changes at low coverage were small. A somewhat greater disordering, but still much less than at saturation, is shown in Fig. 24, representing a surface for which after adsorption at 300 ^{o}K $\Delta\varphi = 0.39$ eV and $\Delta \log A = -0.52$.

It is important to note that a remarkable correlation has been found between the degree of disorder and the changes in φ and log A. To illustrate this, we may compare the final state of Fig. 24 with that of an experiment where the tungsten tip was dosed at 77 °K with about an equal amount of carbon monoxide, which at this temperature causes little or no rearrangement. The tip was then warmed to about 280 °K for two minutes and an F-N plot recorded. The characteristic parameters were $\Delta\varphi = 0.51$ eV and $\Delta \log A = -0.42$, relative to the clean surface. The ion image taken after cooling to 77 °K (Fig. 25) revealed only small changes. Evidently the rate of rearrangement on a partially covered surface is still fairly low at 280 °K. From the F-N data and the ion images obtained in these experiments it follows that the more pronounced disorder of Fig. 24 is accompanied by a larger decrease in log A, while the work function is smaller. These results suggest that at a given coverage rearrangement causes a lowering of both the work function and log A.

(c) Field desorption and evaporation of surface layers

The results presented in sections (a) and (b), above, suggest that under the conditions of image formation the greater part of the adsorbed carbon monoxide is removed from the surface by field desorption. To investigate this point in more detail and to clarify the nature of the surface layers left behind, we took ion pictures of successively advanced stages of field desorption and field evaporation after saturated carbon-monoxide adsorption at 300 °K. After taking an ion picture we reversed the polarity of the metal tip and recorded an F-N plot. Table II summarizes the experimental data and conditions. The corresponding ion images of a representative part of the surface are shown in Fig. 26; the imaging conditions were invariably the same. All $\Delta\varphi$ and $\Delta \log A$ values are referred to the clean surface after field evaporation at 77 °K in the presence of helium. The choice of this reference might be responsible for the relatively low work-function increment after carbon-monoxide adsorption.

Examination of the F-N data and ion pictures reveals many remarkable facts. In the successive stages of field desorption the work function passes first through a minimum value of 4.5 eV and then through a maximum. We will discuss the significance and cause of this alternation later on.

Clearly, the mere application of the required image voltage of 7.8 kV suffices to remove a major part of the chemisorbed layer, and the field desorption effect is markedly enhanced by the presence of helium. After field desorption at 8.4 kV the surface is to be regarded as clean, because from this stage on the values of φ and log A are no longer significantly different from those of the initially clean surface.

Looking at the ion images, we see that Fig. 26(b) represents the characteristic disordered pattern obtained after adsorption at 300 °K. Relatively small changes have occurred after field desorption at 8.2 kV (picture (c)). Field desorption at 8.4 kV (picture (d)) involves more pronounced changes, particularly well visible in the (111) region. Although according to the F-N data the surface is now completely clean, the arrangement of bright spots, showing marked differences in intensity, is still disordered. We also observe relatively large dark areas which are not imaged at all, in contrast with the same areas in photograph (a) of the clean surface. An interesting phenomenon

Table II

Experimental data of field desorption and field evaporation of surface layers after saturated adsorption of carbon monoxide on a field-evaporated tungsten surface at 300 °K; images at 77 °K and 7.8 kV in Fig. 26

Picture No.	φ, (eV)	$\Delta \log A = \log A_{covered} - \log A_{clean}$	Treatment before taking F-N plot and/or picture
26(a)	4.50	0	field-evap. at 8.8 kV, 77 °K with He
	4.95	-1.52	CO adsorption at 300 °K
	4.50	-0.66	tip 5' at 7.8 kV without He
(b)	4.61	0.17	after taking (b)
(c)	4.62	0.21	tip 1' at 8.2 kV with He
(d)	4.53	-0.03	tip 1' at 8.4 kV " "
(e)	4.56	0.09	tip 1' at 8.6 kV " "
(f)	-	-	tip 1' at 8.7 kV " "
(g)	4.51	0.00	tip 1' at 8.8 kV " "
(h)	-	-	tip 1' at 8.9 kV " "
(i)	4.55	0.07	tip 1' at 9.0 kV " "

can be noted by comparing (d) with (b). The latter photograph shows in some regions a slight fuzziness, absent from (d). As the experimental conditions for all photographs were the same, the observed effect is significant; it may originate from small amounts of chemisorbed carbon monoxide, which in view of the F-N data were still present on the surface of (b), but not on the surface of (d).

Photographs 26(e), (f), (g), (h) and (i) show the effect of field evaporation brought about by applying successively higher voltages: surface atom layers are torn off, the disorder gradually decreases and atoms "fill up" the dark areas. At last, after about four layers have been removed, a completely ordered surface is exposed again. The number of layers torn off can be determined most easily by comparing the structure around the (211) and (111) faces on the various photographs. As appears from the last three pictures, bright dots arrange themselves gradually along the [100] zone line. This zone "decoration" is typical of clean field-evaporated tungsten surfaces (see section II-3.2.).

That the removal of surface layers is possible below the voltage initially required to give the field-evaporated end state shown in Fig. 26(a) can be explained as follows. When metal atoms move out of their original lattice positions during the formation of the chemisorption layer, they leave vacancies behind. By diffusion processes these vacancies will partially pene-

trate into deeper-lying atom layers until an equilibrium is established. As a consequence, the surface which becomes exposed after the chemisorption "crust" has been field-desorbed will show a "hill-and-valley" structure on an atomic scale, the valleys being either single vacancies or vacancy clusters. An ion image of such a surface will only reveal atoms on the hills, because above the valleys the ionization probability for the helium atoms will be comparatively small. Field desorption proceeds more easily, i.e. at a lower applied voltage, from such a disordered structure than from a completely smooth surface. The attack will commence at the protruding atoms and edges where the field strength is highest and continue until the increase in the (local) radius of curvature causes the field strength to drop below the value required for evaporation (see section II-3.2.). At consecutively higher voltages the whole process is repeated. Eventually atom layers become exposed which have not more vacancies than are normally observed and the surface is again ideally ordered.

The conclusion that most of the carbon monoxide is removed upon imaging of a saturated surface receives additional support from a comparison of the electron patterns of clean, covered and ion-imaged surfaces as shown in Fig. 27(a), (b) and (d), respectively. The pattern of the covered surface exhibits a marked graininess and the voltage required for 0.5 μA emission has greatly increased. But after imaging the surface (Fig. 27(c)) this emission voltage drops again to almost the same value as for the initially clean surface.

Particular interest attaches to the enhanced emission from several small regions, e.g. the one on the (110) face. The corresponding region in the ion image is marked by bright dots. This correspondence strongly suggests that the bright dots represent tungsten atoms and not carbon monoxide molecules, since the latter would have lowered the electron emission.

The evidence obtained leads us to the following conclusions:

(i) The disorder observed in the ion images taken after carbon-monoxide adsorption cannot be attributed solely to adsorbed carbon-monoxide molecules. The disorder persists even after the carbon monoxide has been removed from the surface and should therefore be associated with disturbances in the initially perfect arrangement of the metal atoms.

(ii) There is evidence that such chemisorbed carbon-monoxide molecules as do escape field desorption during image formation at 77 ^{o}K lower the image contrast instead of showing up as bright spots.

(iii) The adsorption-induced rearrangement of metal atoms strongly influences more deeply lying atom layers by causing vacancies in these layers.

These conclusions and those obtained from the experiments discussed in section (b) seem to confirm the correctness of the interpretation put forward above to explain the phenomena observed in both the electron and the ion microscope after adsorption of carbon monoxide on field-evaporated tungsten surfaces.

IV-2.3. Discussion

(a) Adsorption model

In the foregoing section we gave a description of the adsorption of carbon monoxide on tungsten which satisfactorily explained the results of both ion-microscope and field-emission experiments. It implied a rearrangement of surface metal atoms, which was shown to depend on coverage and which, being an activated process, was far more pronounced at 300 °K than at 77 °K. Some complementary details, including a discussion of the changes in φ and log A, are here appropriate to arrive at a rounded picture.

Adsorption at 77 °K up to a fairly high coverage leads to a chemisorption layer uniformly spread over the surface, with no rearrangement of substrate atoms. The dipole moments of the surface bonds have their negative end pointing outwards, which results in a high work-function increment. For such a chemisorption not affecting the structure of the substrate we propose the name "chemi-adsorption".

Upon formation of the chemisorption bonds the intermetallic bonds are weakened, so that eventually a restricted surface rearrangement can take place, particularly on the less densely packed crystal faces. The rearrangement causes a tighter bonding of some of the adsorbed carbon-monoxide molecules by embedding them in a two-dimensional tungsten carbonyl structure. New adsorption sites are thus created, which we can visualize as being located on top of tungsten atoms having penetrated through the adsorbed carbon-monoxide layer. The additional carbon-monoxide molecules adsorbed on these sites are less strongly bonded than those in the carbonyl layer, as the carbon-monoxide molecules in this layer interact with more than one tungsten atom. Upon saturation at low temperature an additional very weakly bonded layer can be formed on top of the chemisorbed layer.

In assessing the effect of the complex adsorption process upon the work function, we may conceive any rearrangement in the chemisorbed layer to have the effect of decreasing the effective dipole moment vector perpendicular to the surface by introducing components which point with the negative pole parallel to the surface or even inwards. However, as mentioned before, the rearrangement at 77 °K is very limited only. Therefore, the work function will be decreased only slightly as compared with the hypothetical case when no rearrangement takes place. The physisorbed layer most probably lowers the work function.

Heating the 77 °K state to 300 °K causes drastic changes. First, the physisorbed layer is desorbed. If no other processes took place the work function would increase. In actual fact, however, we observe a considerable drop in work function of about 0.5 eV, which can now, because of the ion-microscope results, be correlated with a greatly increased rearrangement in the surface layer. The degree of this rearrangement and the ultimate surface structure will probably be different for the various crystal faces. In some areas changes are presumably such as to justify the term "surface corrosion", i.e. carbon-monoxide molecules are now completely incorporated in the surface structure.

By analogy with what is observed in the formation of oxide layers, we assume that the corrosion layer is mainly formed by metal atoms diffusing outwards. Such a supposition is strongly sustained by the field-evapora-

tion experiments which prove the existence of vacancies underneath the chemisorption layer. As carbon-monoxide molecules in this layer will be held more strongly than those at the surface, different states become distinguishable with respect to the energy required for desorption. Moreover, the states become discernible with respect to the surface potentials, as rearrangements change the component normal to the surface of the bond dipoles.

It can now be understood that after peeling off one or more surface layers, the work function drops to the value of the clean surface, although there is still some carbon monoxide present. This can broadly be explained by visualizing that the surface now contains tungsten atoms with carbon-monoxide molecules underneath. Further field desorption reverses the situation again, and the result is an increase in work function.

Upon redosing the tip at 77 °K, a weakly bonded adsorption layer is formed on top of the corroded surface, which is accompanied by a further decrease in work function.

The critical coverage where rearrangement sets in is much lower at 300 °K than at 77 °K. This result proves that the critical coverage is determined by the prerequisite that metal-metal bonds must be sufficiently weakened by chemisorption such that the activation energy required for rearrangement becomes sufficiently low.

Adsorption, whether at 77 °K or at 300 °K, greatly decreases the pre-exponential factor A of the Fowler-Nordheim relation. Such a decrease has also been found with other adsorption systems; it is certainly not simply caused by a reduction of the emitting surface[8]. Two other explanations have been put forward in the literature, both accounting for the large decrease in log A at low temperature. In the first model, adopted by Menzel and Gomer[9] for carbon monoxide on tungsten, the high electrostatic field polarizes the ad-layer, inducing an extra work function increment which, being proportional to the field strength, to a first approximation does not alter the slope of the F-N plot, but decreases log A. In the second model proposed by Van Oostrom[10] for nitrogen on tungsten the physisorbed layer modifies the image potential such that the resulting barrier for the electrons becomes larger.

Both models may serve to understand the change in log A observed after adsorption of carbon monoxide at low temperature, but are inadequate to explain the decrease of log A at higher temperatures where no physisorbed layer is present. As was pointed out in section IV-2.2.(b), the present results strongly suggest that in that case the decrease in log A is related to the formation of the corrosive chemisorption layer.

An explanation readily follows if one bears in mind that the corrosive chemisorption "demetallizes" the outer surface layers of the metal, so that in fact a dielectric film is formed on the metal surface. This layer not only modifies the potential barrier in vacuo, like the physisorbed layer does in Van Oostrom's model, but probably reduces the transmission of electrons even further by confronting them with an additional barrier.

Apart from decreasing the transmission probability for the electrons, the adsorption may also influence their supply to the barrier. The disordered layer and the induced vacancies can be expected greatly to disturb the periodic potential at the surface. Such disturbances in the periodic potential in the metal are known to increase the resistance of the metal by scattering the

conduction electrons[11,12]. It therefore seems likely that a similar scattering mechanism in the disordered surface layers reduces the number of electrons arriving at the potential barrier, i.e. the supply function (see eq. (4)). This has the same effect as a decrease in emitting area or log A.

In this picture the slow rise in emission current following carbon monoxide adsorption at 300 °K, which rise has an apparent activation energy of about 8 kcal as stated in section IV-2.1., might tentatively be ascribed to an ordering of either the corrosion layer or the disturbed tungsten layers beneath it. This resembles the defect annealing in clean tungsten films requiring a comparable activation energy[13].

A small increase in log A has been observed after field desorption of most of the adsorbate (Table II). Most probably this is due to an increase in emitting surface area, as may be concluded from a comparison of Fig. 27(a) and (b).

A weakly bonded layer on top of a corroded chemisorbed layer, formed at low temperature, gives rise to a relatively small change in log A. In terms of Gomer's model this seems to indicate that carbon-monoxide molecules in such a layer are less polarized by the field than those on top of a chemi-adsorption layer.

Our conception of the different types of adsorption and the specific changes in φ and log A they induce is summarized in the following scheme.

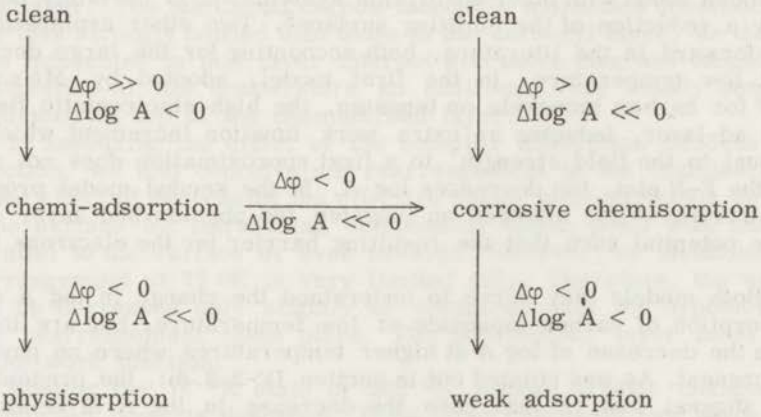

(b) Comparison with previous work

Our experimental results, although obtained on field-evaporated tungsten tips, are in fair agreement with those of Gomer[1,2,14] et al. on tips cleaned by heating, if we identify virgin layers, β-states and α-states of their terminology with what we have called the chemi-adsorption layer, carbon-monoxide molecules incorporated in corrosive chemisorption layers, and the molecules more weakly adsorbed on sites created on top of the corroded layers.

The value of $\Delta\varphi$ for the 77 °K (I) state is about 0.3 eV higher than the one reported by Gomer, while no significant differences are observed for

the 300 °K state and the state obtained after redosing at low temperature. This is in accordance with the model proposed here. At low temperatures where little or no rearrangement of metal atoms takes place, the difference in surface roughness between a thermally cleaned surface and a field-evaporated surface will persist and this, as explained before, will result in a smaller $\Delta\varphi$ for the rougher surface. At higher temperatures, however, the initial differences will be less important, since the original surface structure is drastically changed.

To explain the conversion of a virgin layer into a β-layer, Swanson and Gomer[1] propose "a flipping of a carbon-monoxide molecule into a more tightly bound configuration locally". However, it seems unlikely that the potential barrier between the unstable and stable sites (in this model about 2 Å apart) is so high that a molecule hitting the surface on an unstable site would be unable to immediately "flip over", although being initially in a highly activated state. Moreover, Gomer[2] has found that in the latter stages of the adsorption at low temperature the work function passes through a maximum, suggesting that the terminal section of the adsorption layer consists of the initial portion of the β-layer. This finding is not in agreement with the simple model of an undisturbed surface, for there is no reason why the low-energy binding sites should be occupied earlier and to far greater extent than the high-energy binding sites. However, this is exactly what will happen when the latter sites are not a priori available but are created by surface rearrangement at high coverage.

From their electron-impact desorption experiments Menzel and Gomer[15] concluded that a thermal conversion of virgin states into β- and α-states (the latter occur in their and in our model only together with the former) starts at about 270 °K, in fair agreement with our findings. A careful examination of other results derived with the electron-impact technique reveals that most conclusions fit in with the model here proposed.

The new picture is at variance with some of the conclusions of Ehrlich[16,17], who interpreted the disorderly arranged bright spots in the 20 °K ion images after adsorption of carbon monoxide as individual molecules being unaffected by the severe conditions of ion-image formation. He concluded that the tungsten surface itself had been changed only negligibly. However, he has not reported electron-emission data before and after imaging the surface, thus leaving open the question to what extent the carbon monoxide was field-desorbed. To our way of thinking his experiments do not provide convincing evidence that the bright dots indeed represent carbon-monoxide molecules. In fact, Ehrlich runs into serious difficulties in trying to explain the phenomena on the (110) face. He has observed that this plane fills up later than its surroundings after adsorption at 300 °K. At higher concentrations the "adsorbed" material, which then appears, is stable even at 700 °K. To explain this, Ehrlich proposed a decomposition of the α-state by electron bombardment during image formation. The α-state is thought to be converted into carbon which then shows up as bright atoms. This view is, however, open to some serious objections. Firstly, it is required that the α-state resists field desorption despite its very low bond strength. Secondly, in order to achieve a conversion an appreciable number of electrons must be produced by field ionization above the (110) face. As the (110) face does not show up in the ion image of clean tungsten, this requirement is equivalent to the ad hoc postulate that

α- and β-carbon monoxide, although invisible, drastically increase the ionization. But even if these conditions were fulfilled, the objection remains that the electrons have no or hardly any energy in excess to the Fermi energy which is required to bring about a conversion. Furthermore, as Menzel and Gomer[15] have shown the ratio of dissociation to desorption of the α-state by electron impact is very low ($\approx$ 0.1).

For these reasons we feel that the "retarded" filling up of the close-packed crystal faces at higher concentrations under conditions of high sticking coefficient and very low mobility of the adsorbate favours the surface-rearrangement picture.

Moreover, Ehrlich's interpretation of bright dots in the ion images as chemisorbed molecules is not only in conflict with conclusions (i) and (ii) we arrived at in section IV-2.2.(c), but also difficult to reconcile with theoretical considerations with regard to the theory of image formation of chemisorbed metalloids. This point will be discussed in Chapter V.

IV-3. CARBON MONOXIDE ON TUNGSTEN PRECOVERED WITH HYDROGEN

After saturation with hydrogen both at 77 °K and 300 °K on a field-evaporated tungsten tip the ion image obtained was the same as that of the clean surface. Obviously, hydrogen does not induce any rearrangement of tungsten atoms. When, however, a hydrogen-covered tip was exposed to 10^{-6} Torr for about five minutes both at 77 and 300 °K we obtained the same type of pattern as was found for carbon-monoxide adsorption on clean tungsten at these respective temperatures. Apparently carbon monoxide can displace adsorbed hydrogen, and subsequently induces a rearrangement of tungsten atoms. The field-emission results are summarized in the following scheme:

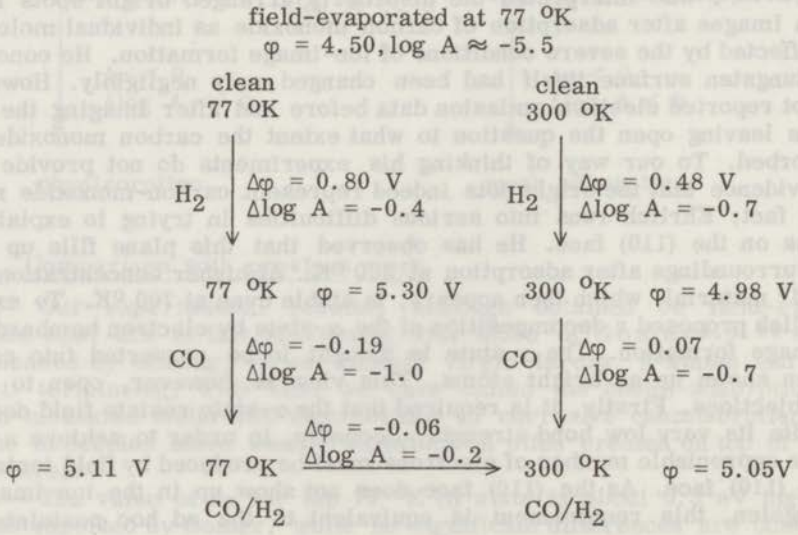

At 77 °K carbon-monoxide adsorption lowers the work function of a hydrogen-covered tip. This can be understood by assuming that carbon monoxide is mainly present in a physisorbed layer, while the major part of the strongly bonded chemi-adsorbed hydrogen layer is not removed. In complete agreement with this assumption is the large drop in log A, characteristic of a more highly polarizable layer.

Upon heating to 300 °K the work function and log A further decrease. Presumably, the greater part of the hydrogen is now replaced by carbon monoxide and a corrosive chemisorption layer is formed. The same state can be achieved by direct carbon-monoxide adsorption at 300 °K on a precovered hydrogen tip.

The displacement of hydrogen by carbon monoxide is accompanied by a relatively small increase in work function and a large decrease in log A, this being again in agreement with the conversion of a chemi-adsorbed hydrogen layer into a carbonylic corrosion layer. The 300 °K state of the mixed adsorption is characterized by having a slightly lower work function than the pure carbon-monoxide adsorption state has at 300 °K. This is most probably due to residual hydrogen in the corrosion layer.

After adsorption at 300 °K or heating of the 77 °K state to 300 °K the same steady increase in current was observed as after adsorption of carbon monoxide on clean tungsten. After intermediate heating to 330 °K, the work function had again changed little ($\Delta\varphi = -0.03$ V), but log A had increased markedly ($\Delta \log A = 0.35$). The activation energy of the process was found to be about 12 kcal/mole.

Hydrogen admitted to a tip which was precovered with carbon monoxide and temporarily heated to 330 °K caused no further change in work function and log A. However, when intermediate heating to 330 °K was omitted, a decrease in both work function (-0.3 eV) and log A (-0.3) was observed. Heating to 330 °K restored the original values of φ and log A characteristic of the pure carbon-monoxide chemisorption layer. This behaviour suggests that in the chemisorption layer saturated at 300 °K with respect to carbon monoxide there are still sites available for hydrogen adsorption. Heating to 330 °K then removes these sites, probably again because of an increased order in the surface layers.

IV-4. NITROGEN ON TUNGSTEN

The nitrogen-tungsten system has been the subject of many studies which primarily made use of flash-filament techniques, the field-emission and field-ion microscope and contact-potential methods. Recently, isotopic mixing experiments have also been reported. Substantial efforts have been made in particular by Ehrlich, whose articles present an extensive survey[3,4,17,18].

The nitrogen-tungsten system resembles the carbon-monoxide-tungsten system in several respects, e.g. in that it exhibits a composite adsorption layer in which at least three different states can be distinguished. Further, as will be shown, similar irreversible effects are observed when the low-temperature adsorption state is heated to room temperature, signifying that

rearrangements of surface metal atoms might take place also in this system.

The phenomena observed, however, turn out to be still more complicated, probably because nitrogen can be adsorbed in either undissociative, predissociative or dissociative forms.

The intricacy of the nitrogen-tungsten system is reflected by, among other things, the values reported for the change in work function after adsorption at room temperature, which range from -0.2 to +0.5 eV for various authors. They were all determined for surfaces on which various crystal faces were exposed, and consequently the experimental values are weighted averages of the contributions of these crystal faces. It has therefore been suggested that the divergence in the results is caused by differences in surface structure.

Results obtained by different methods and with different specimens may in general only be expected to agree if the local surface potentials on individual crystal faces are equal. If they are not, the overall result will depend on the crystallographic nature of the surface and on the manner of averaging inherent in the method of measurement. To explain the discrepancies mentioned it is therefore essential to know the surface potentials of nitrogen on the individual faces of tungsten. As outlined in section III-3. the probe-hole technique is excellently suited for this purpose. We applied it to the adsorption of nitrogen on thermally cleaned as well as on perfectly ordered crystal faces, the latter obtained by field evaporation of the tip. In some experiments we also studied the field desorption of the adsorbate.

Our experimental findings are arranged and discussed in the order of the most disputed points, viz. (i) the possible occurrence of metal-atom rearrangements; (ii) the "visibility" of adsorbed nitrogen in the field-ion microscope; (iii) the crystallographic specificity, particularly the adsorption on the (110) face, and (iv) the simultaneous presence of differently bonded species of adsorbed nitrogen. In presenting the evidence we have taken advantage of the results reported for the carbon-monoxide-tungsten system, so as to avoid a repetition of the detailed arguments concerning the ion-microscope experiments.

IV-4.1. Rearrangement of surface metal atoms

(a) Adsorption at room temperature

Ion images taken at 20 °K after saturated adsorption of nitrogen at 300 °K invariably showed a pattern of disorderly arranged bright dots, the original symmetric structure being hardly, if at all, recognizable. A typical image is given in Fig. 28.

As for the adsorption of carbon monoxide, again the disordered structure cannot simply be attributed to the presence of adsorbed atoms or molecules on a metal surface whose structure has remained unchanged. This was proved by experiments completely analogous to those described in section IV-2.2.(c). After adsorption the surface was subjected to stepwise field evaporation, while the change in electron emission provided information about the degree of nitrogen coverage. The results are illustrated by the series of ion images in Fig. 29, taken under the same conditions of temperature and applied field after adsorption at 300 °K, following preadsorption at 20 °K. Table III summarizes the corresponding F-N data and the conditions of field evaporation.

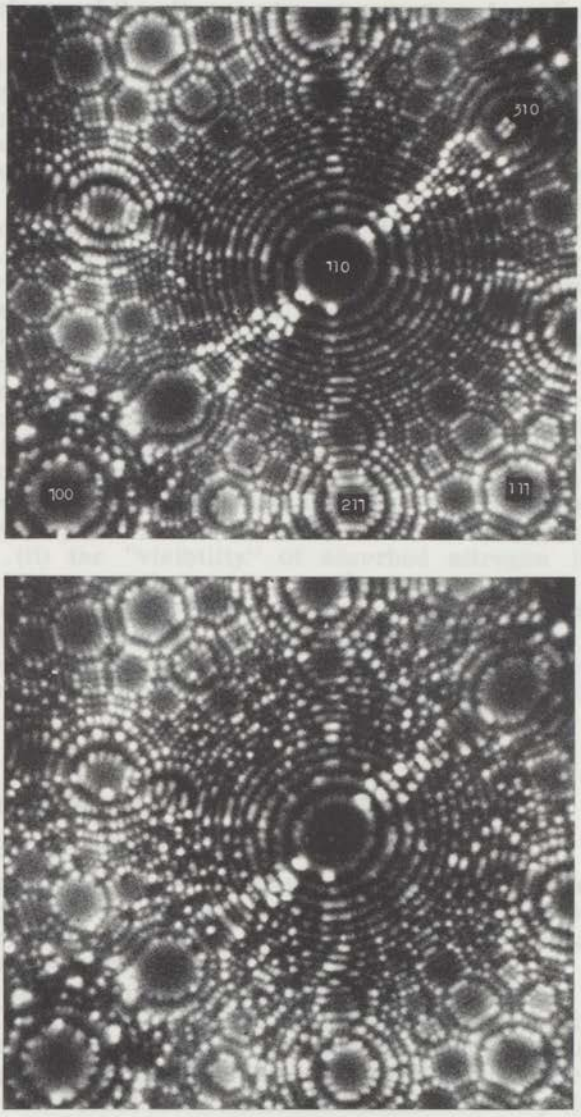

Figure 21

(a) Clean tungsten surface, field-evaporated at 9.6 kV; image at 77 °K and 8.05 kV. (b) Same surface after adsorption of carbon monoxide at 77 °K, partial coverage; image at 77 °K and 8.05 kV

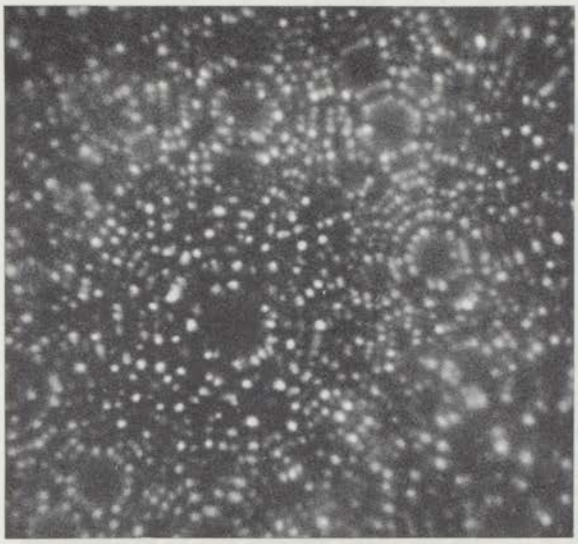

Figure 22

Tungsten surface after saturated adsorption of carbon monoxide at 77 ^{o}K; image at 77 ^{o}K and 7.2 kV

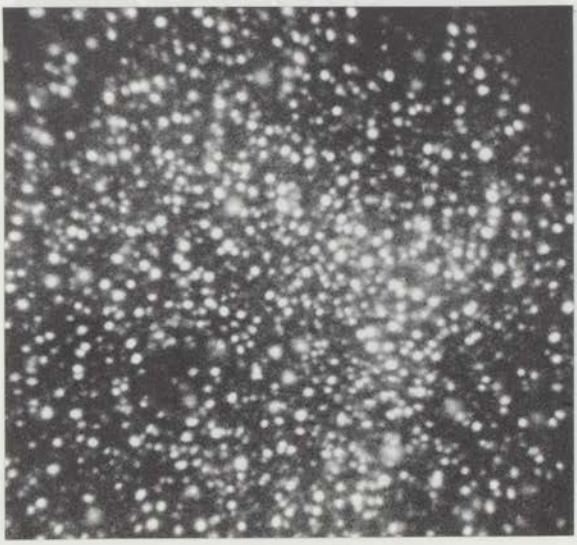

Figure 23

Tungsten surface after saturated adsorption of carbon monoxide at 300 ^{o}K; image at 77 ^{o}K and 9.6 kV

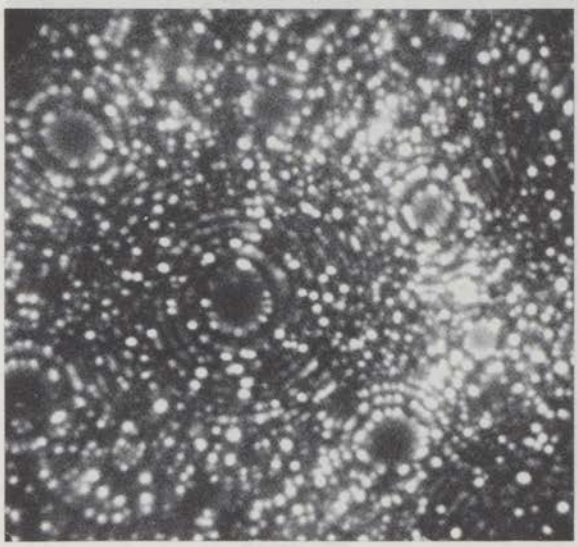

Figure 24

Tungsten surface after adsorption of carbon monoxide at 300 °K, partial coverage; image at 77 °K and 9.2 kV

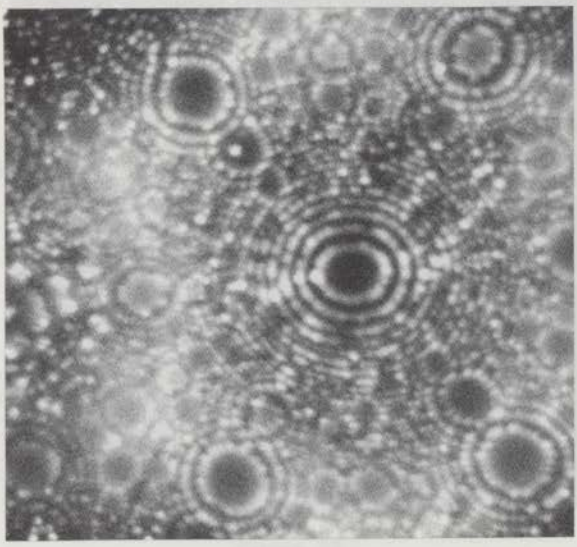

Figure 25

Tungsten surface after adsorption of carbon monoxide at 77 °K, partial coverage, followed by heating to 280 °K for 2 min; image at 77 °K and 9.7 kV

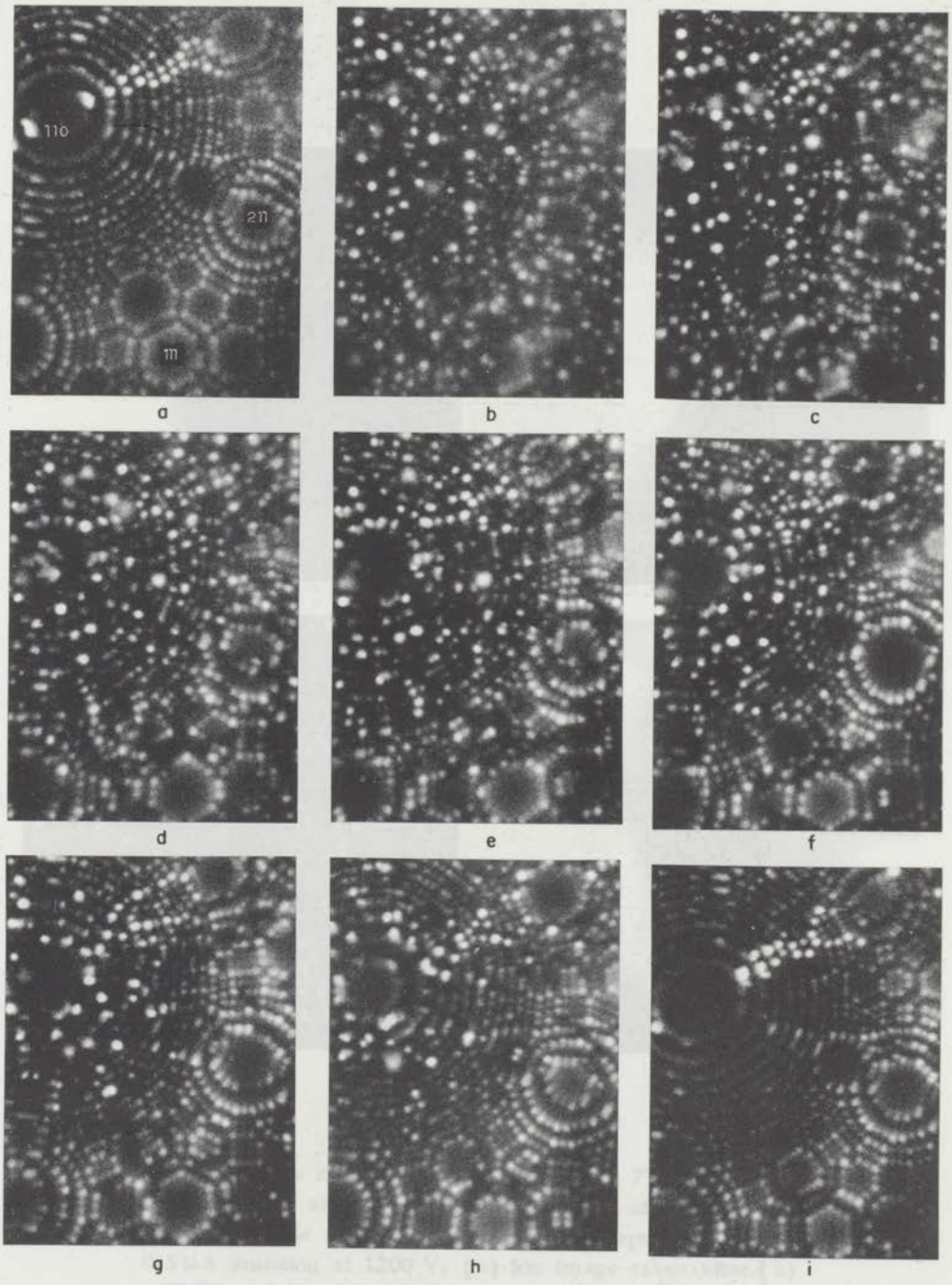

Figure 26

Field desorption and field evaporation of surface layers after saturated adsorption of carbon monoxide on tungsten at 300 ^{o}K; for experimental data and conditions see Table II

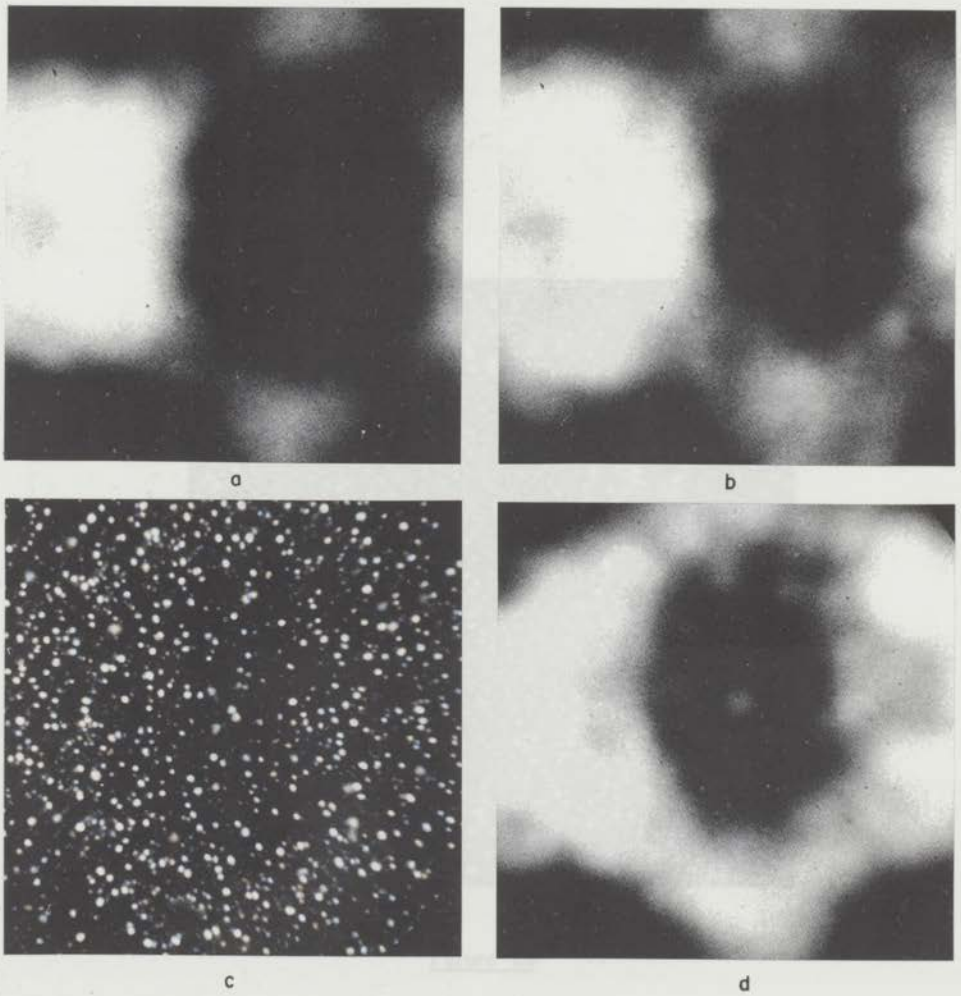

Figure 27

(a) Clean tungsten surface, field evaporated at 77 °K and 11.6 kV; 0.5 μA emission at 840 V. (b) Same surface after adsorption of carbon monoxide at 77 °K following preadsorption at 300 °K; 0.5 μA emission at 1200 V. (c) Ion image taken after (b) at 77 °K and 9.1 kV. (d) Electron pattern after image (c); 0.5 μA emission at 870 V

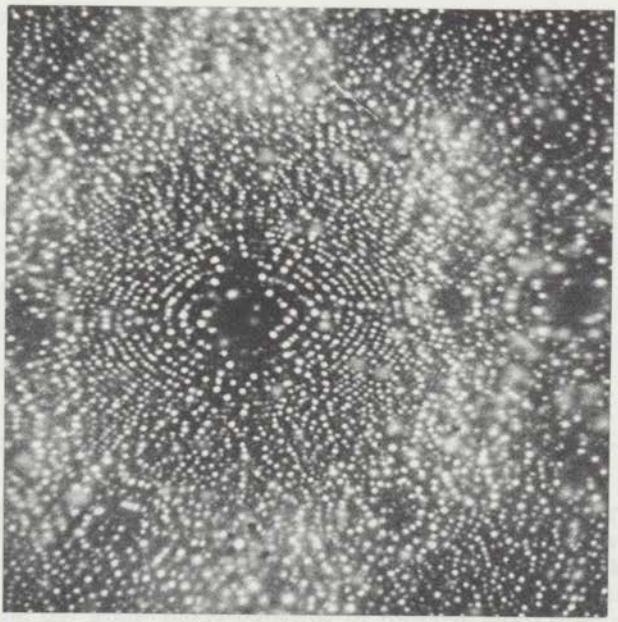

Figure 28

Tungsten surface after saturated adsorption of nitrogen at 300 ^{o}K; image at 20 ^{o}K and 12.0 kV

Table III

Experimental data of field desorption and field evaporation of surface layers after saturated adsorption of nitrogen on a field-evaporated tungsten surface at 300 °K, following adsorption at 20 °K; images at 20 °K and 7.8 kV in Fig. 29

Picture No.	φ, (eV)	$\Delta \log A = \log A_{covered} - \log A_{clean}$	Treatment before taking F-N plot and/or picture
29(a)	4.50	0	field-evap. at 9.2 kV, 20 °K with He
	4.97	-1.01	nitrogen adsorption at 300 °K after preadsorption at 20 °K
	4.90	-0.78	tip 1' at 7.8 kV without He
(b)	4.61	0.02	after taking (b)
(c)	4.61	0.06	tip 1' at 8.2 kV with He
(d)	4.54	-0.02	tip 1' at 8.7 kV " "
(e)	4.50	-0.08	tip 1' at 9.0 kV " "
(f)	4.43	-0.25	tip 1' at 9.1 kV " "
(g)	4.49	-0.12	tip 1' at 9.2 kV " "
(h)	4.51	-0.06	tip 1' at 9.3 kV " "
(i)	4.50	-0.10	tip 1' at 9.4 kV " "

It is seen that mere application of the voltage required for image formation removes only part of the nitrogen but the presence of helium greatly enhances the field desorption of the adsorbate, so that the first image after adsorption shows a surface which is substantially denuded of nitrogen. From the state corresponding to picture 29(d) onwards the values for φ and log A remain approximately constant, so that it seems reasonable to conclude that all nitrogen has been removed from the surface. But the disorder, particularly in the (111) areas, persists until about four atom layers have been peeled off.

If the bright dots in the pictures represented adsorbed nitrogen atoms on an undisturbed surface, as has been proposed by Ehrlich and Hudda[19], the removal of the adsorbate layer would have been sufficient to restore the original surface order, similarly to the behaviour observed for the adsorption of hydrogen on tungsten (see section IV-3.). Even if allowance is made for a possible corrosion of the surface caused by the field desorption of tungsten-nitrogen complexes, an ideally ordered surface should have been exposed after the removal of one metal atom layer, since the field cannot penetrate into the metal beyond this outer surface layer. The experimental results therefore prove that the observed disorder is associated with tungsten atoms and must be mainly caused by the process of chemisorption.

(b) Adsorption at low temperature

When adsorption was carried out at 77 and 20 °K, it was found that, up to a certain coverage, the ion images taken at 20 °K did not differ from those of clean surfaces. This result indicates that at these temperatures no rearrangements take place at low coverage and that upon imaging the nitrogen is removed from the surface. Sometimes some tungsten atoms were removed together with the nitrogen. However, this desorption-induced corrosion was never observed to be so severe that the ion image lost its appearance of an undisturbed surface.

An accurate determination of the degree of coverage was not possible in these experiments. The nitrogen was dosed on the clean tip by letting a certain quantity of the gas expand from the vacuum system before the ball-joint valve into the microscope tube, while only the tip Dewar was filled (to a low level) with either liquid nitrogen or hydrogen. The initial pressures varied from 10^{-7} to 10^{-6} Torr, whereas the final pressures after reaching equilibrium were of the order of $5 \cdot 10^{-9}$ Torr; the adsorption time was about five minutes. Despite the probably still fairly large coverages obtained by this procedure the overall change in both φ and log A after adsorption was rather small. Initially even a rise in log A occurred, in agreement with the data reported by Ehrlich and Hudda[20].

When the coverage was increased we obtained disordered patterns which were completely comparable with those observed after carbon-monoxide adsorption. Initially the (110) and (211) faces remained unaffected, dots appearing only at a coverage close to saturation. This finding is again at variance with the interpretation of "new" bright dots as nitrogen atoms. If the latter should be true, dots would also be randomly distributed at low coverage, since the mobility of nitrogen at 77 °K is much too small to allow a migration of atoms from the (110) and (211) faces to those crystal faces which can provide a more stable bonding.

At full coverage results at low temperature were not as clear-cut as those at room temperature.

In most experiments the disorder in the ion images taken after about five minutes' adsorption at about $5 \cdot 10^{-6}$ Torr followed by pumping was comparable to that observed after adsorption at 300 °K. The penetration depth was also approximately the same. (Perhaps the disorder found after adsorption at 20 °K was even somewhat larger, but at the same time more superficial; this impression could not be substantiated.)

In some other experiments, however, carried out under apparently the same conditions, the atomic arrangement was far less disturbed at 20 °K than at room temperature; notably the (111) faces in these cases were hardly affected by the adsorption. Although the cause of this lack of reproducibility has not yet been established unambiguously, it seems to be related to the initial rate of adsorption, in fact the only experimental condition not easily reproduced in the adsorption procedure. Support for this hypothesis comes from the experiment illustrated by Fig. 30, which shows the surface regions around the (111) and (211) faces. Fig. 30(a) gives the image after adsorption at 77 °K according to the dosing procedure outlined above, but in this case with a preset pressure of 10^{-5} Torr and an adsorption time of about seven minutes. The pressure after the attainment of equilibrium was in the 10^{-8} Torr range. These circumstances indicate that the surface must have been nearly,

if not completely, saturated, as is also borne out by the field-emission measurements, which gave $\Delta\varphi = 0.15$ eV and $\Delta \log A = -1.0$.

The disorder was most pronounced in the region between the (211) and (100) faces (a small part of this region can be seen in the upper left of Fig. 30). However, the general appearance is far less disordered than after saturated adsorption at 300 °K.

The following explanation is tentatively proposed:
Nitrogen can be adsorbed on the surface sites in two modes, a molecular and atomic one, respectively. Now, if it is assumed that a molecular species is a precursor of atomic nitrogen and that the former requires less space than two adsorbed atoms (e.g. one and two sites per molecule, respectively), then the ratio of the rate of adsorption to the rate of conversion of molecular into atomic nitrogen determines the relative amounts of the two types of adsorbed species. A high adsorption rate at low temperature will lead to crowding of molecular nitrogen, leaving no room for dissociative adsorption. In this case little surface rearrangement will occur, since at low temperature it probably requires a fairly large concentration of strongly bonded nitrogen. Atom rearrangements can only take place after partial desorption of the molecular species at higher temperatures.

The above picture is clearly rather simplified, for it does not take into account the existence of a priori different sites. However, this does not seem to be a serious drawback. The issue is how the average lifetime of an adsorbed molecule relative to dissociation compares with the time required for gas-phase molecules to occupy all neighbouring sites of potential use to the molecular species in dissociative adsorption. For example, if it is assumed that in the foregoing experiment these times were about equal and in the order of seconds, an activation energy for dissociative adsorption of 4-5 kcal/mole is calculated.

The present experiment also provides additional information about the nature of the bright dots, since their small number permitted a more detailed study of their removal by field evaporation. Pictures (b) to (f) show the effect of applying for one minute voltages* above the best-image voltage of 10.25 kV ($p = 0.788$) at which all pictures were taken. These voltages were $p = 0.885$, 0.905, 0.923, 0.942 and 0.961, respectively.

First we note that after removing one atom layer (compare (d) with (e)) the order around the (111) face is restored, while after peeling off one more layer (compare (e) with (f)) the other regions also show almost complete order again. The penetration depth of the disorder is evidently very small in this case. It is further interesting to note that the field evaporation in the presence of helium at 20 °K takes place at a voltage which is about 4% smaller than that required for field evaporation in vacuo at 77 °K.

In the sequence of pictures from (a) to (d) only minor changes occur of which two have been marked with arrows. On the right-hand side a bright dot present in (a) has disappeared in (b), leaving a "hole". A similar phenomenon is observed at the bottom right in pictures (b) and (c). In view of foregoing results and those presented in the following section these observations are interpreted as the removal of tungsten atoms which upon adsorption were displaced from their original lattice positions into somewhat more protruding

---

* In order to facilitate a comparison of the applied voltages in these and following experiments, they are characterized by a parameter, p, which gives the ratio to the voltage required for field evaporation in vacuo at 77 °K.

ones. This interpretation would account for the higher intensity of their images and for the fact that they disappear at a voltage which is about 6% smaller than that required to evaporate a complete and nearly perfect surface layer. We much prefer this explanation to one that supposes that the bright dots represent nitrogen atoms which are field-desorbed together with underlying tungsten atoms[21].

IV-4.2. The "visibility" of adsorbed nitrogen

The results obtained in the foregoing section give rise to some questions concerning the possibility of detecting adsorbed nitrogen in the ion microscope. Firstly, it was shown that after nitrogen adsorption at low temperature and up to a certain coverage the helium-ion images made at best-image voltage did not differ from those of clean faces. In these cases the adsorbed nitrogen clearly escapes observation, undoubtedly because it is field-desorbed from the surface. It might now be asked whether the presence of nitrogen will become apparent in one way or another if images are made at a voltage below best-image voltage where a lower rate of field desorption can be expected. Secondly, it followed from field-emission data that after imaging of saturated surfaces some of the initially adsorbed nitrogen remained at the surface. Here the obvious question arises in which form the adsorbate shows up in the disordered images.

An answer to these questions seems of prime importance, not only for the nitrogen-tungsten system but for any adsorption study carried out with the ion microscope. The matter is also of general interest for an understanding of the mechanism of image formation.

Previously Ehrlich and Hudda[19] have put forward the view that adsorbed nitrogen atoms (and also other adsorbates such as carbon monoxide) appear as bright dots indistinguishable from the images of the substrate atoms in a static photograph. Their identification as adsorbed entities is then primarily based on their mobility which is said to exceed that of tungsten atoms (the applicability of the criterion used will be discussed in section IV-4.3.(c)). It seems difficult to reconcile this interpretation of the ion images after adsorption with our results. The discrepancy was already noted before with respect to the adsorption of carbon monoxide on tungsten, but exists equally for the nitrogen-tungsten system.

In an attempt to shed some light on this controversial matter, we examined the changes in the images with the applied voltage hoping that such experiments could supply more information about the field-desorption process and the effect of adsorbed nitrogen on the image formation. Images were made at increasing applied voltage, from a value far below best-image voltage up to a value slightly above it; subsequently, the same series was taken at decreasing voltage so that we obtained pairs of images taken at the same conditions, one from the ascending series and the other from the descending series.

In the coverage range at 77 and 20 °K where the ion images at best-image voltage did not show any disorder, no difference was observed between the "ascending" and "descending" images, even if imaging was started at a voltage as low as $p = 0.5$. Apparently the nitrogen was already removed when the first image was taken.

More conclusive and interesting results were obtained in experiments on saturated surfaces. An examination of the corresponding ion images near best-image voltage, such as are shown in Fig. 28, reveals, besides the large disorder, a diffusiveness in the patterns similar to that observed after carbon-monoxide adsorption. Since such a loss in contrast is never found when clean surfaces are imaged under comparable conditions, it seems logical to attribute it to the presence of adsorbate. This idea is confirmed by the experiment illustrated in Fig. 31(a) and 31(b). Fig. 31(a) shows a tungsten surface after adsorption at 77 °K, followed by heating to 300 °K and readsorption at 77 °K. The image was taken at 20 °K and 21.1 kV ($p = 0.742$), which is somewhat below the best-image voltage for the clean surface ($p \approx 0.79$). A number of more or less isolated diffuse areas lie scattered all over the surface, but are particularly in evidence on and around the (110) face. Fig. 31(b) represents the same surface at identical conditions but after the surface had been imaged at voltages up to 14.1 kV ($p = 0.865$). A drastic change has taken place in that all diffuse spots have now disappeared completely. The conclusion appears inescapable that this striking effect is due to the completion of the desorption of the adsorbate at the highest applied voltage. The disorder still persists, however.

Having established the relation between the diffuse areas and locally adsorbed nitrogen, we must determine whether the latter enhances or lowers the ionization rate above the covered sites. Again this particular point can be clarified by comparing images, viz. those taken at much lower voltage ($p = 0.466$). These images, forming part of the same series as Fig. 31(a) and 31(b), are shown in Fig. 32(a) and 32(b), respectively. Fig. 32(a) exhibits a very remarkable pattern, consisting of triplets all aligned in the same direction and each composed of one most intense dot flanked by two far less intense images. At increasing image voltage the structures are seen to change and eventually disappear irreversibly. This also follows from a comparison of Fig. 32(a) with 32(b). Although these images suggest some kind of order in the chemisorption layer, a definite explanation requires much more research than has so far been carried out. For the present purpose, however, the most important thing to note is the increase in overall intensity after the surface has been imaged at 14.1 kV. Surface areas which were completely non-"emitting" in (a) are imaged in (b), for instance the (100) region, while the (111) areas in (d) also contain much more intense image points than those in picture (a). As the increase of the voltage between pictures (a) and (b) causes desorption of the nitrogen, it must be concluded that the adsorbate lowers the ionization rate.

The present view seems consistent with theoretical considerations about the mechanism of image formation of a covered surface. This subject will be treated in detail in Chapter V, where we will also discuss more fully the changes of the images in the voltage range below best-image voltage, providing further support to the conclusion derived above.

Let us now consider the diffuse spots in more detail. Fig. 33(a) and (b) give typical examples of the changes brought about by a slight increase in applied voltage above best-image voltage. In this case the area depicted is the (110) face and the lattice steps surrounding it, and the images were taken after saturated adsorption at 20 °K. However, many similar effects have been observed in other crystal areas as well as after adsorption under different conditions.

The phenomena on the left-hand side of the (110) face are very illustrative. In picture (a) (p = 0.799) this region contains three diffuse spots (in the encircled area), located roughly between the second and the third lattice step from the centre. In picture (b) (p = 0.826) two spots have disappeared and the atoms belonging to the third lattice step have now become clearly visible. It is difficult to estimate the change in overall intensity in the area in question, but the centres of maximum intensity have distinctly shifted to the left, with an attendant marked increase in contrast.

Most likely these image changes must be attributed to desorption of small protruding "chemisorption clusters" into which the nitrogen is more or less incorporated, making strong bonds with the surrounding tungsten atoms. Nitrogen in a more exposed position would probably have been removed at an earlier stage. The protruding position of these clusters explains why they show a relatively large intensity, despite the presence of nitrogen. The diffusiveness probably stems from a diminished contrast in the potential situation near the surface (see section V-6.). Upon desorption of the chemisorption complex neighbouring atoms may become more prominently exposed; this would account for the shift in the intensity.

Similar changes are observed below the (110) face. On the atom row indicated with an arrow the intensity and contrast have markedly increased in picture 33(b). The same holds for the site indicated above the (110) face. In these cases it is less certain whether a desorption of nitrogen alone can be ruled out. So much is clear from these changes that removal of the nitrogen either as such or as a tungsten-nitrogen complex causes an increase in the ionization rate.

Summarizing the experimental findings, we arrive at the following statements:

(i) At best helium-ion image conditions (10^{-3} Torr He) previously adsorbed nitrogen may remain in small part on the tungsten surface. The bonding of this particular type of adsorbed nitrogen involves rearrangement of surface atoms.

(ii) Nitrogen atoms (or molecules) are not visible as distinct entities; they do not show up as bright image points.

(iii) The presence of nitrogen is marked by a decrease in image contrast and intensity, effects which enable us to trace the location of nitrogen-tungsten chemisorption complexes.

IV-4.3. Adsorption on single faces

(a) Adsorption at room temperature

The ion-microscope investigations showed that after nitrogen adsorption at about 300 °K surface rearrangement takes place in all regions, with a possible exception for the (110) face. Conclusions as to a specific behaviour of the various crystal faces, however, are less easily drawn, although the field-desorption and evaporation experiments strongly suggest that the effect of nitrogen adsorption has the greatest penetration depth in the regions between the (211) and (100) faces. Very little can be said of what happens on the (100) face itself, because this face is normally poorly developed on field-evaporated surfaces and presents a disordered structure also when still clean.

Electron-emission experiments, however, reveal a pronounced crystallographic specificity as regards the change in work function upon adsorption. Fig. 34 shows the emission pattern of a thermally annealed tungsten tip after adsorption of nitrogen at 300 °K. It is evident that the emission anisotropy has completely changed from that for the clean state. The emissivity is strongest for the (411), (310) and (111) regions on clean tungsten, but for the (100) region on the nitrogen-covered tip. For this reason the values of $\Delta\varphi$ and $\Delta \log A$ as determined from the total current do not really give the change in average work function and in pre-exponential factor; they only have some significance as parameters characterizing the overall adsorption state.

From probe-hole measurements, carried out after saturating the surface at about 300 °K and 10^{-6} Torr and pumping off the nitrogen, we derived the changes in work function for the individual faces, including the less strongly emitting ones (such as (110), (211) and (100) faces). The F-N data

Table IV

Changes in work function and in log A for thermally annealed and field-evaporated crystal faces of tungsten after saturated adsorption of nitrogen at 300 °K

Crystal face	φ clean, (eV)	Thermally cleaned surfaces 300 °K		Field-evaporated (77 °K) surfaces 300 °K	
		$\Delta\varphi$, (eV)	$\Delta \log A$	$\Delta\varphi$, (eV)	$\Delta \log A$
100	4.9	-0.5	-0.8	$\approx$ -0.15	$\approx$ -1.2
110	$\approx$ 6.0	0.05	-0.5	0.08	-0.9
111	4.40	0.30	-0.7	0.17	-0.9
211	4.90	0.43	-0.5	0.11	-1.6
311	4.50	0.26	-0.6	$\approx$ 0.15	-1.3
611	4.30	0.29	-	$\approx$ -0.1	-2.1
n11*	4.40	-0.14	-	-	-
310	4.35	0.39	-	-	-
total surface	4.50	-0.18	-0.8	0.3	-0.8

* Denotes area in the [110] zone imaged at the edge of the (100) face.

are assembled in Table IV (third column). The values for the work function of the clean faces were derived from a comparison of the F-N plots for the single faces with the plot for the total surface, assuming for the latter a

value of $\varphi = 4.50$ eV*.

A remarkable finding is that the local $\Delta\varphi$ values differ not only in magnitude but even in sign. This was also observed by Oguri[23] who used the method of measuring the light output of the screen. He found for the (610) face $\Delta\varphi = -0.2$, for the (210) face $\Delta\varphi = 0.5$ and for the (111) face $\Delta\varphi = 0.15$ eV.

The occurrence of both positive and negative changes in work function in dependence of surface structure makes it possible to understand the disagreement in the values reported for the overall change in work function. For example, values obtained by diode methods (Hill and Pethica[24]: 0.0 eV on a saturated tungsten ribbon, after an initial drop of -0.1 eV; Redhead[25]: 0.09 eV on a tungsten wire) apply to surfaces on which the faces of the [110] zone, including the (100) and (311) faces, are known to prevail. Since the changes in φ for these faces are of opposite sign, a slightly different face distribution on the samples may account for the difference in the overall values observed.

Although the results of other authors[10,18,26,27] confirm the observation that the change in work function has an opposite sign on different crystal faces, there remain discrepancies when the data are compared in more detail. One reason for this may well be a difference in surface structure, even though the data which are compared refer to faces indicated with the same Miller indices.

Ion images taken from flashed or thermally annealed tungsten tips show that on the surface the stable (211) and (110) faces are well developed whereas the other regions contain a large frozen-in disorder in the arrangement of the surface atoms. For the latter surface areas the designation with crystallographic indices becomes somewhat arbitrary, because one cannot at all be sure that a particular face, e.g. the (611) face, has indeed been developed. Moreover, on all less closely packed faces present, the configuration of the outer surface layers deviates widely from the ideally ordered structure which can be deduced from marble models. This holds not only for metal tips, but also for crystal faces obtained after cutting a single crystal in a known direction and subsequently cleaning it in vacuo (e.g. by electron bombardment). In the latter type of experiment stable low-index facets may be formed also on a face cut normal to a direction with higher indices.

The above arguments might explain why Van Oostrom[10] reported a $\Delta\varphi = -0.14$ eV for the (411) face, whereas we have found almost the same change for a surface region very close to the (100) face. The region to which we have given the indices (611), on the contrary, shows an increase in work function which is about equal to that for both Van Oostrom's and our (311) face. It seems very likely that the indefiniteness in the crystallographic structure is here indeed the cause of the differences.

Such an explanation, however, does not hold for the behaviour of the (110) face, for which both Ehrlich and Van Oostrom have reported that no adsorption takes place at room temperature, contrary to our results. This question merits a fuller discussion, for which see section IV-4.3.(c).

---

* The values for the (100) face reported previously by the present author[22] proved to be too high according to repeated experiments. The new values are also in better agreement with those reported by other authors.

The use of field-evaporated tips which expose almost ideally ordered surfaces allows a far better characterization of the initial surface structure. We have therefore also carried out probe-hole measurements with tips field-evaporated at 77 °K. The data referring to adsorption at 300 °K (after heating of the clean tip from 77 to 300 °K) and 10^{-6} Torr are listed in the fourth column of Table IV, where it is assumed that the clean faces have the same work functions as a thermally annealed tip has.

As could be expected from the change in the emission pattern after adsorption, which closely resembled that shown in Fig. 34, the data for field-evaporated tips follow much the same trend as those for thermally annealed tips. Still, there are some differences.

Firstly, the decrease in work functions on the (100) face is far smaller than for thermally annealed tips. This is probably due to the fact that on thermal tips the (100) face is much better developed, as can be concluded from the emission patterns. The (100) face on a field-evaporated tip never shows up as a well-defined dark area as it does on a thermal tip.

However, the data obtained for the (100) face and also for the surrounding regions (e.g. the (611) faces) showed a great spread, even in the F-N plots taken in one and the same experiment, although all conditions were maintained constant and the accuracy of the individual plots was good. For example, in one case a change in work function as low as -0.48 eV was measured for the (611) face. In general it was found that the larger the decrease in work function, the larger also the drop in log A, so that the emission current varied very little.

Cooling the tip and readsorption at 77 °K gave results which were quite reproducible, proving that the spread in results at room temperature was indeed due, not to experimental inaccuracies, but to changes in the adsorption layer. As all measurements were made after pumping off the gas, a slow desorption of a weakly bound molecular species cannot completely be excluded as a possible cause, but it seems unlikely, since no particular trend of the F-N data with time was observed. A more probable explanation therefore seems to be that there are species which can undergo a change in bond type at room temperature, but remain in a particular bonding mode when at low temperature the coverage increases. A definite explanation cannot be given yet, however.

We do not know whether other authors have observed similar effects, for in general little is said about the reproducibility of reported results. As will be outlined later it might also be possible that such structural fluctuations only become apparent with the probe-hole technique using very small tips (see section IV-5.1.). Van Oostrom[10] has mentioned an unexpected large increase in work function of the (321) face after exposing the surface to a large dose of nitrogen and has tentatively attributed it to impurities in the nitrogen. In our view, however, the effect of impurity adsorption has often been given too much weight in the explanation of conflicting results.

Secondly, it can be seen from Table IV that the apparent change in work function for the total field-evaporated surface is positive, although experimental conditions were not changed and nitrogen was used from the same storage flask as in experiments with the thermally annealed tips which led to a decrease in overall work function.

A further point of interest is the far greater decrease in the pre-exponential factor A in the case of field-evaporated tips. This can be understood if one assumes that, similarly to what was observed upon carbon-monoxide adsorption, the decrease in log A again originates at least in part from the disordering of the surface upon adsorption. Field-evaporated surfaces undergo a much greater loss in order than do thermally annealed surfaces which show a relatively large disorder even in the clean state. It should be noted here that the disorder of thermal surfaces extends to a depth of several layers, as was observed by following the gradual change from an annealed surface to an ideally ordered one upon field evaporation in the ion microscope.

It could be argued that for one and the same crystallographic direction, once metal-atom rearrangements occur, the structure of the chemisorption layer must be the same, irrespective of whether the surface was initially ordered (field-evaporated) or disordered (annealed). However, this uniformity of structure can only be expected when the mobility in the surface layer is large enough to allow the attainment of the equilibrium configuration. If this is not the case, and it probably will not be at the relatively low temperature of 300 ^{o}K, the initial differences in surface structure may well influence the ultimate structure, as they will determine the course of the rearrangements and the ease with which they take place.

(b) Adsorption at low temperature

The adsorption state at 77 ^{o}K showed a dependence on the way it was brought about somewhat similar to that observed in the low-temperature adsorption of carbon monoxide, but more complicated. For several crystal faces three different sets of F-N data were obtained depending on whether the adsorption at 77 ^{o}K took place (i) completely at 77 ^{o}K, (ii) after preadsorption at 300 ^{o}K, or (iii) after preadsorption at 77 ^{o}K and subsequently at 300 ^{o}K. The data presented in Table V relate to adsorption on field-evaporated crystal surfaces at a pressure of about 10^{-6} Torr.

The lowest work functions were obtained after preadsorption at 300 ^{o}K and the highest, though still below those after adsorption at 300 ^{o}K (except for the (211) face), after adsorption at 77 ^{o}K only. Preadsorption at low temperature resulted in intermediate values for the (211), (311), (611) and (100) faces, while it made little difference to the (110) and (111) faces. Differences were also found in the sets of values of Δlog A.

The occurrence of the third low-temperature state implies that the adsorption state at 300 ^{o}K also depends on whether or not preadsorption at low temperature has taken place. Such a phenomenon has been noted before by the present author[28] from a comparison of emission patterns and F-N data obtained for thermally annealed tips. The measurements at the individual faces of field-evaporated tips provide more detailed proof, as can be concluded from the data presented in Table VI. For the (611) face the preadsorption at 77 ^{o}K even reverses the sign of the change in work function, compared with direct adsorption at 300 ^{o}K (Table IV). In further contrast the data for this face now showed a very good reproducibility.

In agreement with the increase in all changes of local work function the average value for the total surface also proved higher when the surface had first been saturated at low temperature; preadsorption at 20 ^{o}K even gave rise to a work function increment at 300 ^{o}K of about 0.5 eV (see Table III).

Table V

Changes in work function and in log A for field-evaporated crystal faces of tungsten after saturated adsorption of nitrogen at 77 °K

second column: after adsorption at 77 °K only,
third column : following preadsorption at 300 °K,
fourth column : following preadsorption at 77 °K and heating to 300 °K

Crystal face	77 °K		300 °K → 77 °K		77 °K → 300 °K → 77 °K	
	Δφ, (eV)	Δ log A	Δφ, (eV)	Δ log A	Δφ, (eV)	Δ log A
100	-0.2	-2.4	-0.6	-2.7	-0.51	-2.2
110	0.02	-1.9	-0.23	-1.6	-0.25	-1.7
111	-0.18	-1.9	-0.05	-1.4	-0.03	-1.4
211	0.26	-1.5	-0.38	-2.5	0.13	-1.6
311	-0.24	-2.4	-0.45	-2.3	-0.28	-2.1
611	-0.30	-2.6	-0.53	-2.9	-0.43	-2.5

Table VI

Changes in work function and in log A for field-evaporated crystal faces of tungsten after saturated adsorption of nitrogen at 300 °K, following preadsorption at 77 °K

Crystal face	77 °K → 300 °K	
	Δφ, (eV)	Δ log A
100	≈0.0	-1.6
110	0.11	-1.1
111	0.18	-1.1
211	0.5	-1.0
311	0.18	-1.5
611	0.14	-1.7

The effect of preadsorption on the 300 °K state has also been observed by Delchar and Ehrlich[18], who reported a $\Delta\varphi = 0.03$ eV for the (100) face, while they obtained values ranging from -0.4 to -0.1 eV when adsorption only took place at 300 °K.

The ion images corresponding with the three low-temperature states discussed above all showed a large disorder. (No effect of the adsorption rate on the adsorption state at 77 °K was detected at the pressure (10^{-6} Torr) applied in the probe-hole experiments.) The various images were not markedly different and did not allow any definite conclusion as to whether the three states imply different arrangements of the substrate atoms. Most likely, however, this will be the case, at least for the states after a treatment at 300 °K compared with the one obtained after adsorption at 77 °K only. For, in the former case the mobility of the metal atoms will be greater, so that the surface can come closer to the equilibrium configuration.

Perhaps preadsorption at 77 °K has an effect on the 300 °K state, and consequently also on the state obtained after readsorption at 77 °K, similar to that which a high adsorption rate has on the course of the adsorption at low temperature. The surface might be partly "immobilized", the occupation of the sites hampering further rearrangements at 300 °K. The configuration so obtained can be visualized as being intermediate between the other two low-temperature states, which would be in agreement with the work function data of Table V.

Clearly these interpretations are rather speculative and need more experimental evidence to prove their validity.

(c) Adsorption on the (110) face

In so far as the results of foregoing sections can be compared with those obtained by other authors, they reasonably agree except, as was noted before, for the (110) face. We will therefore discuss the behaviour of this particular face in more detail. The point at issue is whether or not at room temperature and low pressures nitrogen is adsorbed on the (110) face of tungsten. The absence of such an adsorption had previously been reported by Van Oostrom[10] and Ehrlich and co-workers[18,19]; the former also applied the field-emission technique, while the latter authors derived their conclusions from contact-potential and flash-desorption experiments at single crystals and from a study with the ion microscope. On the other hand, Quinn and Roberts[29] have observed a negative surface potential ($\Delta\varphi = 0.12$ eV) at 300 °K on evaporated tungsten films, the surface of which they believed to be predominantly composed of the (110) face.

Our field-emission results (Table IV) show that the change in work function at 300 °K and about 10^{-9} Torr is rather small. This in itself is in fair agreement with Delchar and Ehrlich's[18] finding that $\Delta\varphi = 0$. They observed a (negative and reversible) change in work function only at pressures above 10^{-2} Torr. However, the change in log A in our experiments provides another parameter indicative of any adsorption taking place. Since this change is appreciable we must conclude that adsorption of nitrogen does occur.

Additional evidence is furnished by the possibility of obtaining two different low-temperature states also for the (110) face (Table V). For, if the sequence comprising exposure to nitrogen at 300 °K, pumping off, cooling to

77 °K and re-exposure to nitrogen at 77 °K results in a completely different state than does direct exposure to nitrogen at 77 °K, nitrogen must inevitably have been present at the surface at 300 °K, and in a different configuration than after adsorption at low temperature. Once the surface has been warmed to 300 °K adsorption at 77 °K gives a reversible change in work function of about -0.3 eV; the same value has been reported by Quinn and Roberts. Delchar and Ehrlich also studied the low-temperature adsorption and found at 110 °K a change in work function of -0.15 eV, but according to their results it makes no difference whether the surface has been exposed to nitrogen at 300 °K prior to the adsorption at 110 °K. From flash-desorption experiments it was concluded that adsorption took place in the form of atoms.

The reason for the discrepancy between various results is obscure. We have considered two possible causes: the adsorption of impurities and the special features of the probe-hole technique.

While the presence of impurities in the nitrogen can be ruled out in view of the purification, it might have been possible that upon pumping nitrogen with the sputter-ion pump other gases are released. However, experiments in which the nitrogen was cryo-pumped by using liquid hydrogen gave the same results. Besides, the adsorption of impurities would also have affected results for all other faces, for which no discrepant results are found.

The second possibility deserves more consideration. When the (110) face is not large compared with the area obtained by projection of the probe-hole back onto the tip surface, electrons having large tangential velocities originating from the edges of the (110) face could conceivably enter the probe-hole. If the latter current exceeds that of the flat portion of the face, the F-N data provide information about the edges only. We sometimes noted such an effect when the tip was field-evaporated by stepwise increasing the voltage. Normally the current from a single face then steadily decreases, but for the (110) face we often observed an alternation which evidently corresponded with the alternation of the apparent diameter of the (110) face, as can be seen in the ion microscope. We always took care to start any experiment in the situation where the current had a relative minimum.

Thermally annealed tips show a much larger (110) face, so that edge effects are not likely to interfere with results obtained with these tips. Besides the adsorption at room temperature (see Table IV), we therefore studied also the adsorption at low temperature on "thermal" (110) faces. Again the occurrence of two different low-temperature states was established ($\Delta\varphi$ = 0.13 eV, $\Delta \log A$ = -1.9 and $\Delta\varphi$ = -0.35 eV, $\Delta \log A$ = -1.8, respectively), proving that nitrogen is indeed adsorbed on the (110) face at 300 °K.

Let us now consider the evidence provided by experiments in the ion microscope. Particular interest attaches to it because it was such evidence that first led Ehrlich and Hudda[19] to the conclusion that nitrogen is bound (in the form of atoms) on the (110) face only at temperatures below 190 °K. The arguments were mainly based on the following observations: (i) when the surface was imaged after adsorption at 300 °K the (110) face remained bare, whereas adsorption at 145 °K and below gave rise to bright dots; (ii) when an imaged surface showing bright dots on the (110) face was warmed to 300 °K these dots disappeared.

For several reasons we do not agree with these interpretations. Firstly, as we have demonstrated in section IV-4.2., adsorbed nitrogen lowers the ionization probability, so that if a particular crystal region does not show

new "emission" centres after adsorption, it does not necessarily follow that adsorption has not taken place. (After oxygen adsorption on tungsten the (110) face also remains bare in the ion image[17]!) If new emission centres appear, then according to our interpretation the ionization probability has increased owing to changes in the configuration of the metal atoms at that place. But apart from this more general remark, we observed in several experiments that the (110) face does not remain unaffected upon adsorption of nitrogen at 300 °K. Two examples are given in Fig. 35 (image voltage p = 0.811) and Fig. 36. The latter is particularly interesting in that it reveals the changes in the ion images with increasing image voltage. Only picture (d) (p = 0.823) gives the impression that nothing has happened on the (110) face. But a comparison with (b) (p = 0.753) shows that at a lower voltage the edge of the (110) face is largely non-emitting. The slight increase in voltage from (b) to (c) (p = 0.791), however, is sufficient to make them visible again. This abrupt change in intensity can only be caused by the desorption of nitrogen and therefore demonstrates once more that adsorbed nitrogen causes the ionization probability to decrease. Similar effects can be noted in other regions.

Adsorption at low temperatures indeed mostly gives rise to more randomly localized dots in the (110) region. However, their number does not simply increase with decreasing temperature as would follow from Ehrlich's interpretation. For example, the images of a surface covered at 20 °K often showed a smaller number of new dots on the (110) face than those taken after adsorption at 77 °K.

Adsorption at low temperature can even take place without the appearance of new dots on the (110) face. This happened in some of our experiments where the surface after adsorption at low temperature was warmed to 300 °K, saturated at this temperature and subsequently at 77 °K. An example is given in Fig. 37 (image voltage p = 0.801). It provides further evidence for the conclusion that the "bareness" of a particular face in the ion image need not imply that no adsorption has taken place.

According to the second of Ehrlich's arguments the disappearance of emission centres upon warming of an imaged surface to 300 °K means that these centres have a large mobility and therefore cannot be tungsten atoms. We, however, are of opinion that the procedure introduces some artifacts. Upon heating of an imaged surface which has previously been covered at low temperature, nitrogen is desorbed from the densely covered shanks of the tip and from its support. Readsorption therefore takes place on the front surface which, as was shown in section IV-4.1., is almost clean after imaging. Small wonder, then, that when the surface is again imaged at 20 °K the original array of bright dots has drastically changed. Changes are observed all over the surface and are not confined to the (110) area. This observation in fact lends support to our view that bright dots are tungsten atoms, for it is difficult to understand why strongly bound nitrogen atoms on, for example, the (111) face should be affected by prolonged exposure to nitrogen at 300 °K.

Although it is evident from the discussions above that we are still far from a complete understanding of the ion-microscope results for the (110) face, we feel justified in concluding that they prove, rather than rule out, the possibility of nitrogen being bound at 300 °K.

There is one more remark to be made with regard to the view held by Ehrlich. If nitrogen, bound as atoms, were indeed stable on the (110) face

only below 190 °K, it should be possible at this low temperature to achieve isotopic mixing of $^{14}N_2$ and $^{15}N_2$ over tungsten substrates exposing the (110) face. Madey and Yates[30], however, have reported that over tungsten filaments no isotopic mixing occurs at temperatures below 1000 °K.

IV-4.4. Different states of adsorbed nitrogen

It has become general usage among those who study the nitrogen-tungsten system to discuss their results in terms of an atomistic model in which the adsorbed nitrogen is divided according to three main types: the α-, β- and γ-states. This designation originates from flash-filament experiments[31] and is therefore based on the stability of the adsorbate, the heat of adsorption for the three states being roughly 20, 75 and 10 kcal/mole, respectively. After the earliest flash-filament experiments, the improvement of techniques and crystallographic characterization of samples led to a refinement in the differentiation of the nitrogen states. Both the original β-state and γ-state had to be subdivided into two states[32], while at present it seems that at least for the β-state the classification is still less simple, since this species has a fairly broad desorption spectrum.

Isotopic mixing experiments[32] have provided evidence that the α- and γ-states are to be identified with molecularly bound nitrogen. The β-states on the contrary are isotopically mixed upon desorption and therefore most probably consist of atomically bound nitrogen, although part of this strongly bound species shows first-order desorption kinetics according to results reported by Madey and Yates[30]. At 300 °K adsorbed nitrogen is mainly present in these β-states and only to a limited extent in the α-state. Oguri[23,34] has discussed his experiments in terms of α-, ε- and ζ-states. In his model, the α- and ζ-states can be identified with the α- and β-states as defined above. The ε-state has a stability intermediate between those of the α- and β-states, and is supposed to be non-dissociative.

Work-function measurements, on the other hand, give rise to a division of adsorbed nitrogen species according to the specific change in work function they induce (or, in other words, according to their surface potential). Values of the latter, as was noted in the previous section, differ widely for the various crystal faces both in sign and in magnitude.

On account of the subdivision it is not surprising that attempts to correlate the classification based on stability with that according to surface potential result in a somewhat embarrassing number of "different states", being primarily β- and γ-substates[18]. This circumstance obviously interferes with a simple interpretation of the formation and structure of the nitrogen-tungsten chemisorption layer. One of the problems that has aroused much discussion concerns the sign of the surface potential of nitrogen present in the β-states.

The finding that atomically bound nitrogen in the β-state on some crystal faces lowers the work function of tungsten conflicts with the generally adopted view[35] that adsorption of an atom on a metal surface leads to an increase of the work function when the electronegativity of the atom is larger than that of the metal, which is indeed the case for the nitrogen-tungsten system (on Pauling's electronegativity scale: N - 3.0 and W_{metal} - 1.6 [36,37]). The validity of this "rule" hinges essentially on two assumptions: (i) the dipole

moment of the chemisorption bond is determined by the difference in the electronegativities, while the latter are known accurately enough to give the correct direction of the bond moment, and (ii) the surface potential has the same sign as the bond dipole moment calculated with the electronegativity relation.

Recently Delchar and Ehrlich[18] have questioned the first assumption. They quite rightly pointed out that besides electronegativity differences there are other factors playing a role in determining the bond dipole of simple molecules. Firstly a difference in atomic size of the bond partners might give rise to a homopolar dipole with the positive end on the larger atom. A further important factor is the hybridization of bonding orbitals; also, the presence of a lone electron pair in a non-bonding orbital can produce a large atomic dipole. However, there is no reason why in the case of the nitrogen-tungsten bond these effects should oppose and even overwhelm the effect due to the difference in the electronegativities. On the contrary, comparison with e.g. a compound like ammonia suggests that any lone-pair contribution to the bond dipole should have the same direction as that arising from the electronegativity difference. For the present we therefore see no manifest cause for rejecting the assumption that the electronegativity difference determines the sign of the moment of the nitrogen-tungsten bond. We rather feel that there are good reasons to criticize the second supposition mentioned above.

In the ordinary electrostatic picture set up to account for the change in work function upon adsorption, a chemisorption layer is visualized as a dipole layer on a plane surface having either its positive or negative side pointing outwards. According to eq. (16) the surface potential is proportional to the magnitude of the individual dipoles and their number per unit area. In applying this model to real chemisorption systems, however, we should be aware that the bond moments need not all be aligned perpendicular to the metal surface. In fact the dipole moment used in the electrostatic picture corresponds with the dipole component perpendicular to the surface in the actual case. When adsorption takes place on an atomically rough surface, the normal components may be expected to become appreciably smaller than for the case of a very smooth surface, or even have opposite direction. Neglecting for the moment any surface rearrangement, we therefore arrive at the conclusion that an electronegative adsorbate, such as nitrogen, will show the more positive surface potential on the rough surface areas.

Delchar and Ehrlich derive an exactly opposite conclusion from their contact potential data: the surface moment of nitrogen on tungsten is positive on a flat and negative on a rough surface. This conclusion implies that the electronegativity picture would fail in the present case, contrary to our view on this matter.

However, the views diverge in another way as well. In the classification of rough and flat faces Delchar and Ehrlich consider the (111) face to belong to the former category, and the (100) face to the latter on the ground that the smoothing-out of the conduction electrons prevents a nitrogen atom from sinking into the gaps between the protruding atoms of the (100) face. Such a reasoning seems invalid, however, because upon adsorption the electronic configuration drastically changes, the conduction electrons at the surface taking part in the bonding of the nitrogen. Consequently, on the understanding that no rearrangements take place, we see no reason why geometrical

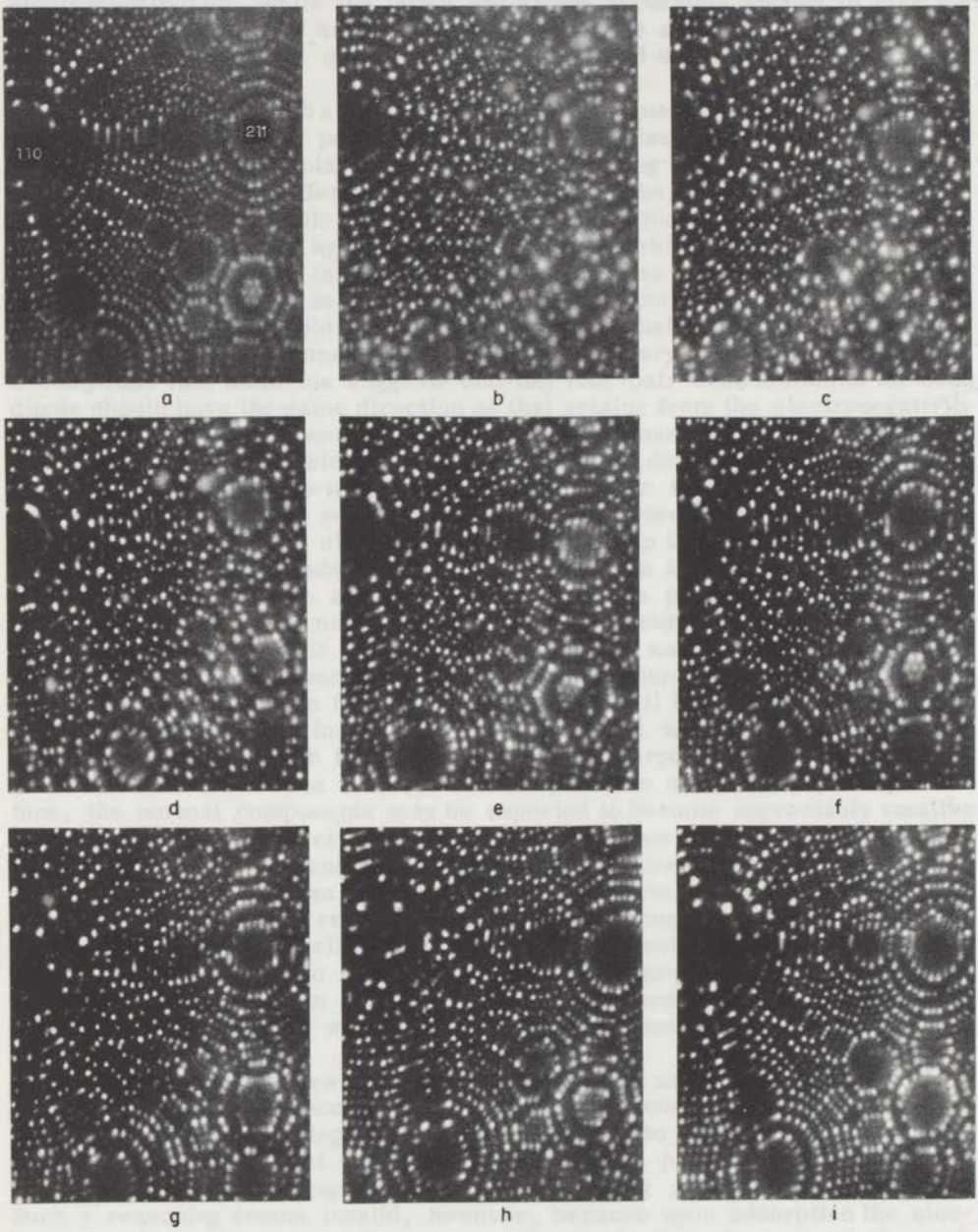

Figure 29

Field desorption and field evaporation of surface layers after saturated adsorption of nitrogen on tungsten at 300 ^{o}K; for experimental data and conditions see Table III

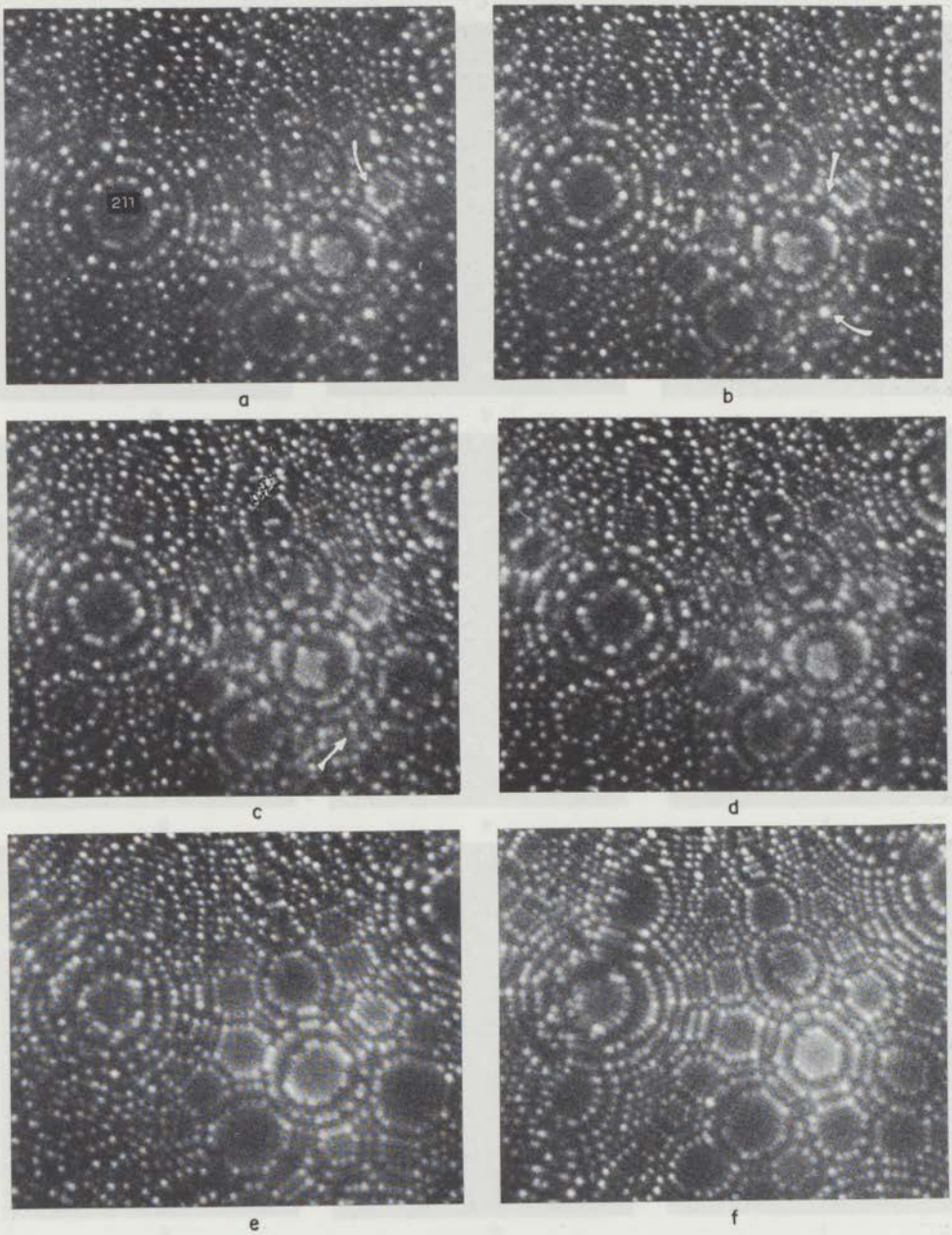

Figure 30

(a) Tungsten (211) - (111) region after adsorption of nitrogen at 77 °K; (b), (c), (d), (e) and (f) show same surface after applying, 11.75, 12.0, 12.25, and 12.5 kV, respectively, for one minute; images at 20 °K and 10.25 kV

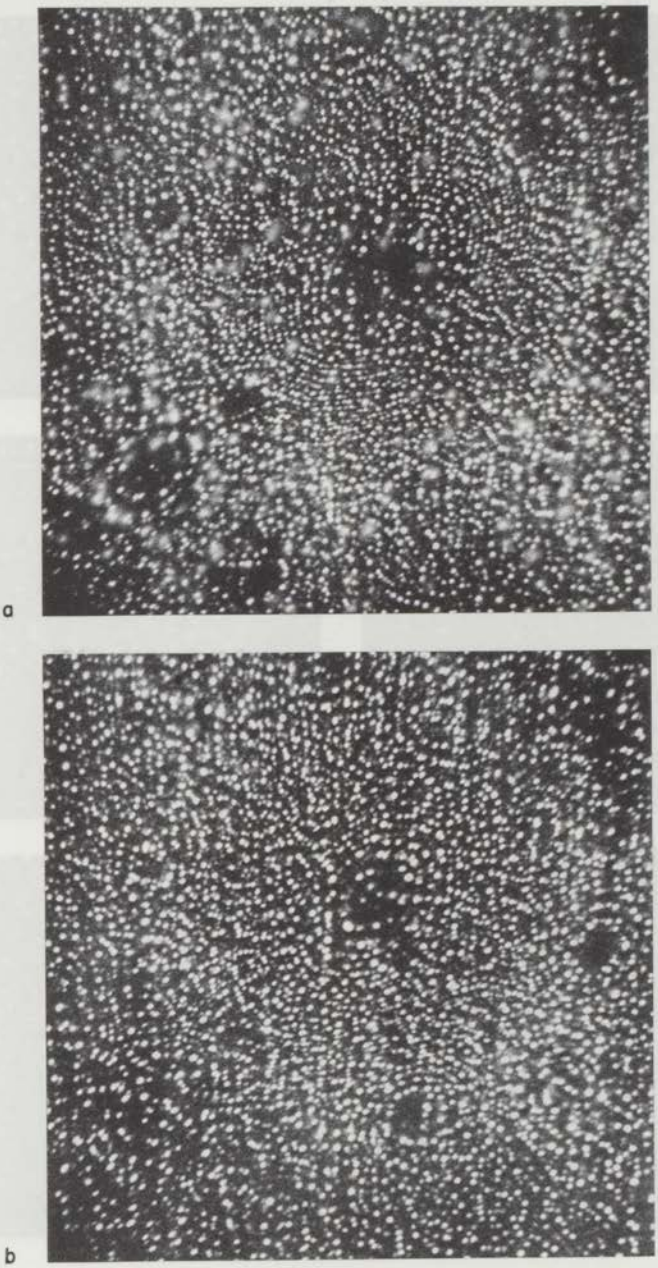

Figure 31

Tungsten surface after adsorption of nitrogen at 77 °K following preadsorption at 77 and 300 °K; images at 20 °K and 12.1 kV; (a) before and (b) after imaging at higher voltages (maximum 14.1 kV)

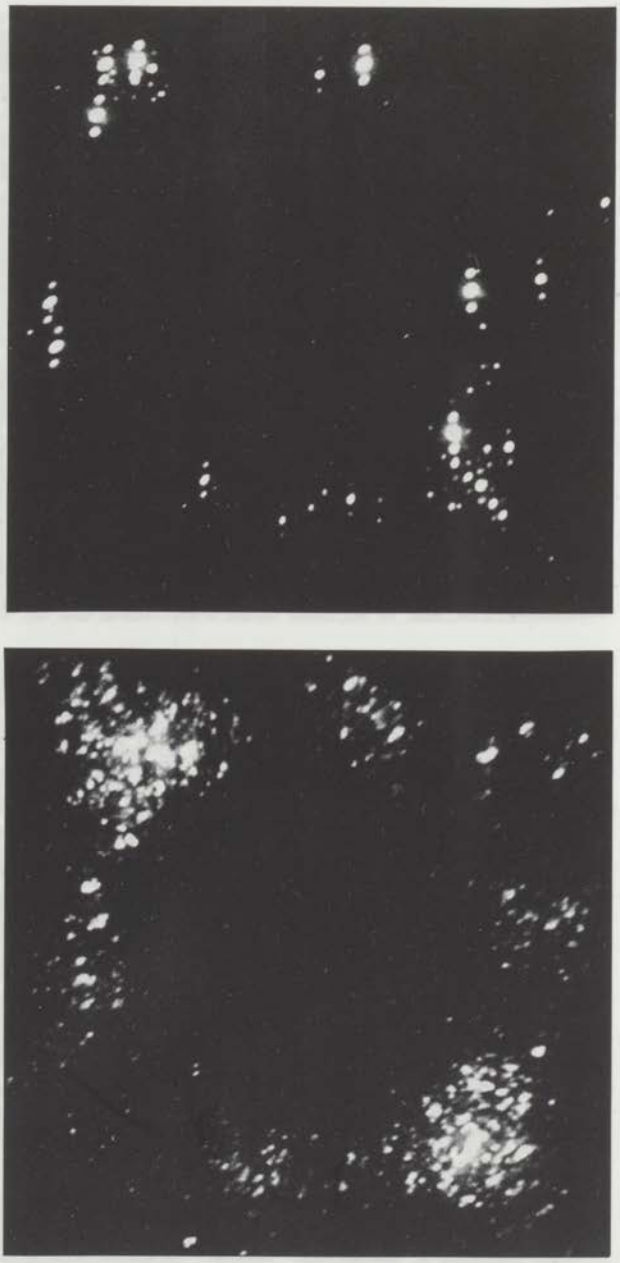

Figure 32

Same surface as in Fig. 11, but images taken at 20 ^{o}K and 7.6 kV; (a) before and (b) after imaging at higher voltages (maximum 14.1 kV;)

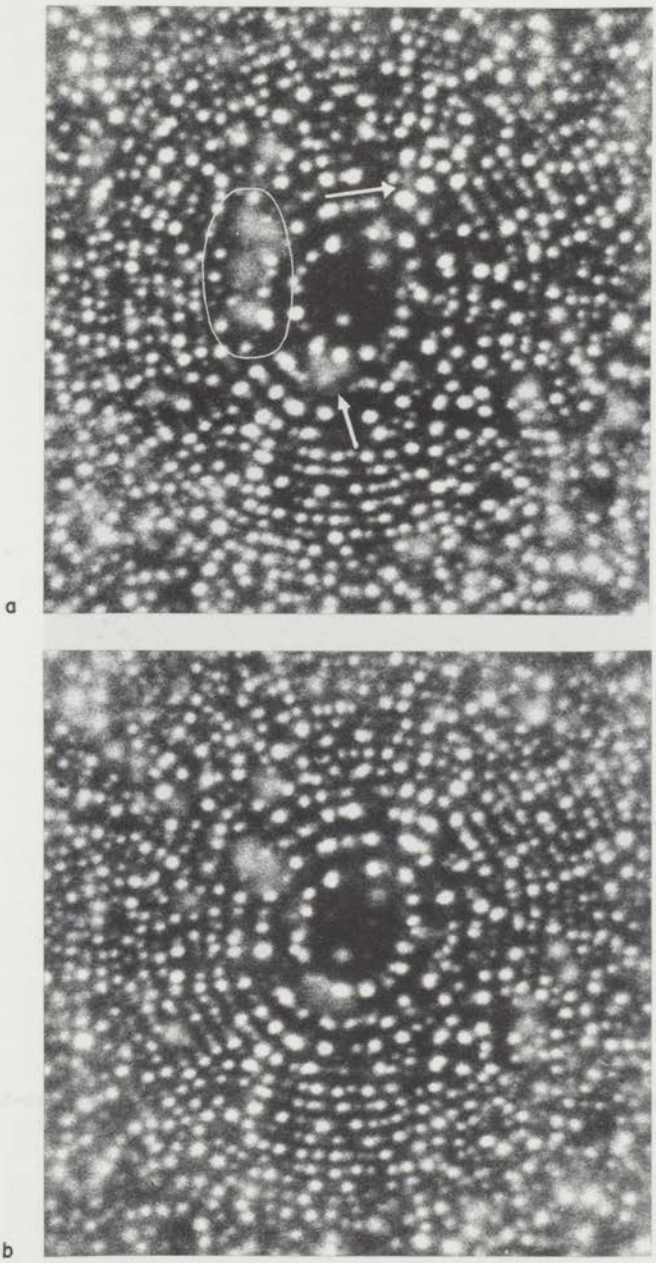

Figure 33

Tungsten (110) region after saturated adsorption of nitrogen at 20 °K; images at 20 °K, (a) at 9.4 kV and (b) at 9.7 kV

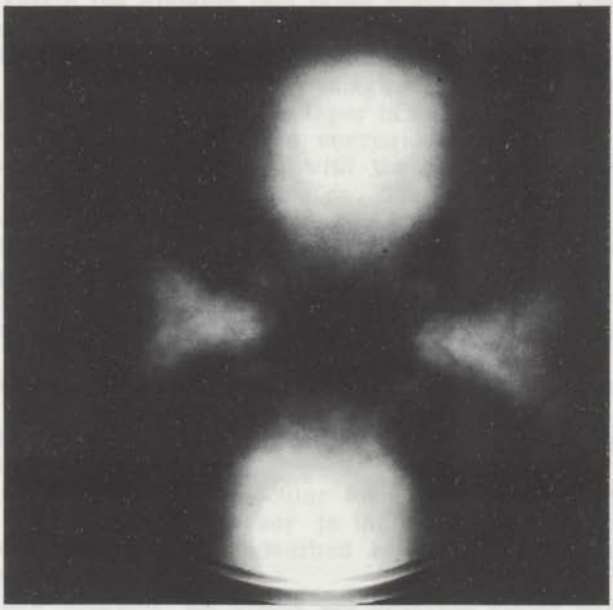

Figure 34

Field-emission pattern of a thermally annealed tungsten surface after saturated adsorption of nitrogen at 300 ^{o}K

considerations using a hard-sphere atomic model and assuming a reasonable value for the dimension of a strongly bonded nitrogen atom ($\approx$ 0.6 A radius) should lose their validity. Once it is accepted that a nitrogen atom can sink into the (100) surface structure there is no need to doubt the electronegativity relation any more.

The results of the present study, indicating that the adsorption of nitrogen causes a reconstruction of nearly all crystal faces of tungsten, largely supersede all previous considerations which were essentially based on the assumption that the metal surface is an assembly of sites having a fixed configuration. The new interpretation we now arrive at closely resembles that given in section IV-2.3. for the adsorption of carbon monoxide on tungsten.

If we retain the division into three main types of adsorbed nitrogen for the moment, the most stable species is that incorporated into the metal surface; undoubtedly it will be present in the atomic form corresponding with the β-state or Oguri's ζ-state. We may imagine a special dissociative species to be formed in the chemi-adsorption layer in the initial stages of adsorption at low temperature when no surface corrosion takes place. Most probably this type of nitrogen interacts less with the metal atoms than the β-state does, but more than the α- and ϵ-states do. The bond strength of the chemi-adsorbed nitrogen, however, is not easily determined, because on heating (e.g. in flash-filament experiments) a conversion into β-states will take place.

On top of what again may be called the corrosive chemisorption layer, sites will be available for less strongly bound species. The latter can conceivably occur in both a dissociative and a predissociative form without differing much in bond strength. Evidently the α- and ϵ-states belong to this type. In the present picture the formation of the states in question follows on that of the most strongly bound nitrogen. This conclusion is in excellent agreement with the experimental findings for the α-state as reported by Delchar and Ehrlich.

In the γ-nitrogen all molecular forms of low stability are grouped together, i.e. the possible precursor in the dissociative adsorption and the nitrogen that can be physically adsorbed at low temperature on top of a chemisorbed layer.

If we now consider the effect the different states have on the work function, we can utilize the arguments made above in discussing the surface potential of nitrogen adsorbed on rough and smooth surfaces, and those advanced for the carbon monoxide-tungsten system. It follows that the low-temperature chemi-adsorption state at low coverage and the states formed on top of the corroded layer must have negative surface potentials, whereas the surface potential of the β-state will be positive or at least far less negative than the former. Physically adsorbed nitrogen certainly has a positive surface potential. The assignment proposed here compares well with the one given by Oguri[23]: at full coverage ζ-nitrogen gives $\Delta\varphi = -0.2$ eV, while ϵ-nitrogen gives $\Delta\varphi = 0.5$ eV.

It is particularly interesting to note that Ehrlich and Hudda[20] already observed in the field-emission microscope that in the early stage of adsorption at 77 ^{o}K the work function is raised, while simultaneously an entirely different arrangement of the β-state was found. It turned out that only the initial adsorption was really different. If first small amounts were added

at 300 °K, continued adsorption at low temperature only lowered the work function still more. These findings seem in very good accord with the formation of a chemi-adsorption layer at low temperature.

From the present model it is also readily understood that an irreversible change takes place when the surface is warmed after saturation at low temperature, because the reconstruction of the surface will proceed at higher temperatures and probably result in the formation of more β-species. This explains why the work functions obtained after readsorption at low temperature are lower than those obtained after adsorption at low temperature only. As regards the changes in the pre-exponential factor A for the F-N relation, we think that the explanation given in section IV-2.3.(a) for the adsorption of carbon monoxide also holds for the nitrogen-tungsten system.

So far we have made a rather simplified classification without referring to the observed crystallographic specificity. But it should be fairly easy to understand, if only qualitatively, that adsorption can proceed differently for various crystal faces and results in different surface potentials. Although the outer surface layer(s) will be reconstructed upon adsorption, the structural differences for the various crystallographic directions need not necessarily have lost their important effect on the structure of the chemisorption layer. On the contrary, the more easily the rearrangements take place, the greater will be the influence of subsurface layers on the ultimate structure of the outer layers, in a way comparable with the effect encountered in epitaxial growth. We must therefore expect that within a main group of states species will have slightly different stabilities and surface potentials on different crystal faces. Moreover, the amount of nitrogen adsorbed in a particular state may vary for individual crystal faces. Oguri, for example, has accounted in this way for the increase in work function on the (111) face and the decrease on the (100) face. From his experiments he has concluded that on the (111) face both the ε- and ζ-states exist in about equal amounts, so that $\Delta\varphi$ becomes roughly $(0.5-0.2)/2 = 0.15$ eV. On the (100) face only ζ-nitrogen is supposed to be present. This interpretation agrees well with out corrosive-chemisorption model, but is in conflict with that proposed by Delchar and Ehrlich, who do not distinguish between two strongly bound states on the (111) having surface potentials with opposite sign.

In an effort to reach an unambiguous decision, we have studied the effect of field desorption on the work function of the (111) face after adsorption at 300 °K (following preadsorption at 77 °K). Such experiments should indeed permit removal of the nitrogen bound on top of the β-layer, without appreciably affecting the structure of this layer. The results are shown in Fig. 38. The removal of adsorbate takes place in distinct stages. In the initial stage the work function drops approximately to the value for the clean surface and there is little change up to a voltage of 4.8 kV. Increasing the applied voltage by 0.2 kV then causes the work function to drop abruptly to a value -0.15 eV below that for a clean surface. However, the value of log A has little changed in comparison with that obtained for the covered surface. It can therefore safely be concluded that a major part of the original adsorbate is still present on the surface. Further increase of the desorbing field causes both the work function and log A to approach the values for the clean surface.

The interpretation is obvious. The nitrogen that desorbs first probably has a negative surface potential and is loosely bound in a (predissociative) molecular form; the second stage consists in the desorption of more strongly

bound nitrogen atoms also having a negative surface potential. After these stages have been completed the surface exposes tungsten atoms shielding the nitrogen atoms buried in the surface. This structure then has a positive surface potential in accordance with expectation. In this way we have obtained direct evidence for the simultaneous occurrence of states differing in both stability and surface potential and more generally for the adsorption model put forward here.

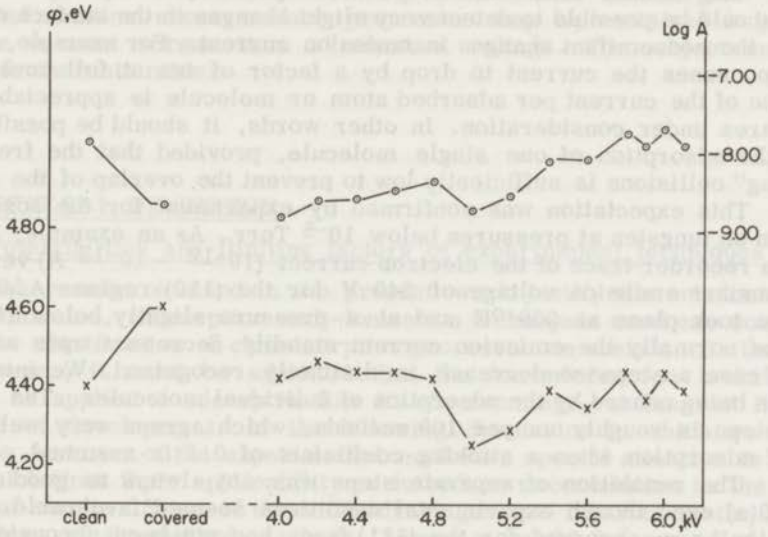

Figure 38

Changes in work function and in log A for the tungsten (111) face (field-evaporated at 77 °K and 7.5 kV) after saturated adsorption of nitrogen at 300 °K and subsequent stepwise field desorption at 300 °K; the applied desorption voltages are indicated on the ordinate

IV-4.5. The detection of individual atomic events with the probe-hole technique

As the cleaning of metal tips by field desorption and field evaporation (see section III-2.) almost completely preserves the sharpness which tips have when leaving the etch bath, our experiments were normally started with clean tips giving an electron emission of 0.5 μA at a voltage of about 400 V, sometimes less. Such tips are even too sharp to give an ion image of reasonable intensity and must therefore be blunted purposely in the ion microscope, either by careful heating or by prolonged field evaporation. No inconvenience, however, attaches to their use in the probe-hole tube. On the contrary, the availability of extremely sharp tips has permitted some most remarkable observations not reported before. These are discussed below.

Consider a tip with a radius of curvature of 200 Å at 5 cm distance from the anode screen. Then the magnification amounts to $2.5 \cdot 10^6$, which means that the hole in the screen (0.2 cm in diameter) corresponds with an area on the tip surface having a diameter of 8 Å. This area will contribute most to the electron current passing through the probe hole, but electrons with high tangential velocity emitted from the borders around the main area can also enter the probe hole (see section IV-4.3.(c)). Accordingly, it seems a good estimate if we consider the probe beam to originate from an area with a diameter of about 20 Å. If we further assume an average surface-atom density of 10^{15} atoms/cm^2, the probed area thus exposes roughly 30 atoms.

The number of atoms "seen" in the probe-hole experiment indicates that it should be possible to detect very slight changes in the surface configuration by the concomitant changes in emission current. For example, when adsorption causes the current to drop by a factor of ten at full coverage, the decrease of the current per adsorbed atom or molecule is appreciable for the small area under consideration. In other words, it should be possible to observe the adsorption of one single molecule, provided that the frequency of "sticking" collisions is sufficiently low to prevent the overlap of the individual events. This expectation was confirmed by experiment for the adsorption of nitrogen on tungsten at pressures below 10^{-8} Torr. As an example, Fig. 39(a) shows a recorder trace of the electron current (10^{-12} - 10^{-13} A) versus time at a constant emission voltage of 340 V for the (110) region. Adsorption of nitrogen took place at 300 °K and at a pressure slightly below 10^{-8} Torr. Whereas normally the emission current steadily decreases upon adsorption, in this case a stepwise decrease is distinctly recognized. We interpret the steps as being caused by the adsorption of individual molecules. The frequency of the steps is roughly one per 100 seconds, which agrees very well with the rate of adsorption when a sticking coefficient of 0.1 is assumed.

The resolution of separate steps was not always as good as that in Fig. 39(a) even though experimental conditions seemed favourable. This bad resolution, e.g. observed for the (111) face, has not been accounted for unequivocally, but it might be caused by changes in the surface structure which did not follow instantly upon adsorption, but took place in subsequent surface reactions. In that case the number of (overlapping) current changes exceeds the number of particles adsorbed. A bad resolution might therefore be indicative of surface rearrangements. However, a more systematic study is required in order to verify this supposition.

Fig. 39(b) shows another interesting example of stepwise changes in the probe-hole current. The latter was recorded at a constant voltage of 587 V for a partially field-evaporated region on the edge of the (110) face, at 300 °K and at a pressure of about 4.10^{-10} Torr. Initially the current ($\approx 10^{-11}$ A) is extremely stable, proving that the noise of instrumental origin is very small. Then suddenly a stepwise drop in current occurs, after a few seconds followed by an equivalent rise. But now a remarkable increased "noise" becomes noticeable. After about 18 minutes the current slightly increases and so does the noise structure. The subsequent drop in current is accompanied by a fine structure which is far better resolved than the preceding one. Ten minutes later the situation has changed again.

The current variations shown in Fig. 39(b) were the only ones observed over a period of about one hour and even after a two hours' run no

appreciable net change of the current was measured. The fact that the variations occur stepwise and reversibly strongly suggests that they, too, are caused by single events at the metal surface. We have not inquired deeply into the temperature dependence of the phenomenon, but it appeared that the number of steps and the noise diminish with decreasing temperature. This would rule out adsorption of molecules of the residual gas as a possible cause and prove that changes in the surface configuration as such are involved. The large steps could then be due to the transitions of an atom between adjacent sites, while the fine structure would correspond to short-range oscillations around the equilibrium position.

The present experiments clearly demonstrate that a good deal of valuable information about surface processes may be contained in plots of probe-hole current versus time at constant voltage. The subject certainly deserves further attention.

IV-5. GENERAL DISCUSSION

IV-5.1. Potentialities and limiting factors of experimental techniques

The results obtained in the present work justify the conclusion that the field-emission, -desorption and -ionization techniques used can contribute much to the clarification of chemisorption processes on metals. At the same time, however, it must be admitted that the ion-microscope technique in particular as applied to adsorption has its shortcomings, at least at its present stage of development. In the following discussion in which we review the various features of the experimental methods, special attention is paid to factors which limit their applicability or introduce uncertainties in the interpretation of results. Some of these disadvantages are inherent in the microscopic nature of the methods; others, however, might be remedied in the future as further experimental and theoretical progress is made.

(i) The field-emission (probe-hole) microscope and the field-ion microscope permit the study of adsorption on perfectly ordered metal surfaces of well-defined crystallographic orientation.

Conventional methods for obtaining clean metal surfaces, e.g. heating, electron or ion bombardment of contaminated surfaces and the evaporation of films, invariably introduce a more or less severe disorder at the surface. Annealing at appropriate temperatures can remove the disorder only for the most stable crystal faces of the metal. Field evaporation at low temperature as applied in the present techniques, on the contrary, uniquely provides the possibility of obtaining clean and atomically ordered crystal faces of high indices, too. Moreover, the cleaning procedure and the crystallographic orientation can be checked by means of the ion image of the surface. As was already noted in section II-3.3., however, the study of metals in the ion microscope is restricted to those with relatively high melting points, though recent improvements in imaging techniques have greatly extended the range of metals that can be investigated[38].

(ii) With the combined use of the electron- and ion-microscope techniques it is possible to arrive at a fairly detailed atomistic interpretation of adsorption processes.

As demonstrated in this work, the electron and ion technique supplement each other very favourably as regards their respective potentialities for adsorption studies. The electron-emission technique supplies information about the various adsorption complexes which can be distinguished according to their surface potential and stability. Surface processes like adsorption, diffusion and desorption can kinetically be investigated by studying them at different temperatures. With the probe-hole technique the dependence on crystallographic orientation can be established. The field-ion technique, on the other hand, contributes largely to a better understanding of surface processes by furnishing atomic details such as about a possible rearrangement of surface metal atoms which cannot be detected by the electron-emission microscope.

Particular interest attaches to the application of field desorption and field evaporation, since by using these methods the adsorbate layer and the subsurface atom layers can gradually be removed at very low temperature. In this way a reconstruction of the surface layers, which would occur upon thermal desorption, is avoided. During field desorption the surface structure passes through stages which may completely differ from those traversed during the adsorption or thermal desorption processes. The emission characteristic and the ion image corresponding with the successive stages of field desorption and field evaporation then can provide additional information not accessible by any other technique.

The ion microscope offers an atomic view because of the high resolution obtained with it, provided that the operating temperature is kept very low. This requirement obviously limits the use of the technique because it means that in practice only frozen-in states can be observed. Besides the necessity of maintaining a high resolution the occurrence of enhanced field desorption and eventually of field evaporation prohibits the use of the instrument at temperatures much above 77 ^{o}K.

A drawback inherent in the high resolution and magnification obtained with both field-emission and field-ion microscope is that the surface areas viewed are extremely small ($\approx 10^{-10}$ cm^2) compared with those exposed in experiments using filaments, single crystals or evaporated films. With the microscope techniques the total number of surface and adsorbate atoms taking part in the surface processes therefore only amounts to about 10^5. As in the probe-hole measurements the number of atoms considered is even much smaller, the statistical prerequisite of thermodynamics is not valid for the observations with this technique. In consequence, it is not surprising that the results obtained with this method sometimes show a slight irreproducibility (cf. section IV-4.3.). Evidently, possible fluctuations in the configuration of the surface atoms do not average out completely in these cases. For the same reason experiments carried out under exactly the same conditions never resulted in identical ion images of the surface after adsorption.

(iii) Under normal operating conditions of the field-ion microscope, i.e. 20 or 77 °K, 10^{-3} Torr helium and ≈ 4.5 V/Å, the greater part of a chemisorbed layer is removed from the surface.

Obviously, the most disadvantageous feature of the helium-ion microscope in adsorption studies is that the image conditions themselves strongly interfere with a chemisorbed layer. This follows directly from a comparison of the low-field and high-field images of one and the same adsorption experiment (cf. Fig. 31 and 32). The observation of chemisorbed species is thus largely prohibited by the promoted field desorption of these species.

It might now be asked whether field effects similar to those causing field desorption of the adsorbate might also be responsible for the observed displacements of metal atoms. In our view the rearrangements have largely taken place already during the adsorption process. The most important argument in favour of this conclusion is the finding that the extent of the disorder, as observed for the adsorption of carbon monoxide and nitrogen on tungsten, largely depends on the conditions of adsorption, which always took place while the field was switched off. Moreover, the disorder penetrates into deeper-lying atom layers which are shielded from the high field.

Nevertheless, it is admitted that in the process of field desorption during imaging some atom displacements might be induced in addition to those already brought about by the adsorption itself. Being aware of such additional field effects, we have refrained from advancing too detailed an interpretation of the observed ion patterns, which in fact show almost only the debris of the original chemisorption layer.

In order to avoid or at least diminish the field desorption of the adsorbate, the operating conditions of the microscope have to be modified. This can be done in several ways. Firstly, our experiments showed that the rate of field desorption markedly increases in the presence of helium. It therefore seems advantageous to resort to one of the methods for image intensification discussed in section II-3.3., which would permit the use of lower helium pressures at equal image-recording times. Secondly, as demonstrated in this work, helium-ion images can be taken at about half the field strength required for making an optimal image of the clean surface. Such images show very remarkable structures for the case of nitrogen adsorbed on tungsten and undoubtedly contain much valuable information about the chemisorption layer, which under these image conditions is hardly disturbed. Thirdly, we may use image gases other than helium, such as neon or argon. Since the best-image voltage is lower for these gases than for helium, it can accordingly be expected that field desorption takes place to a lesser extent under best-image conditions. This has recently been confirmed experimentally by Bassett[39] for the case of an oxygen-covered tungsten tip imaged with neon. The recording of neon images, and a fortiori of images obtained with other rare gases, however, also requires image intensification.

In view of the foregoing we regard the making of images with neon or argon at low pressures and image fields, using the most powerful method of image intensification available, as the most promising approach to evade high-field-induced effects during the imaging of covered tips.

(iv) The presence of nitrogen or carbon monoxide at a tungsten surface causes a decrease of the ionization probability compared with the value at the clean surface; the image contrast is also lowered.

The question whether an adsorbed atom or molecule gives rise to an increase or a decrease of the probability of field ionization has so far received little attention in the literature. It even seems that this question has not been posed before. However, the answer is clearly of crucial importance for the interpretation of the ion images obtained in adsorption experiments. In the present study we arrived at the conclusion that adsorption of metalloids lowers the ionization probability and the image contrast, thus rejecting the view held by others that bright dots in the ion patterns can be identified unequivocally with adsorbed species. As all the arguments presented were based on experimental evidence, the problem should be reconsidered from a theoretical point of view. This will be done in the next chapter.

IV-5.2. Atomic processes in chemisorption on metals

The atomistics of the adsorption of carbon monoxide and nitrogen on tungsten have been discussed at length in sections IV-2.3. and IV-4.4., respectively. At this place it seems appropriate to summarize the most important conclusions of these discussions and reconsider them in a somewhat wider scope, since we feel that they bear not only on the particular systems investigated but also upon other adsorption systems. At the same time this gives us the opportunity to express our view on several aspects of chemisorption and surface reconstruction which have recently aroused some discussion[40].

(i) The adsorption of both carbon monoxide and nitrogen on tungsten causes a rearrangement of the metal surface, the adsorption of hydrogen does not.

In considering the feasibility of surface reconstruction from a thermodynamic point of view one should differentiate between chemisorption systems according to whether or not a corresponding bulk compound is stable under the same conditions of temperature and gas pressure. In the group of systems where a solid compound is stable (e.g. the nitrogen- and carbon monoxide - tungsten systems) it is thermodynamically favourable that the intermetallic bonds are broken in order that new chemical bonds can be made with the reaction partner[41]. Since this equally holds for the intermetallic bonds at the surface the occurrence of surface rearrangements in these systems is in agreement with thermodynamics.

For systems or conditions where the formation of bulk compounds is thermodynamically unfavourable predictions are less easily made. If in such cases chemisorption takes place, this is due to "unsaturated valencies" available at the metal surface. The simplest way we can visualize them to be saturated is by the formation of a chemi-adsorption layer. According to the present results this seems to be the case in the hydrogen-tungsten system. In general, however, surface reconstruction a priori cannot be ruled out, since the formation of a surface phase involving rearrangements of metal atoms and a (partial) breaking of intermetallic bonds may conceivably lead to a further decrease in free energy of the system.

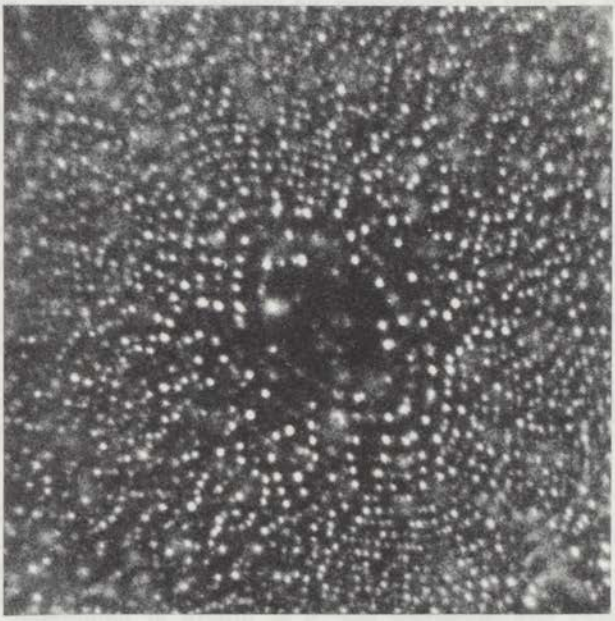

Figure 35

Tungsten (110) region after saturated adsorption of nitrogen at 300 ^{o}K following adsorption at 77 ^{o}K; image at 20 ^{o}K and 15.0 kV

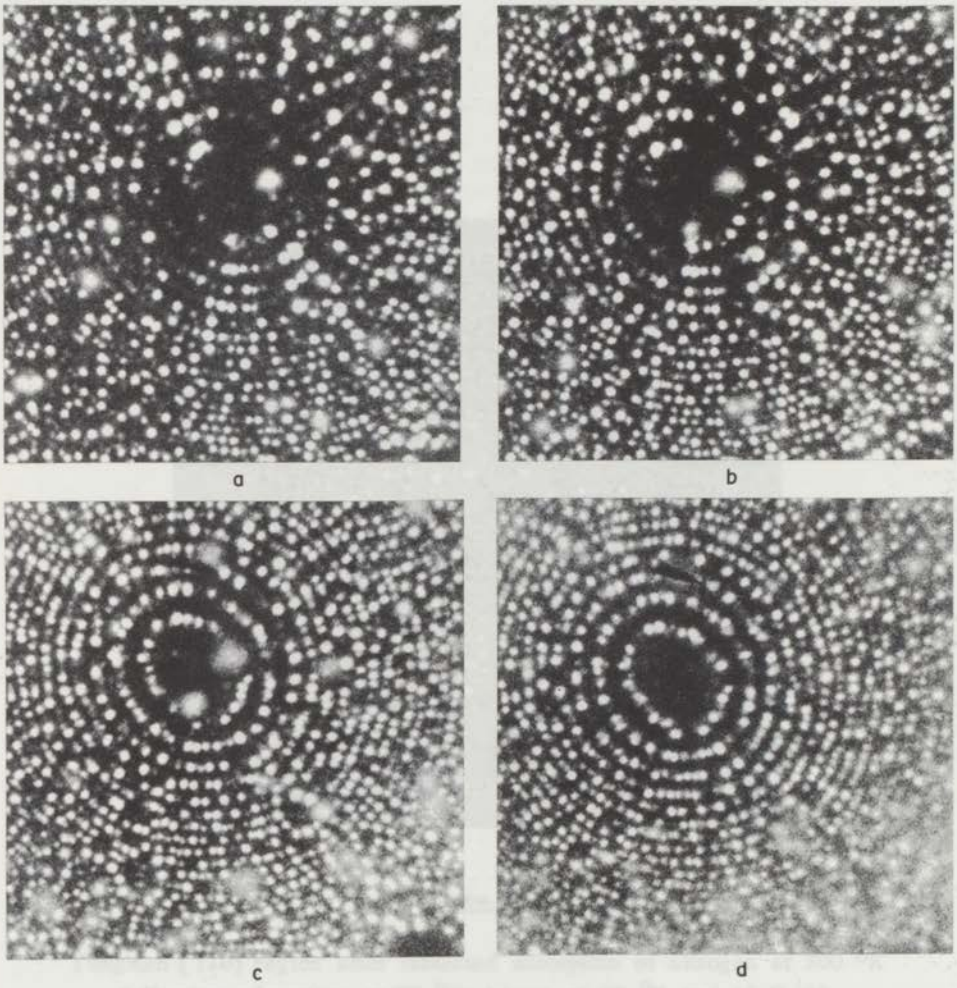

Figure 36

Tungsten (110) region after saturated adsorption of nitrogen at 300 ^{o}K; images at 20 ^{o}K and (a) 11.5, (b) 11.9, (c) 12.5 and (d) 13.0 kV

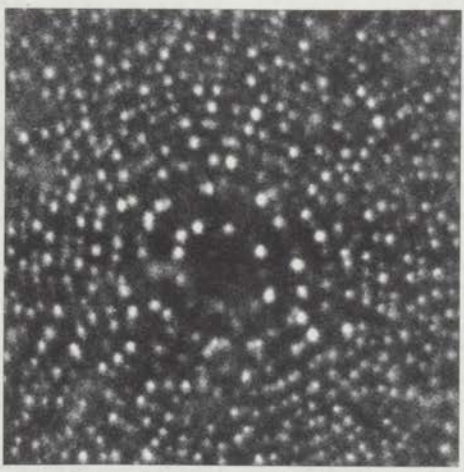

Figure 37

Tungsten (110) region after saturated adsorption of nitrogen at 77 °K following preadsorption at 77 and 300 °K; image at 20 °K and 10.9 kV

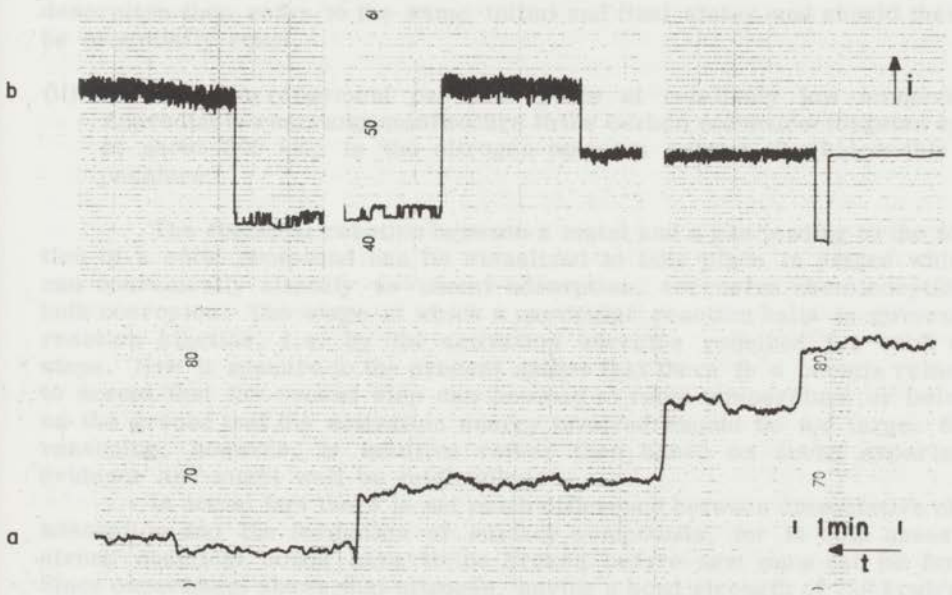

Figure 39

Recorder traces of the probe-hole current versus time at constant applied voltage for the tungsten (110) region; (a) during nitrogen adsorption on a clean surface at 300 ^{o}K and p $\approx 10^{-8}$ Torr, voltage 340 V and current 10^{-12}-10^{-13} A; (b) for a partially field-evaporated surface at 300 ^{o}K and p $\approx 10^{-10}$ Torr, voltage 587 V and current 10^{-11}-10^{-12} A

An argument occasionally brought forward against our interpretations assumed that the heats of adsorption and desorption should be different if metal atoms are displaced upon chemisorption[19,42]. Since these heats prove to have roughly the same value, the possibility of rearrangements was ruled out. This argument, however, is incorrect for the following reason. Heats of desorption are determined from kinetic measurements at high temperature, e.g. for the nitrogen-tungsten system above 1000 °K. At these temperatures the mobility of the surface atoms becomes appreciable, even on a clean tungsten surface, as has been shown by Müller[43] and Ehrlich and Hudda[20]. Thus, if adsorption causes a rearrangement of the surface it is most likely that upon desorption at high temperature the metal surface is reconstructed in reverse. The measured values of the heats of adsorption and desorption then refer to the same initial and final states and should therefore be essentially equal.

(ii) Surface rearrangement can take place at relatively low temperature. Appreciable rearrangement occurs in the carbon monoxide-tungsten system at about 300 °K, in the nitrogen-tungsten system far below this temperature.

The chemical reaction between a metal and a gas leading to the formation of a solid compound can be visualized to take place in stages which we can conveniently classify as chemi-adsorption, corrosive chemisorption and bulk corrosion. The stage at which a particular reaction halts is governed by reaction kinetics, i.e. by the activation energies required for each of the steps. Now it appears to the present author that there is a certain reluctance to accept that the second step can proceed at room temperature or below it, on the ground that the activation energy involved should be too large. Such a reasoning, however, is intuitive rather than based on sound experimental evidence and might well be misleading.

In actual fact there is not much difference between dissociative chemi-adsorption and the formation of surface compounds, for in both cases very strong chemical bonds have to be broken before new ones can be formed. Since experiment shows that nitrogen, having a bond strength of 226 kcal/mole, is dissociatively adsorbed at low temperature, we see no reason to reject the possibility that intermetallic bonds can likewise dissociate at this temperature.

We may imagine the rearrangement to take place according to a concerted mechanism in which the rupture of intermetallic bonds is accompanied and compensated by the formation of new adsorbate-metal bonds. Such a mechanism is quite similar to the one that suggests itself for dissociative adsorption, and may also involve a small activation energy. Obviously the activation energy increases when the corrosion starts penetrating more deeply into the surface and diffusion processes become rate-limiting.

The considerations presented above, suggesting that surface corrosion can take place at relatively low temperature, are strongly supported by numerous instances of surface corrosion in actual practice, occurring at room temperature and extending over far greater depth than was found for the systems discussed here. Moreover, the formation of ordered surface compounds at room temperature has been convincingly shown by many low-energy electron diffraction experiments in recent years[44].

Furthermore it is interesting to note that tungsten hexacarbonyl is formed in macroscopic quantities by the interaction of carbon monoxide and elementary tungsten at a temperature as low as 225 °C. In this process the intermetallic bonds are completely broken. A tungsten atom can only be removed from the surface as a hexacarbonyl molecule if some carbon-monoxide molecules are attached to the atom from underneath. It follows that either carbon-monoxide molecules are capable of penetrating into the surface or surface tungsten atoms can migrate into the chemisorbed carbon-monoxide layer. In view of this similar rearrangements may conceivably become noticeable at lower temperatures and pressures, where no macroscopic hexacarbonyl production takes place.

The surprising ease with which a surface can reconstruct itself at room temperature does not seem an exclusive feature of metal surfaces, for it has also been found for oxide surfaces[45]. In brief, all evidence goes to show that a solid surface, when allowed to interact chemically, is far more mobile than was thought in the past.

A fortiori the surface mobility must be large under conditions at which catalytic reactions normally take place. Gwathmey and co-workers[46] beautifully demonstrated this many years ago with the reaction of hydrogen and oxygen over copper at about 400 °C. Spherical copper single crystals developed very pronounced facets having a specific crystallographic orientation.

(iii) Upon adsorption of carbon monoxide and nitrogen on tungsten at low temperature (77 °K) surface rearrangement only takes place above a certain minimum coverage.

This finding constitutes experimental proof of the ideas expressed by Sachtler and Van Reijen[7]. These authors suggested that the formation of chemisorption bonds requires the rupture of intermetallic bonds in the surface layer. In their view the metal valencies used in the initial stage of chemisorption are not real free valencies ("dangling" bonds), but have combined in the metal surface, so that the latter behaves like a "polyolefin" rather than like a "polyradical". Upon increasing coverage these easily available valencies become exhausted, and the regular metal-metal bonds in turn also become weakened, losing more strength as the chemisorption bonds formed are stronger. From this picture it readily follows that a point might be reached where the weakening has proceeded far enough to allow a rearrangement to take place. In view of the difference in strength between the carbon monoxide-tungsten and the nitrogen-tungsten bond ($\approx$ 90 and $\approx$ 150 kcal, respectively) it can also be understood that a far greater rearrangement is observed at low temperature for nitrogen than for carbon monoxide.

For different metals one expects rearrangements to occur the more easily as the cohesive energy of the metal is smaller and the chemisorption bonds are stronger.

(iv) For both the carbon monoxide-tungsten and the nitrogen-tungsten system the simultaneous occurrence of various adsorbed states distinguishable according to their stability and surface potential readily follows from an adsorption model which takes into account rearrangements of the metal atoms at the surface.

In the past few years many attempts have been made to explain the experimental results for the nitrogen and carbon-monoxide systems in terms of models which pictured the surface as an assembly of adsorption sites whose configuration is not altered upon chemisorption. The present study shows that the assumption of a fixed surface configuration is not justified. In the two systems considered here, chemi-adsorption is followed by the formation of a corrosive chemisorption layer, which in the case of nitrogen probably even exhibits a partly ordered structure, differing markedly for different crystal faces. Atoms or molecules incorporated in these corrosion layers are more strongly held than those on top of these layers. This situation naturally brings about a differentiation between the adsorbed species according to their stability.

Running parallel with the foregoing differentiation is another one, based upon the changes induced in the work function of the metal surface. We have established the relation between the two classifications, having made it plausible that the conversion of the chemi-adsorption layer into the corrosive layer is attended with a decrease in work function. Still, carbon monoxide always causes an increase in work function compared with the value of the base metal, whereas in the case of nitrogen adsorption decreases are also found, depending on the crystal face. To the nitrogen incorporated in the surface layer we have assigned a positive surface potential. For one crystal face, viz. the (111) face, this assignment was checked by experiment and found to be correct. A negative surface potential is attributed to nitrogen stably bound on top of the rearranged layer. In view of these results we see no reason to doubt the validity of the electronegativity rule for estimating the moments of nitrogen-tungsten bonds as well. We would point out that these conceptions agree very well with the view advanced by Burshtein and co-workers[47,48] that a decrease in work function in the case of adsorption of electronegative gases results from the penetration of the adsorbate below the upper layer of metal atoms.

From the foregoing we can conclude that this study presents a novel atomistic interpretation of the current classifications of adsorbed states. Classifications of this kind are useful for schematizing experimental results and discussing the principal modes in which the adsorbate can be present on the surface. Within these main types a further differentiation can obviously be made, since it seems likely that the environment of, for example, a β-nitrogen will slightly vary for different crystallographic directions and perhaps on one and the same crystal face. Still, little seems to be gained from elaborating the classifications in more detail, for it must be kept in mind that they inevitably provide greatly simplified interpretations. The concept of an adsorbed state having a well-defined surface potential and stability is, strictly speaking, valid only when adsorbed entities of that particular species can be removed without affecting the bonding of the species remaining on the surface. This is so, for example, at very low coverage or for weakly bound (physisorbed) species. But in a chemisorption layer at full coverage the interdependence of the bonds is presumably strong, so that the definition of a state becomes more or less arbitrary.

One question which has not so far been discussed is why the change in work function of a tungsten surface after adsorption of nitrogen depends so markedly on crystallographic orientation, whereas no such dependence seems to exist for carbon monoxide. As a particular change in work function reflects a specific structure of the chemisorption layer, this problem reduces to find-

ing out why the structure of the chemisorption layer depends on crystallographic direction in the case of nitrogen, while it does not for carbon monoxide. We tend to the view that upon nitrogen adsorption the structure of a nitride-like surface phase adapts itself to that of the underlying metal atom layers. Owing to the smallness of a nitrogen atom it then seems likely that the specific structure of the substrate is largely preserved in the rearranged surface layers. By contrast, the larger size of the carbon-monoxide molecule probably prohibits a reasonable fit of the lattice of the surface phase onto that of the metal substrate. Differences in the latter, therefore, can be expected in this case to import less in determining the structure of the chemisorption layer.

However, the above reasoning remains speculative as long as we do not know the precise structure of the chemisorption layer on the various crystal faces. In this study it has been shown that the metal surface is reconstructed; the next step should be to demonstrate how it is reconstructed.

REFERENCES

1. L. Swanson and R. Gomer, J. Chem. Phys. 39, 2813 (1963).
2. R. Gomer, Discussions Faraday Soc. 41, 14 (1966).
3. G. Ehrlich, Proceedings of the Third International Congress on Catalysis, North-Holland Publ. Co., Amsterdam (1964) Vol. 1, p. 113.
4. G. Ehrlich, Advan. Catalysis 14, 255 (1963).
5. G. Ehrlich and F.G. Hudda, Phil. Mag. 8, 1587 (1963).
6. O. Nishikawa and E.W. Müller, J. Appl. Phys. 35, 2806 (1964).
7. W.M.H. Sachtler and L.L. van Reijen, J. Res. Inst. Cat. 10, 87 (1962).
8. M.J. Duell, B.J. Davis and R.L. Moss, Discussions Faraday Soc. 41, 43 (1966) and remark by A.A. Holscher.
9. D. Menzel and R. Gomer, J. Chem. Phys. 41, 3311 (1964).
10. A.G.J. van Oostrom, Thesis, Amsterdam (1965).
11. N. Mott and H. Jones, "Theory of the Properties of Metals and Alloys", Dover, New York (1958).
12. T. Toya, J. Res. Inst. Cat. 10, 236 (1962).
13. J.W. Geus, H.T.L. Koks and P. Zwietering, J. Catalysis 2, 274 (1963).
14. R. Gomer, J. Chem. Phys. 28, 168 (1958).
15. D. Menzel and R. Gomer, J. Chem. Phys. 41, 3329 (1964).
16. G. Ehrlich, Trans. N.Y. Acad. Sci. 101, 722 (1963).
17. G. Ehrlich, Discussions Faraday Soc. 41, 7 (1966).
18. T.A. Delchar and G. Ehrlich. J. Chem. Phys. 42, 2686 (1965).

19. G. Ehrlich and F.G. Hudda, J. Chem. Phys. 36, 3233 (1962).

20. G. Ehrlich and F.G. Hudda, J. Chem. Phys. 35, 1421 (1961).

21. J.F. Mulson and E.W. Müller, J. Chem. Phys. 38, 2615 (1963).

22. A.A. Holscher, J. Chem. Phys. 41, 579 (1964).

23. T. Oguri, J. Phys. Soc. Japan 19, 83 (1964).

24. M.P. Hill and B.A. Pethica, J. Chem. Phys. 36, 3095 (1962).

25. P.A. Redhead, J. Chem. Phys. 38, 566 (1963).

26. F.H. Hayes, M.P. Hill, S.M.A. Lecchini and B.A. Pethica, J. Chem. Phys. 42, 2919 (1965).

27. M.P. Hill, S.M.A. Lecchini and B.A. Pethica, J. Chem. Phys. 44, 2170 (1966).

28. A.A. Holscher, Chem. Weekblad 62, 229 (1966).

29. C.M. Quinn and M.W. Roberts, J. Chem. Phys. 40, 237 (1964).

30. T.E. Madey and J.T. Yates, J. Chem. Phys. 44, 1675 (1966).

31. G. Ehrlich, J. Chem. Phys. 34, 29 (1961).

32. L.J. Rigby, Can. J. Phys. 43, 532 (1965).

33. J.T. Yates and T.E. Madey, J. Chem. Phys. 43, 1055 (1965).

34. T. Oguri, J. Phys. Soc. Japan 18, 1280 (1963).

35. A. Eberhagen, Fortschr. Phys. 8, 245 (1960).

36. L. Pauling, "The Nature of the Chemical Bond", Cornell University Press, Ithaca, New York (1960).

37. D.O. Stevenson, J. Chem. Phys. 23, 203 (1955).

38. E.W. Müller, Science 149, 591 (1965).

39. D.W. Bassett, Discussions Faraday Soc. 41 (1966), General Discussion, p. 65.

40. See e.g. Discussions Faraday Soc. 41, 54-74 (1966).

41. O. Kubaschewsky and E. Evans, "Metal Physics and Physical Metallurgy", Pergamon Press, New York (1958).

42. G. Ehrlich, Discussions Faraday Soc. 41 (1966), General Discussion, p. 69.

43. E.W. Müller, Z. Physik 126, 642 (1949).

44. J.W. May, Ind. Eng. Chem. 57, 19 (1965).

45. L.L. van Reijen and P. Cossee, Discussions Faraday Soc. 41, 277 (1966).

46. A.T. Gwathmey and A.F. Benton, J. Phys. Chem. 44, 35 (1940).

47. R.Ch. Burshtein and M.D. Surova, Dokl. Akad. Nauk 61, 75 (1948).

48. R.Ch. Burshtein and N.A. Shurmoskaya, Surface Science 2, 210 (1964).

CHAPTER V

IMAGE FORMATION IN THE FIELD-ION MICROSCOPE

V-1. INTRODUCTION

In the past few years appreciable efforts have been made to elucidate the mechanism of image formation in the field-ion microscope. Müller and co-workers[1,2], Gomer[3], Brandon[4] and Southon[5] in particular have done much experimental and theoretical work with this objective in view. Nevertheless there still remain many important problems to be solved and in some respects the theoretical developments seem not to keep pace with the experimental progress in making images of all kinds of metals. This situation is rather unsatisfactory, for if it is not possible to give an unequivocal interpretation of the experimentally observed phenomena, we might on the one hand arrive at false conclusions regarding the systems in question, while on the other hand we would be unable to fully utilize the potentialities of the ion-microscope technique. This seems true in particular for the use of the ion microscope in adsorption studies, which as we have discussed in the previous chapter, has given rise to completely different interpretations of essentially similar ion images. So far, however, little attention has been paid to the effect of adsorbed gases on image formation.

The possibility of calculating the ion current generated at the metal tip and the understanding of image formation in the ion microscope, operated under certain conditions, depend on a knowledge of

(i) the supply of gas particles to the area where ionization can take place;
(ii) the value of the ionization probability of a particle in this area; and
(iii) the way these two factors vary with the shape and structure of the metal surface, the latter being either clean or (partially) covered with adsorbate.

To evaluate the variation of ion current and image structure with operating conditions, i.e. with the applied voltage, the temperature and the pressure of the image gas and of any other residual gas, we need to know the effect of varying conditions on supply and ionization probability, taking into account the possibility that at a metal tip, having a heterogeneous surface, the events at neighbouring patches may influence each other.

The gas supply to the ionization region is governed by gas kinetics in the highly inhomogeneous field. A quantitative treatment will be extremely difficult, but at least a qualitatively correct kinetic model is required to understand the current-voltage characteristics at different temperatures.

The theories developed to explain the ionization near a metal surface have so far provided only a rough picture, as they fail to describe adequately the effects of the non-uniformity of the surface structure on an atomic scale. The very existence of high-resolution ion microscopy, however, depends on this fine structure, clearly demonstrating the need for more advanced theories.

In the present chapter an attempt is made to review the most important aspects of current generation and image formation, some of which

have already attracted much attention, while others have not. The author realizes that the discussion presented here is mainly qualitative, sometimes even speculative and in no way conclusive. Nevertheless it seems worthwhile, if for no other reason than to draw the attention to some intriguing problems which need more experimental and theoretical effort to be solved.

V-2. GAS SUPPLY AND ION CURRENT

(a) General

Owing to the highly inhomogeneous field applied during operation of an ion microscope, gas particles present in the field are attracted by polarization forces to the tip region which acts as a potential-energy well. For a particle with a permanent dipole moment P and a polarizability α in a field with strength F the potential energy is given by

$$V(F) = -PF - \tfrac{1}{2}\alpha F^2 \qquad (32)$$

if it is assumed that the dipole moment is completely oriented in the field direction. In the following only gases having P = 0 are considered.

With respect to the polarizability the question arises whether at these high fields (≈ 4.5 V/Å) we may still use values derived from low-field experiments. There are indications that at high fields the induced dipole moments do not vary linearly with the field strength any longer. However, since it is by no means clear whether there is question of a saturation of the polarization or a hyperpolarizability[6], we will further assume that the known values of α remain valid at high field strength.

The moment the field is switched on, the initially Maxwellian velocity distribution of the gas particles drastically changes and there is a net flow of particles to the tip, so that they arrive at its surface at a greatly increased rate.

For a spherical geometry, i.e. when

$$F(r) = F(r_t)\left(\frac{r_t}{r}\right)^2 , \qquad (33)$$

where F(r) is the field strength at a distance r from the centre of a spherical tip with radius r_t, Gomer[3] has calculated that the ratio of the effective capture cross-section to the geometrical one is given by

$$\sigma = \left(\frac{\rho}{r_t}\right)^2 = 1 - 2/3\ V(F_t)/kT , \qquad (34)$$

where ρ is the radius of a "sphere of capture", and T the temperature of the gas.

According to Southon[7] the calculation has to be corrected and eq. (34) replaced by

$$\sigma = (-\pi V(F_t)/kT)^{1/2} \quad . \tag{35}$$

This formula, however, cannot be of general validity since at very low fields σ must approach unity and not zero.

The gradient of the polarization energy, i.e. the force acting on a gas particle, can be found by differentiating eq. (32) with the aid of eq. (33). It follows that

$$\frac{dV(F)}{dr} = \frac{2}{r}\,(PF + \alpha F^2) \quad . \tag{36}$$

Further, the full polarization velocity of a particle is given by

$$v = F(r_t)\left(\frac{\alpha}{m}\right)^{1/2} \quad , \tag{37}$$

where m is the mass of a particle.

When no ionization takes place and metal tip and gas have the same temperature, equilibrium is obtained when the particles have transferred their polarization energy to the metal and the Maxwellian velocity distribution is restored. The rate of this process is determined by the accommodation coefficient, i.e. the fraction of kinetic energy transferred in one collision.

The equilibrium gas concentration C_e (number of particles per cm^3) in a region with field F is given by

$$C_e = C_g \exp\left(-\frac{V(F)}{kT}\right) \quad , \tag{38}$$

where C_g is the concentration in a region where $F = 0$.

With field ionization occurring there is again a flow of gas particles to the tip region, replenishing the depleted ionization region; consequently, in this case there is also a small net energy transfer.

When particles need a time Δt for traversing the ionization region, the fraction of them that will become ionized during the passage amounts to

$$S = 1 - \exp\left(-\int_0^{\Delta t} \frac{dt}{\tau}\right) \quad , \tag{39}$$

where τ is the characteristic time required for ionization at a particular distance from the surface (cf. eq. (21)). In what follows we will call S the "integrated ionization probability".

If, as a fair approximation, ionization is considered to take only place in a thin zone in which τ is assumed to be constant, eq. (39) reduces to

$$S = 1 - \exp(-\frac{\Delta t}{\tau}) \ , \tag{40}$$

signifying that a larger integrated ionization probability can be achieved either by a decrease in τ (at a higher field strength) or by an increase in Δt (e.g. by a smaller particle velocity). The ionization process is thus selective with respect to the particle velocity, or more correctly, to the time of residence in the ionization zone, preferentially "picking out" those particles which, if there were no ionization, would gradually have built up the equilibrium concentration near the tip.

In principle the ion current can be calculated by taking the sum over all particles entering the ionization zone per unit time, each being multiplied by its integrated ionization probability.

In an alternative approach the ionization rate per unit volume can be expressed as a product of a rate constant times the steady-state concentration in the ionization zone. The rate constant is obviously equal to $\frac{1}{\tau}$ and can be considered to be practically independent of temperature. The temperature-dependent rate constant as derived by Gomer[3] for a special case (case (d) hereafter) does not seem to be a true one, because it implicitly involves the particle concentration.

A quantitative treatment of the most general case requires a detailed description of the particle-velocity distribution in the tip region. Although at present this seems rather difficult to achieve, it is possible to consider the limiting cases and come to qualitative predictions for the intermediate ones.

The following applies to the generation of current at a surface which is uniform in field strength and ionization probability, while metal tip and gas are at the same temperature.

(b) Ion current at high field strength

When every particle entering the ionization zone is ionized, either during its first passage or on its rebound from the surface, the current is limited by the supply function Z,

$$Z = \sigma N \ , \tag{41}$$

where

$$N = C_g \left(\frac{kT}{2\pi m}\right)^{1/2} \tag{42}$$

gives the number of particles striking per second unit area if F were zero.

The ion current is then given by

$$i = q\ 4\pi r_t^2\ Z\ , \tag{43}$$

where q is the electric charge of the ion.

Equation (43) is an approximation because the actual capture surface for a real tip need not be exactly equal to $4\pi r_t^2\ \sigma$ (see section V-3.).

The zero-field rate of arrival per unit area N can also be expressed

$$N = \frac{p}{(2\pi mkT)^{1/2}}\ , \tag{44}$$

where p is the gas pressure in the region with F = 0. With $p = C_g kT$ eq. (44) transforms into eq. (42).

The use of (42) or (44) depends on the experimental conditions, i.e. on whether C_g or p is kept constant while varying the temperature. In the former case the ion current should be temperature-independent when σ conforms to eq. (35), whereas σ of eq. (34) implies a dependence on $T^{-1/2}$ since normally $-2/3V(F_t)/kT \gg 1$. If the pressure in the tube is kept constant there is a dependence on T^{-1} or $T^{-3/2}$, respectively.

Recently Feldman and Gomer[8] have conducted low-temperature experiments in which they immersed the tube in a cryostat and measured the pressure in a side-arm at 300 °C; in that case $p = p_{300}(\frac{T}{300})^{1/2}$.

At constant temperature the current will increase in proportion to pressure and field strength owing to a larger supply according to eq. (44) and (35).

The case of a supply-limited current occurs when τ is much smaller than the time $\Delta t_{in} + \Delta t_{out}$ a particle would need to pass in and out through the ionization zone. The average steady-state concentration C_s in the ionization zone with width d is equal to $Z\frac{\tau}{d}$, which, multiplied by the ionization volume and the rate constant $\frac{1}{\tau}$, of course leads to the same expression for the ion current as eq. (43).

If the accommodation of incoming particles having a kinetic energy $\frac{1}{2}\alpha F_t^2 + 3/2\ kT$ is very small, $\Delta t_{out} \approx \Delta t_{in}$ and the field would have to be very high to ionize all incoming particles. For helium atoms with the polarization velocity (37), assuming a width d = 0.5 Å, and taking τ equal to its value at the critical distance x_c (eq. (24)), it is calculated that $S(\Delta t_{in}) \approx 1$ at a field strength of about 7 V/Å.

The more efficient the accommodation is, the more Δt_{out} increases, so that lower fields can ionize all particles on their way out.

(c) Ion current at low field strength

The other extreme of current generation is represented by the case where the rate of ionization is so low that the gas concentration in the ionization zone remains nearly equal to the equilibrium concentration. This situation occurs at relatively low fields, when τ is so large that every particle can pass many times back and forth through the ionization zone and become completely accommodated before being ionized. Then

$$i = q\ V\ \frac{1}{\tau}\ C_g\ \exp(-\frac{V(Ft)}{kT}) \qquad (45)$$

where V is the volume of the ionization zone in which τ is assumed to be constant.

With decreasing temperature the gas concentration near the tip and hence the ion current increases. The particular situation where the concentration near the tip becomes very large, approaching the value for the liquid state, will be discussed under (e).

(d) Ion current at moderate field strength

In the cases intermediate between those discussed in (b) and (c) the ionization is far from complete, but the steady-state concentration C_s in the ionization zone less than C_e. Conditions of accommodation and field strength are such that on the average particles traverse the zone several times and are at least partly accommodated before they are ionized.

The ion current can be formally expressed by

$$i = q\ V\ \frac{1}{\tau}\ C_s\ . \qquad (46)$$

The temperature dependence of (46) at constant field can be expected to lie between that of (43) and (45). This would mean that the ion current will always increase with decreasing temperature, and will do so more sharply as case (c) (high value of τ) is approached more closely. Only if the current is limited by the supply function Z and C_g is kept constant, will it be temperature-independent.

In an attempt to describe the "hopping" motion of the particles in a detailed kinetic model Gomer[3] arrived at a less general conclusion regarding the temperature dependence. Thus he calculated a larger current for the ionization of helium atoms at 20 °K than at 4 °K.

Gomer[3] and Müller[1,9] considered particles which become accommodated at the tip surface and derived an average hopping height h. They argued that when at very low temperatures h, which is proportional to the tip radius, falls below the critical distance x_c, most incoming particles will diffuse out of the high-field region towards the shanks of the tip without becoming ionized. This diffusion mechanism should hold whether or not ionization takes place. If for simplicity the mechanism is considered for the case

where ionization can be neglected it would follow that, while net energy is no longer taken up from the field, a directed flow of mass takes place. This is obviously incompatible with first principles and the model should therefore be rejected. Some time ago Southon and Brandon[5] also pointed out that the gradient of polarization energy along the tip surface is comparable with the radial gradient, which makes a preferential diffusion to the shanks unlikely.

The concept of an average hopping height seems of limited use here as it gives only the height of the jumps of a particle at the surface with a kinetic energy equal to kT; it does not tell anything about the distribution of the particles. Incidentally, when ionization can be neglected the hopping height averaged over all particles must be equal to the weighted average of the positions of the particles at equilibrium. With decreasing temperature the atmosphere around the tip becomes denser and thus the average hopping height will decrease. But the hopping-height distribution will change, too, and it can easily be understood that a decrease of the average is accompanied by an increase in the number of particles with a hopping height equal to x_c. Consequently, it is unlikely that there is an optimum operating temperature which depends on the tip radius, as was suggested by Müller[1].

Brandon[4] has divided the incoming particles into a fraction that completely escapes from the potential well near the surface and a fraction which is "trapped". Now the latter fraction, a net supply function, is considered to replace Z in calculating the ion current with eq. (43). However, this reasoning would be valid only if any incoming particle is either ionized on its first passage and rebound or completely escapes. Such an approach ignores the fact that at intermediate fields the steady state is marked by a gas concentration around the tip which has increased compared with C_g. The increase comprises the "hopping" particles which, though they can be regarded as being trapped, are not ionized.

It is also essentially the increased gas concentration which causes the number of atoms arriving in unit time at unit area of the ionization zone to differ from the supply function Z, contrary to what is often supposed. In our view the function Z is only useful when almost every incoming particle is indeed ionized.

Although the following picture is not easily cast in a more quantitative form, it might give an adequate kinetic description of the field ionization process.

When the ionization rate is still so low that the gas concentration in the region from which the supply is drawn remains about equal to the equilibrium concentration, the velocities of the particles entering the ionization zone still obey a Maxwellian distribution corresponding with the operating temperature. As the particles pass through the zone the velocity distribution changes, because the ionization process preferentially removes the particles with a relatively long time of residence. In consequence the average velocity of the emerging particles has increased. For the same reason the distributions in the various directions are no longer the same: relatively more particles are now travelling in radial direction towards the tip surface. After they have struck this surface, there will be a certain amount of accommodation and directional randomization. These two processes tend to restore a Maxwellian distribution, the former of them decreasing the average velocity of the reflected particles[10]. Upon passing back through the zone, the particles go through a similar process.

Now a decrease in temperature at constant field will increase the rate of arrival, because the exponential increase of the concentration in the supply region far overcompensates the decrease in velocity ($\sim T^{-\frac{1}{2}}$). In addition, the integrated ionization probability increases with the time of residence. An effect of probably minor importance is the change in accommodation efficiency, which, according to calculations by McCarrol and Ehrlich[11] for atoms on a linear lattice, should rise with decreasing incident energy.

All effects thus lead to an increase in ion current upon lowering the temperature. Obviously case (c) above presents the limit for very low fields, where even the velocity distribution in the ionization region does not deviate from Maxwell's law.

The combined effects of an increase in the supply and in the time of residence can equally well be expressed as an increase in the steady-state concentration C_s of eq. (46).

Analogous arguments hold at higher field strength. The ionization now lowers the concentration in the supply region below the equilibrium value. The rate of supply to the ionization zone will therefore be diminished, while the incoming particles no longer have a Maxwellian velocity distribution corresponding with their thermal energy kT. The gas has become effectively "hotter" owing to the ionization of low-energy particles. Also, particles travelling in radial direction predominate more markedly. The effect of a decrease in temperature will be smaller in this case than at lower field strength. No great increase in the gas concentration in the supply region can be expected, because the particles which bounce off from the tip without being ionized are precisely those with a relatively high kinetic energy of which the thermal energy is only a small fraction. A decrease in the latter will therefore have less effect in keeping these particles close to the tip.

Ultimately a situation is reached where the current becomes limited by the supply function Z. In that case all - nearly radially arriving - particles have about the kinetic energy $\frac{1}{2}\alpha F(r_t)^2$. Compared with this polarization energy the thermal energy can be neglected; for example, for helium atoms in a field of 6 V/Å, $\frac{1}{2}\alpha F(r_t)^2 = 0.25$ eV or equivalent to 2900 °K. The temperature dependence can then only be small (see case (b)).

We thus arrive at the general statement that the dependence on thermal energy will be smaller as the effective gas temperature is higher, that is as the rate of ionization is higher. This rule seems to be confirmed by the experimental current-voltage characteristics at 20 °K and above, which are discussed in section V-3.

(e) Liquid films

So far the particle concentration near the tip has been assumed to be less than that in the liquid state, a situation which applies to most experiments with the field-ion microscope. It is, however, well conceivable that field ionization occurs under conditions where a liquid film is formed around the tip, even of the less polarizable rare gases, such as helium and neon. In that case the previous discussions are not valid any more.

Whether liquid film formation is possible can be estimated by applying eq. (38). Thus it is calculated that for helium with $\alpha = 2.02 \times 10^{-25}$ cm^3 at $p = 10^{-3}$ Torr and $F(r_t) = 4.5$ V/Å the equilibrium concentration C_e (when

ionization is neglected) near the tip at 20 °K would be $\approx 10^{49}$ and at 4 °K even $\approx 10^{132}$ atoms/cm^3. As the concentration in liquid helium is about 10^{22} atoms/cm^3 this obviously would mean that a liquid layer is formed having about the latter concentration.

In the 20 °K case no distinction can be made between the liquid and the gaseous phase because the critical temperature of helium is lower than 20 °K (T_{cr} = 5.2 °K). However, above T_{cr} the "liquid" film can be considered to terminate at the point where the value of C_e calculated with eq. (38) becomes about equal to that in the liquid. Calculation for helium at 20 °K shows that this happens at a field strength $F \approx 2$ V/Å. With the aid of eq. (33) the thickness w of the liquid layer can then be roughly estimated at 0.5 r_t. At 4 °K and $F(r_t) = 4.5$ V/Å the helium film, being in equilibrium with the gas phase at $p = 10^{-3}$ Torr and F = 0, terminates at $F \approx 0.8$ V/Å, i.e. at a distance $w \approx 1.4\ r_t$.

Similar calculations for neon at $p = 10^{-3}$ Torr and 3.5 V/Å (which is about the best image voltage) give a value of $w \approx 0.8\ r_t$ at 20 °K, while "liquid" (T_{cr} = 44.4 °K!) formation at 77 °K is negligible.

We thus note that with a tip radius r_t = 500 Å the calculated thicknesses range from 250 to 700 Å. A more rigorous derivation of film thicknesses should take into account that owing to the presence of the dielectric material, the variation of field strength with distance from the tip is different from that in vacuum. At equal applied voltage the field at the same distance will be smaller in the liquid film than in vacuum and show a discontinuity at the meniscus (of course, a decrease in field strength near the tip also occurs before liquid is formed). With helium and neon the effects are small owing to the small dielectric constant of the liquids (e.g. $\epsilon_{He} = 1.05$) and a fortiori of the gases. Besides, the small droplet will have a higher vapour pressure than a liquid with a plane surface. However, calculation shows that in most cases this correction can also be neglected in making an estimate of film thicknesses.

In reality the ionization process causes the particle concentration near the tip to fall below C_e and tends to increase the effective gas temperature. However, if we assume for the sake of argument that even under these conditions a liquid film can still be present, it is interesting to consider field ionization from such a layer in more detail.

In liquid films of an appreciable thickness the layers closest to the metal surface will have a rather rigid structure since the polarization forces acting on the particles will greatly restrict their mobility. An estimate of this effect can be made by comparing the value of the gradient of the polarization energy (eq. (36)) near the tip surface with kT. For helium at 4 °K, $F(r_t) = 4.5$ V/Å and $r \approx r_t = 500$ Å these values are 1.8×10^{-15} erg/Å and 0.55×10^{-15} erg, respectively.

Furthermore, with helium at 4 °K and a fortiori with neon at 20 °K the first atom layer is kept to the metal surface also by physisorption bonding forces which become of importance at these low temperatures.

A point which has not so far been taken into account but which can no longer be neglected is the fact that the gas particles have finite dimensions. The ionization region is not a continuous zone but is essentially made up of small discs above the clearly protruding atoms. Measurements of energy distributions in field ionization by Tsong and Müller[12] have revealed that these discs have a depth of about 0.2 Å only and that they are located at a

distance $x_c \approx 4$ Å from the surface. It thus follows that the thickness of the ionization region is far less than the atomic radii of all gases, while the critical distance x_c is of the order of interatomic distances (e.g. about 3.6 Å in liquid helium).

These facts are important with regard to the supply of particles to the ionization "zone". It is easily seen that in a completely rigid structure the steric configuration of the first layers determines whether atoms are located most favourably, having their centres coinciding with the ionization discs, or whether they cover the discs imperfectly.

The definition of a concentration in regions that are small compared with the atomic dimensions now becomes meaningless, for there is no longer an averaging-out over all points of space as is possible for the gas phase.

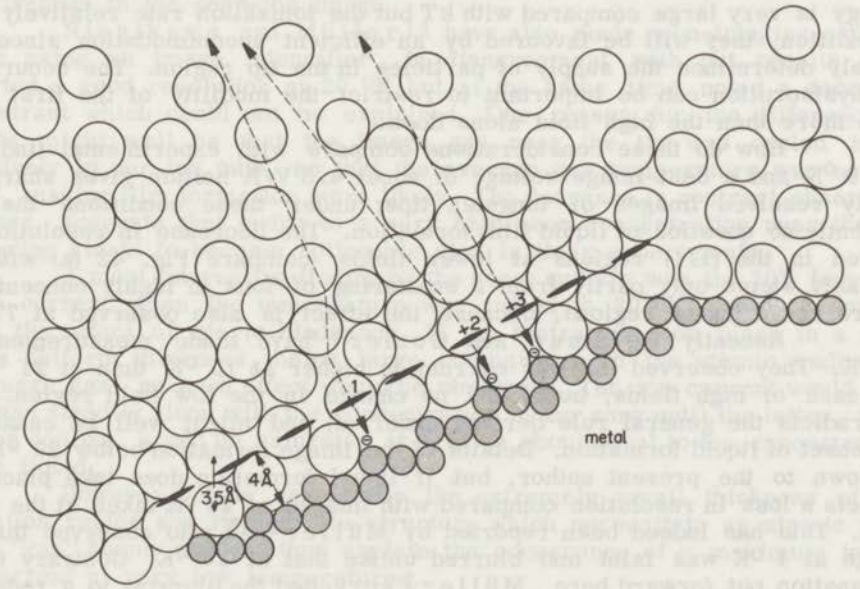

Figure 40

Steric hindrance in field ionization from liquid films; assumed values of critical distance x_c and interatomic distance in liquid being 4 and 3.5 Å, respectively

An unfavourable configuration leading to what might be called "steric hindrance", can be dissolved by the inducement of structural fluctuations such that atoms get a chance to pass through an ionization disc. This is a question of creating holes in the structure which requires a certain amount of activation counter to the polarization forces. It is therefore more

likely to occur according as the (effective) temperature is higher. Such a situation is schematically represented in Fig. 40, where the temperature is assumed to be above T_{cr} of the gas, so that no meniscus is present. The interatomic distance in the liquid is taken to be 3.5 Å, while $x_c = 4$ Å relative to a rather arbitrarily chosen surface. Ionization will only take place at site 1 and, with far smaller probability, at sites 2 and 3, whereas it can proceed elsewhere only when locally a fluctuation in the configuration occurs similar to the one assumed to have taken place at site 1. The few ions which are then produced will be scattered by the densely packed layers; consequently they lose energy and do not give rise to a resolved image on the screen.

When the field strength is increased the ionization rate rises and eventually becomes so high that the supply cannot maintain the concentration at the value of the liquid state. For these conditions the discussion given under (d) becomes valid again.

More generally, it follows that effects of steric hindrance due to formation of liquid films are most likely to appear when the polarization energy is very large compared with kT but the ionization rate relatively low. In addition, they will be favoured by an efficient accommodation since this largely determines the supply of particles in the tip region. The occurrence of physisorption can be important to restrict the mobility of the first layer even more than the high field alone does.

How do these considerations compare with experimental findings? At 20 °K and a best-image voltage of about 4.5 V/Å helium gives sharp and highly resolved images of tungsten tips; under these conditions there is evidently no question of liquid film formation. The decrease in resolution observed in the (111) regions at lower fields (compare Fig. 42 (a) with (e)) probably stems only partly from a scattering of ions in highly concentrated layers above these regions, because the effect is also observed at 77 °K.

Recently Feldman and Gomer[8] have made measurements at 15 °K. They observed that the current is higher at 15 °K than at 21 °K in the case of high fields, but found no change in the low field region. This contradicts the general rule derived under (d) and might well be caused by the onset of liquid formation. Details of the image formation below 20 °K are unknown to the present author, but if liquid formation does take place one expects a loss in resolution compared with images at 20 °K taken at the same field. This has indeed been reported by Müller[9,13] who observed that the image at 4 °K was faint and blurred unlike that at 20 °K. Contrary to the explanation put forward here, Müller[1] attributed the blurring to a reduction of the contrast in field profile due to the presence of a mobile physisorbed helium layer.

More pronounced effects should be found with gases having larger polarizabilities and higher boiling points. We have made some preliminary experiments by imaging tungsten with neon. Although for lack of an image intensifier the photographs obtained were rather faint and not suitable for reproduction, yet they produced interesting evidence. At 10^{-3} Torr and 77 °K the neon-ion image was highly resolved and comparable to a helium-ion image. But when we replaced the liquid nitrogen in the tip Dewar by liquid hydrogen, the image turned completely diffuse except at the outer edges where disorderly arranged atoms were present. A comparison of the overall intensity of the patterns suggested that the total ion current was less at 20 °K than at 77 °K, which agrees well with a model of rigid neon layers unfavourably

packed relative to the location of the loci of maximum ionization probability. It should be remarked, however, that a loss in energy owing to scattering also gives rise to a decrease in intensity. Warming to 77 °K caused reappearance of the detailed image with an attendant increase in intensity.

The finding that the protruding atoms at the edges remained sharp and were even more intense at 20 °K than at 77 °K can be explained as follows:

The calculations mentioned above showed that there is no "liquid" formation at 77 °K. The optimum operating temperature corresponding with the maximum steady-state concentration (and hence maximum ion current) consistent with a good resolution might therefore be somewhat below 77 °K. Now at 20 °K the same optimum gas concentration can be found in regions with lower field strengths, for instance, near the shanks of the tip, which are imaged along the edges of the pattern. In fact, it should be possible to obtain a map of the differences in local field strength by slowly cooling a tip from 77 °K down to 20 °K and observing the onset and progress of the diffusiveness in the neon-ion image.

Nishikawa and Müller[14] have also made neon-imaging experiments using an image intensifier. In disagreement with out results they reported a good resolution at 20 °K but at the same time noted a decrease in contrast which could not be explained. One reason for the difference in results might well be that the image gas near the tip was cooled more effectively in our ion tube, so that the average gas temperature was nearer 20 °K, making film formation more likely. The decrease in contrast observed, however, suggests that owing to a very high neon concentration near the tip scattering starts to become noticeable also in their experiments.

A most interesting finding by the same authors was the 10% increase in ion current when the temperature was raised to 30 °K, which seems to prove the effect of steric hindrance. If the ionization took place in a zone with a uniform thickness, being large compared with the atomic radius of the image gas, no such effect would be observed. The ion current would then increase steadily along with the concentration in the zone until the latter, upon further cooling, would be saturated at a value about equal to the concentration in the liquid.

However, it is essentially the extremely small thickness of the ionization region and its discrete structure which necessitate an atomic view of the "gas" supply and can thus explain the occurrence of a maximum in the ion current at very low temperatures.

Scattering of ions passing through a liquid layer should have a pronounced effect of the energy distribution of the ions, smearing it out to lower energies. The effect has already been pointed out by Beckey[15], who noticed its absence in his field ionization experiments with H_2O at 1 V/Å and 300 °K. Under these conditions the equilibrium film thickness is about 0.2 r_t only, so that the ionization itself probably prevents the film becoming thicker than a few layers. This, however, seems sufficient to give the association complexes of water as observed by Inghram and Gomer[16] and by Beckey[15].

A conclusive proof of the model proposed here should be obtained by measurements of energy distributions of neon ions (or those of other rare gases) under conditions where the image is diffuse.

It is interesting to note that in field ionization from a liquid layer the rate of removal of the ions might become a limiting factor too. A very crude estimate of this effect can be made by solving the equation of motion of an ion under the action of the applied field and the frictional force exerted by the liquid. For neon ions with a radius of 1.2 Å, assuming a constant field of 3.5 V/Å and a viscosity of 10^{-4} poise at 20 °K, it is calculated that after a time interval equal to τ (x_c) $\approx 10^{-13}$ s the ion is only about 20 Å removed from the surface. This distance is indeed of such an order of magnitude that the potential near the surface might become influenced during the time required to ionize the next atom.

In the discussion presented above we only paid attention to changes in the supply, but the presence of "adsorbed" layers might also modify the ionization probability by changing the potential situation near the surface (decrease in field strength). However, for a physisorbed helium or neon layer the effect on the ionization probability will most likely be small in contrast with that expected for a chemisorbed layer which strongly interacts with the outer layers of metal atoms. The point will be discussed in more detail in section V-5.

V-3. i-V CHARACTERISTICS OF THE HELIUM-ION MICROSCOPE

Measurements of ion currents in the field-ion microscope were first reported by Drechsler and Pankow[17] and Müller and Bahadur[10]. The results of the latter authors, though not allowing a detailed analysis, confirmed the general aspects of the theory they gave at that time.

A far more extensive study including a correction for secondary electron emission effects was made by Southon and Brandon[5] (hereafter referred to as S and B). They investigated the characteristic variation of the ion current with the applied voltage in a helium-ion microscope as a function of tip radius, temperature and pressure. From their experimental findings they concluded that there were several disagreements with the theory given by Müller[1,10] and Gomer[3], in particular as regards the dependence of the ion current on the voltage and the tip radius. Also, assuming the ionization to be complete, the current at high fields was always less than calculated from the supply function as derived by Gomer (eq. (41)). Only the predicted proportionality between current and pressure could be confirmed.

However, in the discussion of their results S and B did not take into account that the "emitter" surface in the ion microscope is not uniform with respect to field strength and ionization probability as is tacitly assumed in the theories outlined in the previous section. Although the non-uniformity of the surface greatly complicates a quantitative treatment of the current generation, it might give a reasonable explanation for many of the features of the i-V characteristics. To discuss the question in more detail, we will use the experimental data of S and B.

(a) The basic i-V characteristic

The upper curve of Fig. 41 shows in a logarithmic plot the typical variation of the total helium ion current with applied voltage for a clean field-evaporated tungsten tip at 77 °K. The interpretation generally[5,8] given is that the integrated ionization probability (39) increases rapidly with the field in the region AB and is nearly unity at the "cut-off" B, remaining constant in the working range BC, while in this region the limiting supply function Z increases with the field. At C the evaporation field is reached.

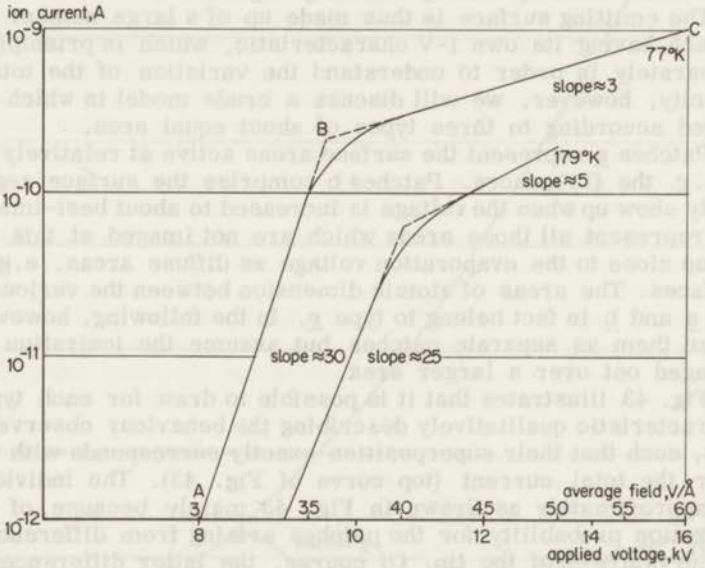

Figure 41

Current-voltage characteristics for field ionization near a tungsten tip at 77 °K and 179 °K, respectively (after Southon and Brandon[5])

Whereas the large slope (≈ 30) in the range AB seems reasonable in view of the dependence of the ionization probability on the field, the slope (≈ 3) in the range BC is in conflict with theory. As discussed above, the latter predicts either a proportionality to F^2 (eq. (34)) or a variation with F when instead of eq. (34) eq. (35) applies.

However, the characteristic shape of the experimental curves can be understood when it is realized that the measured total ion current is the sum of the contributions from surface areas whose individual i-V characteristics might be different. To illustrate this, Fig. 42 shows a sequence of helium-ion images of a clean and ordered tungsten tip taken at different applied voltages, all other conditions being kept the same (tip temperature 20 °K). It is observed that at voltages far below the best-image voltage only certain

areas, particularly the (111) regions, emit while other regions do not yet show up. This causes a highly non-uniform intensity distribution in the image. Near the best-image voltage the emittancy is far more spread over the whole surface, except in the most densely packed regions like the (110) and (211) faces. A non-uniformity on an atomic scale, in fact the basis of the ion microscope, remains and is only gradually removed by applying still higher voltages (pictures not shown).

The most remarkable thing here is that the intensity in the initially highly emitting regions drops at higher voltages. The ion current from these regions apparently goes through a maximum when the applied voltage is inincreased. In the initially weakly emitting regions this is not observed.

The emitting surface is thus made up of a large number of different patches, each having its own i-V characteristic, which in principle should be studied separately in order to understand the variation of the total current. For simplicity, however, we will discuss a crude model in which the patches are arranged according to three types of about equal area.

Patches a represent the surface areas active at relatively low applied voltages, e.g. the (111) faces. Patches b comprise the surface regions which subsequently show up when the voltage is increased to about best-image voltage. Patches c represent all those areas which are not imaged at this voltage but only show up close to the evaporation voltage as diffuse areas, e.g. the (211) and (110) faces. The areas of atomic dimension between the various ionization centres of a and b in fact belong to type c. In the following, however, we will not consider them as separate patches but assume the ionization probability to be averaged out over a larger area.

Fig. 43 illustrates that it is possible to draw for each type of patch an i-V characteristic qualitatively describing the behaviour observed from the ion images, such that their superposition exactly corresponds with the characteristic for the total current (top curve of Fig. 43). The individual curves should be approximately as drawn in Fig. 43 mainly because of differences in the ionization probability for the patches arising from differences in local radius of curvature[18] of the tip. Of course, the latter differences also give rise to a non-uniformity in the supply. This becomes the more pronounced as the ionization rate is lower, for reasons similar to those previously discussed with respect to the temperature dependence. At low rates the concentration in the supply region is an exponential function of F, while at high rates the supply is proportional to F (eq. (35)).

When ionization starts at patches a, initially the current will steeply rise owing to a sharp increase in both ionization probability and concentration. At the field strength where the integrated ionization probability for every impinging particle approaches unity the current becomes limited by the supply of particles to the ionization zone above patches a. However, this supply is not simply what might be called a "radial" supply from the gas phase, but owing to the fact that little or no ionization occurs on all other patches a "lateral" supply from these patches to patches a will take place as well. This circumstance has recently also been noted by Müller et al.[19].

The limiting situation would be that every particle arriving at the other patches would be ionized above patches a without having a chance to escape through the ionization zone back to the gas phase. The current would then be limited by the total supply to the tip surface. In the other extreme the ionization above patches a does not decrease the equilibrium concentration above all other patches.

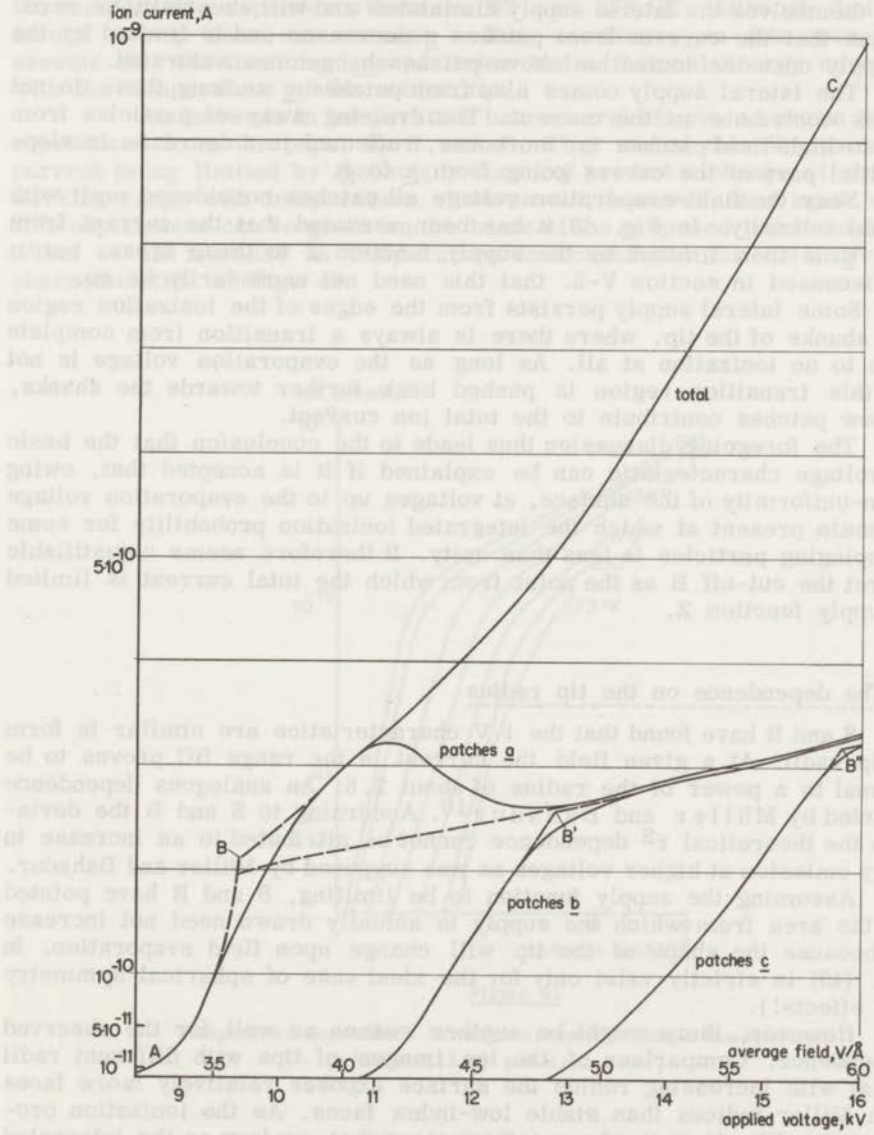

Figure 43

Analysis of the current-voltage characteristic at 77 °K of Fig. 41

In the analysis given in Fig. 43 it is assumed that the real situation is between the two extremes and that in particular the neighbouring patches b contribute to the ionization above patches a. Once ionization starts above patches b themselves the lateral supply diminishes and will eventually be zero. This means that the current from patches a decreases and is limited by the radial supply once the ionization above patches b becomes saturated.

The lateral supply comes also from patches c as long these do not themselves contribute to the current. The draining away of particles from low-field to high-field patches is, moreover, reflected in a decrease in slope of the initial part of the curves going from a to c.

Near the field-evaporation voltage all patches considered emit with about equal intensity. In Fig. 43 it has been assumed that the current from a, b and c is then limited by the supply function Z to these areas, but it will be discussed in section V-5. that this need not necessarily be so.

Some lateral supply persists from the edges of the ionization region near the shanks of the tip, where there is always a transition from complete ionization to no ionization at all. As long as the evaporation voltage is not reached this transition region is pushed back further towards the shanks, making new patches contribute to the total ion current.

The foregoing discussion thus leads to the conclusion that the basic current-voltage characteristic can be explained if it is accepted that, owing to the non-uniformity of the surface, at voltages up to the evaporation voltage areas remain present at which the integrated ionization probability for some of the impinging particles is less than unity. It therefore seems unjustifiable to interpret the cut-off B as the point from which the total current is limited by the supply function Z.

(b) The dependence on the tip radius

S and B have found that the i-V characteristics are similar in form for all tip radii. At a given field the current in the range BC proves to be proportional to a power of the radius of about 2.5. An analogous dependence was reported by Müller and Bahadur[10]. According to S and B the deviation from the theoretical r^2 dependence cannot be attributed to an increase in secondary emission at higher voltages as was supposed by Müller and Bahadur.

Assuming the supply function to be limiting, S and B have pointed out that the area from which the supply is actually drawn need not increase with r^2 because the shape of the tip will change upon field evaporation. In fact, eq. (43) is strictly valid only for the ideal case of spherical symmetry (no edge effects!).

However, there might be another reason as well for the observed $r^{2.5}$ dependence. Comparison of the ion images of tips with different radii shows that with increasing radius the surface exposes relatively more faces with high Miller indices than stable low-index faces. As the ionization proceeds more readily above the former this means that, as long as the integrated ionization probability for impinging particles is not unity everywhere above the surface, the current will increase faster than corresponds with the increase in total surface area.

(c) The effect of operating temperature

The total i-V characteristic discussed above is typical of the helium-ion microscope operated at low temperature (77 °K). S and B have investigated the temperature dependence between 63 and 273 °K. Although their experimental set-up does not warrant a firm conclusion on this score, we will assume that the incoming gas particles had a thermal energy corresponding with the temperature of the cooled tip.

An increase in temperature has several effects as shown by Fig. 44 reproduced from the paper by S and B. They stated that the theory of the current being limited by the supply does not predict a change of slope in the working range with temperature. It turns out, however, that again a reasonable explanation can be given on the basis of the proposed patch model, if the effect of an increase in temperature is considered for the individual i-V characteristics of Fig. 43.

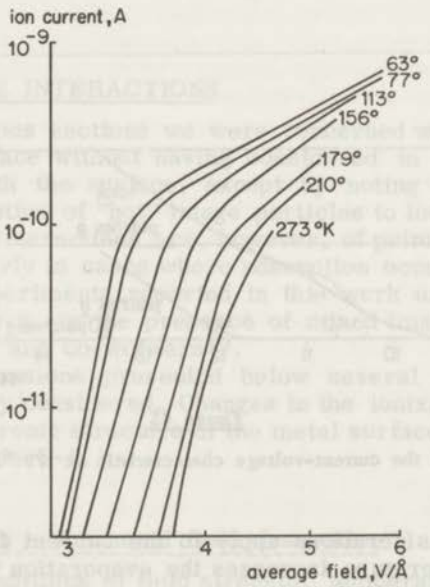

Figure 44

Temperature dependence of tungsten current-voltage characteristics (after Southon and Brandon[5])

It was shown in section V-2. that at a given field strength, i.e. a fixed value of τ, the steady-state concentration near the tip surface and hence the ion current decreases with increasing temperature. The initial part of all i-V characteristics will therefore shift to higher applied voltages. At higher field strengths the temperature dependence is smaller in fair agreement with the prediction made previously.

For patches a it is expected that the lateral supply will diminish faster than the radial supply because the former, being determined by the concentration above patches b, decreases sharply with increasing temperature, while the supply function Z depends less on temperature. In other words, in the low-field region particles impinging on b stand a better chance of escaping instead of being ionized above a according as the temperature is higher. Consequently the maximum in the i-V curve will become less pronounced and perhaps completely disappear at higher temperature.

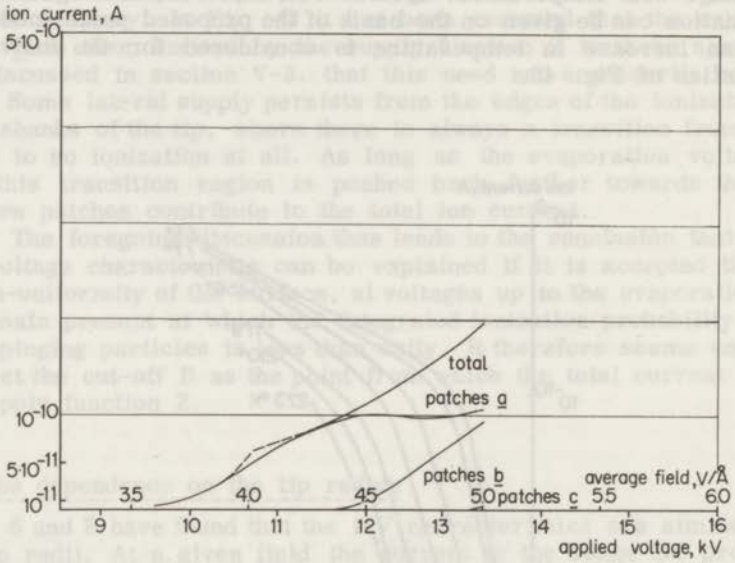

Figure 45

Analysis of the current-voltage characteristic at 179 °K of Fig. 41

Similar considerations apply to the current from patches b and c. However, as the temperature increases the evaporation voltage decreases and evaporation might start before b and c have reached saturation point. The overall effect on the total ion current consists in an increase in slope in the working range. This is illustrated by Fig. 45, which shows an analysis of the lower curve of Fig. 41. The latter approximately corresponds to the i-V characteristic at 179 °K as reported by S and B.

The curves of Fig. 44 indicate that at a temperature higher than about 200 °K even patches a do not reach saturation.

S and B have already pointed out that the magnitude of the temperature dependence of the location of the cut-off B indicates that the gas atoms must have about thermal velocities when they are ionized. This agrees well with the present conclusions, for it means also that the cut-off must still be far removed from the field strength where the total ion current is limited by the supply function Z.

If the foregoing is true, it follows that the temperature dependence of the supply function Z cannot be determined from measurements of the total ion current. Experimentally, this must be done by measuring patch ion currents at a field strength and in a temperature range where Z, if ever, is really the limiting factor in the current generation at the patch. Moreover, an experimental set-up is required such that tip and gas have the same temperature. For, if in actual fact only the tip is cooled and every incoming particle is ionized either before or after hitting the tip, the supply is determined by the temperature of the surrounding walls from which the particles "evaporate". Even the conventional electrode in contact with the cold finger and shielding the tip cannot completely ensure the desired control of gas temperature.

Much better temperature control is possible in cryostat experiments as recently reported by Feldman and Gomer[8]. Their results obtained at 15, 21 and 78 °K seem also to be in agreement with the ideas put forward here.

V-4. GAS-SURFACE INTERACTIONS

In the previous sections we were concerned with current generation at a clean metal surface without having considered in detail the interaction of the image gas with the surface, except by noting the importance of the process of accommodation of "hot" image particles to lower effective temperatures. Gas-surface interactions are, however, of prime interest in field-ion microscopy, particularly in cases where adsorption occurs, either only before imaging as in the experiments reported in this work or also during imaging or field evaporation e.g. in the presence of mixed image gases as have been reported by Müller and co-workers[19].

In the discussions presented below several types of gas-surface interactions are briefly considered. Changes in the ionization probability owing to changes in the electronic structure of the metal surface upon adsorption will be discussed in section V-5.

(a) Accommodation - Promoted field desorption

At fixed conditions of field strength, temperature and pressure the steady-state concentration or, equivalently, the supply of low-velocity image gas particles to the ionization zone is determined by the efficiency with which the gas particles transfer their excess kinetic energy to the metal tip. (When no ionization takes place the efficiency of energy transfer determines the rate at which equilibrium is attained.) Accordingly the accommodation coefficient γ plays an important role in the current generation and image formation in the ion microscope.

For helium to clean tungsten γ is very small. A theoretical value of 0.02 has been derived for γ_{He-W} at large impact energies (above 500 °K)[11]; experimental values[20,21] are as low as 0.016.

Nishikawa and Müller[14] have pointed out that because protruding metal atoms under imaging conditions are close to field evaporation the energy

transfer to these atoms approaches that between free particles. If adsorption effects can be neglected (for helium above 4 °K), an upper limit is provided by the classical expression for elastic collisions between free hard spheres: $\gamma = \frac{4m\,M}{(m + M)^2}$, m and M being the masses of the colliding particles. This gives for helium to tungsten $\gamma_{He-W} = 0.083$.

By determining the difference in applied voltage required to field-evaporate tungsten in vacuum and in helium, Nishikawa and Müller have shown that under evaporation conditions indeed $\gamma_{He-W} \approx 0.1$. For neon to tungsten at 20 °K they similarly found $\gamma_{Ne-W} \approx 0.85$ compared with a classical value of 0.35, which indicates that owing to adsorption effects neon-tungsten collisions at this temperature can no longer be considered elastic. At higher temperatures, however, the experimental γ approaches the classical value.

Since the experiments by Roberts[22] it is known that adsorbed atoms or molecules increase the efficiency of accommodation of helium atoms by acting as intermediate collision partners[11]. A considerable improvement of the accommodation obviously requires a fairly high degree of coverage of the surface. However, at the field strength applied during image formation with helium, most adsorbates are very near to field desorption and need little activation to be removed from the surface. When, moreover, the energy transfer approaches that for free particles it is very probable that by the impact of fast helium atoms the adsorbed species are excited into the ionization zone and become ionized there. This phenomenon has indeed been observed experimentally and is known as promoted field desorption since Ehrlich and Hudda[23] detected that under normal helium-image conditions a hydrogen layer on tungsten is completely desorbed.

In the absence of helium the hydrogen layer almost completely withstands field desorption at the same field strength. That promoted field desorption is also nearly complete for more strongly bonded adsorbates like nitrogen and carbon monoxide on tungsten has been proved in this work. While Ehrlich and Hudda attributed the promotive effect of helium to a bombardment by electrons originating from the helium ionization, Nishikawa and Müller have presented arguments in favour of the polarization-energy transfer mechanism[14]. But the question seems not yet solved unambiguously.

The occurrence of promoted field desorption prevents a permanent improvement of the accommodation unless the removal of adsorbate is compensated by a continuous supply during imaging. Such a supply could take place either directly from the gas phase by penetration through the ionization zone or by surface diffusion along the shanks. For most gases the former mechanism will not apply since radially approaching particles with a relatively low ionization energy stand little chance of escaping ionization at helium-image fields. On the other hand surface diffusion from the shanks requires the presence of a species which is mobile under the operating conditions.

Accommodation effects are supposed to account for the improved performance of the ion microscope which Müller et al.[19] obtained when adding small amounts (1-10%) of neon or hydrogen (deuterium) to the helium-image gas. Whereas addition of neon only slightly decreased the best-image voltage, admixture of hydrogen resulted in a sharp image particularly round the (111) regions at a voltage of about 70% of the value required for pure helium, in which these areas do not show up at the same field strength

(3.2 V/Å). The authors attributed this result to complete accommodation of the helium atoms to the tip temperature (20 °K).

Although the proposed explanation seems interesting some points remain to be clarified. Firstly, one expects promoted field desorption to supply hydrogen continuously to the ionization zone in excess of that entering directly from the gas phase. For instance, in the limiting case where every incoming helium atom in the act of accommodation knocks off one adsorbed atom or molecule, there would be an equal contribution to the ion current by H^+ or H_2^+ ions, probably accompanied by a loss in resolution. However, it is reported that the contribution of hydrogen ions is negligible, while the images remain highly resolved.

If, on the other hand, the rate of field desorption is still relatively small the degree of hydrogen coverage in the steady state must remain large. Then the question arises whether an adsorbed hydrogen layer would not appreciably affect the ionization probability and thus change the image compared with that of the clean surface*.

Secondly there is a remarkable improvement in the resolution, particularly in the (111) region with the helium-1% hydrogen mixture at 3.2 V/Å compared with the image in pure helium at the same field strength, which is far more diffuse in the few areas which then show up.

The bad resolution in the low-field helium images could be due to two causes:

(i) scattering of the ions by the dense gas phase or liquid layers above the protruding areas, or
(ii) an intrinsic lack of contrast in the ionization probability for helium atoms at this field strength.

Whichever of the two may apply, it is difficult to understand how an improvement of the accommodation can result in a better resolution of the image. A greater accommodation efficiency at the same field strength has the effect of increasing the concentration in the tip region and could therefore only enhance the scattering.

In the accommodation model a much larger concentration is indeed required to give at 3.2 V/Å an image intensity which is about equal to that at 4.5 V/Å, for according to eq. (24), the decrease in field strength causes a drop in ionization probability at x_c by a factor of roughly 270. While at 4.5 V/Å particles completely accommodated at 20 °K have a 40% change of being ionized in a single pass, this chance at 3.2 V/Å is only 0.2% if the ionization zone is assumed to have an effective width of 0.5 Å.

The low value of the single-pass ionization probability also shows that particles above the areas round (111) should have ample chance of being drained away to the protruding (high-field) (111) area itself owing to the field

---

* When this chapter had been completed an article by Tsong and Müller[24] appeared, in which they concluded more precisely that the increase in the rate of accommodation is due to a hydrogen layer adsorbed on the shanks of the tip. Such a mechanism is also subject to criticism, however, because (i) helium atoms arriving at the shanks possess little polarization energy, so that accommodation cannot be very important, and (ii) any helium atom with thermal energy, passing from the (low-field) shanks to the (high-field) front of the tip, is again accelerated owing to polarization.

gradient. This constitutes the "lateral" supply previously mentioned.

The second possible cause of a bad resolution obviously is not affected by any change in the accommodation.

(b) Steric effects

Steric effects have been discussed at length in connection with the formation of liquid layers at the metal surface. In a similar way a chemisorbed layer, when it is not field-desorbed, can form a barrier preventing the image atoms from reaching the ionization region. Whether this will occur again depends on the width and the configuration of the adsorption layer and the minimum distance to which an image atom can approach it. In this context details of the accommodation process might become of interest. An atom approaching the surface to which it cannot be bonded slows down when the repulsive forces become active. At the turning point the velocity is zero and then increases again up to a value which is determined by the energy transfer that has taken place. Thus there is a very small region over which the velocity of the particle is low. Three cases can now be distinguished:

(i) the region of low velocity lies between the surface and the ionization zone,
(ii) it coincides with this zone, and
(iii) it lies outside the zone.

In the first case no special effect is observed; it applies, for example, to collisions with a clean surface. The occurrence of the second possibility, though being a remote one, would increase the integrated ionization probability for impinging and rebounding particles. In the third situation the steric hindrance lowers the ionization rate.

However, steric effects in the presence of chemisorption layers are probably of less importance than the change in ionization probability resulting from the change in the electronic surface structure upon formation of chemisorption complexes (see section V-5.).

(c) Formation of ion complexes

Mass-spectroscopic analysis of the ions produced in field ionization has shown that besides the simple parent ion other ionic complexes are often produced as well. Many examples of such complexes can be found in the work of Beckey[15], who showed that hydride ions such as N_2H^+, ArH^+, COH^+ and CO_2H^+ are formed at field strengths of 1-2 V/Å when the presence of traces of water gives rise to a thin liquid film. According to Beckey the parent ions react with this liquid layer.

Particular interest attaches to the occurrence of H_3^+ ions during field ionization of hydrogen as first reported by Clemens and Müller[25]. In this case no liquid film is present, while on the other hand the occurrence of a gas-phase reaction seems precluded since Jason et al.[26] have shown that the H_3^+ ion must be formed very close to the surface. For the latter reason two mechanisms might account for the formation of the H_3^+ ion:

(i) the field desorption of an H_3 species, which is adsorbed as such or temporarily formed in the adsorption layer, and
(ii) the ionization of a short-lived H_3 collision complex formed by the impact of an H_2 molecule from the gas phase with an adsorbed H atom.

Clearly these two mechanisms differ only on minor points, such as the way the required hydrogen is supplied. There are, however, some experimental findings which seem to favour the second mechanism. Firstly, Clemens and Müller noted that the relative abundance of the H_3^+ species as a function of the field strength goes through a maximum at a field strength of about 2.2 V/Å. The reason for this might be that at higher field strengths most of the incoming H_2 molecules are ionized before they can collide with the surface. A second argument in favour of the collision mechanism is provided by the mixed-gas experiments of Müller et al.[19]. They found no H_3^+ ions in any voltage range when helium was present. This then could be due to a shielding of the tip from the impact of H_2 molecules by helium atoms, which at 20 °K and 2 V/Å are present at a high concentration near the tip.

If the ionization of collision complexes is a possible side reaction in field ionization, it will probably occur fairly generally. For example, in the mixed-gas experiments just mentioned one could imagine the formation of a hydride ion like HeH^+, which is already known from ordinary mass spectroscopic studies[27] and resembles the ArH^+ ion detected by Beckey. The helium hydride ion also has been the subject of many theoretical studies[28,29,30].

It is tempting to attribute the improved image formation to the occurrence of the HeH^+ species, as such a mechanism seems less subject to the objections which can be raised against the accommodation mechanism.

If τ is assumed to be the same in the experiments with pure helium and with helium/1% hydrogen, according to eq. (22) the ratio of the respective best-image fields should correspond[1] with an ionization potential of the image-forming species of about 19 eV which, incidentally, is about the average of the ionization potentials of helium and hydrogen.

It should, of course, be borne in mind that the suggested explanation is highly speculative and that much more experimental evidence is required to prove its validity than is now available.

V-5. THE PROBABILITY OF FIELD IONIZATION AT A CLEAN SURFACE

(a) Uniform surface

The tunnel barrier model as described in section II-3.1. has the obvious disadvantage that it is only one-dimensional. Also, it leads to a half-width of the energy distributions larger than experimentally observed[12]. In order to arrive at a three-dimensional treatment of field ionization another procedure is more suitable.

The problem of calculating the ionization probability is essentially one of determining the time behaviour of a system under the influence of a perturbation. In principle such a problem can be treated by using the methods of time-dependent perturbation theory[31,32] by which it is possible to derive an expression for the probability of a transition from one quantum state into another as a result of a perturbation acting on the system.

Let a perturbation $\mathcal{H}'$ act on a system during a time t, $\mathcal{H}'$ being independent of time during this period. Further suppose that at t = 0 the system is in an initial state with energy E_i represented by a wave function ψ_i. Then the chance that after a time t' < t the system is in another (final) state with energy E_f and wave function ψ_f is given by

$$a_i^f = 2\left|H'_{if}\right|^2 \frac{1 - \cos(E_f - E_i)\, t'/\hbar}{(E_f - E_i)^2} , \tag{47}$$

where

$$H'_{if} = \int \psi_i^* \mathcal{H}' \psi_f \, dv . \tag{48}$$

When transitions take place into a continuous group of states the probability of a transition in time t' is found by integrating eq. (47) over all E_f values. As the value of the integrand is very small except for $E_f = E_i$, the result becomes

$$A_i^f = \frac{2\pi}{\hbar} \left|H'_{if}\right|^2 \rho_f \, t' , \tag{49}$$

where ρ_f is the density of final states which have an energy close to E_f and give the same value for the matrix element (eq. (48)). From eq. (49) it follows that the occurrence per unit time of the transition process, i.e. the transition probability, is given by

$$P_i^f = \frac{2\pi}{\hbar} \left|H'_{if}\right|^2 \rho_f , \tag{50}$$

with the condition that $E_f = E_i$.

Gomer and Swanson[33] have made use of time-dependent perturbation theory in considering field desorption, in which case vibrational transitions also have to be taken into account.

Recently Boudreaux and Cutler[34] have applied the theory to the one-electron transition in the field ionization of a hydrogen atom. They took the initial state in this case to be a hydrogenic wave function, and represented the final state by a plane wave inside the metal and an exponentially decaying function outside the metal. For the energy distribution of the hydrogen ions they calculated a half-width of 0.11 Å, which is somewhat less than the experimental values of about 0.2 Å.

The perturbation which can induce a transition from the initial into the final state consists of the applied field and the interaction of the electron with the metal surface, which becomes noticeable when the atom approaches the surface. While the latter interaction at all distances should apparently be

zero when the electron is "on" the nucleus, the expression given by Boudreaux and Cutler results for that case in a repulsion.

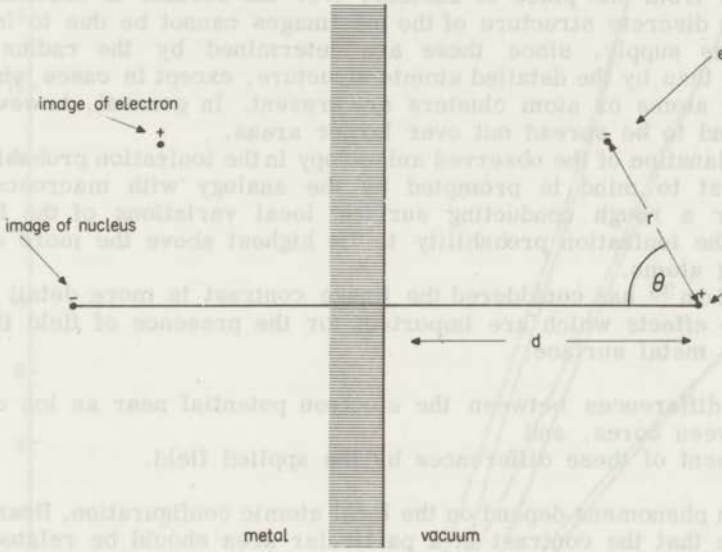

Figure 46

Coordinate system chosen for evaluating the interaction energy, $V_{e\text{-metal}}$, of an electron in a hydrogen atom with a metal surface

Using the coordinate system as shown in Fig. 46 and taking the zero point of the interaction energy for the atom at infinite distance from the surface, we derived for the classical interaction energy $V_{e\text{-metal}}$ of an electron in a hydrogen atom having its nucleus at a distance d from the surface

$$V_{e\text{-metal}} = \frac{-e^2}{4(d - r\cos\theta)} + \frac{e^2}{2r\sin\theta}\cot^{-1}\left(\frac{2d - r\cos\theta}{r\sin\theta}\right), \qquad (51)$$

where the first term gives the interaction of the electron with its image and the second term that with the image of the ion. For very small values of r $V_{e\text{-metal}}$ indeed becomes zero.

The classical approach for evaluating the interaction potential is clearly invalid for very small values of the electron-metal distance. For the electron-electron image interaction a correction factor which includes quantum-mechanical effects has been proposed[35]. A similar correction seems required for the electron-ion image interaction.

(b) Non-uniform surface - The image contrast

The foregoing discussions concerned ionization at a uniform surface. However, from the highly resolved images obtained in the ion microscope it is readily concluded that the ionization probability above the metal surface must vary widely from one place to another, i.e. the surface is essentially non-uniform. The discrete structure of the ion images cannot be due to local differences in gas supply, since these are determined by the radius of curvature rather than by the detailed atomic structure, except in cases where highly protruding atoms or atom clusters are present. In general, however, supply effects tend to be spread out over larger areas.

An explanation of the observed anisotropy in the ionization probability which comes first to mind is prompted by the analogy with macroscopic electrostatics for a rough conducting surface: local variations of the field strength cause the ionization probability to be highest above the more distinctly protruding atoms.

Brandon[36] has considered the image contrast in more detail and distinguishes two effects which are important for the presence of field fluctuations near the metal surface:

(i) the a priori differences between the electron potential near an ion core and that between cores, and
(ii) the enhancement of these differences by the applied field.

As both phenomena depend on the local atomic configuration, Brandon made it plausible that the contrast in a particular area should be related to the number of nearest neighbours and be smallest in the densely packed planes. This conclusion proved to be in agreement with experimental findings.

Let us consider the tunnel barrier model in further detail using the diagram shown in Fig. 47. For the sake of convenience the zero of the x-coordinate, being normal to the surface, is taken to be so far away from the surface that the potential in this point does not depend on the surface structure or any applied field.

In the presence of an external field the potential for an electron approaching the surface is the sum of the applied potential and the potential arising from the interaction of the electron with the metal ion cores and the conduction electrons. Although the exact form of the latter potential is unknown it will have a steeper gradient near a core than between cores[36]. However, at a distance large compared with the surface roughness the effect of the latter is no longer felt and the potential can be approximated by an image potential for a uniform planar surface. For simplicity the "surface" is considered here to be located at the edge of the Fermi sea of conduction electrons.

On an atomically smooth surface such as that of a field-evaporated metal tip, the contour of the highest filled level, i.e. the surface roughness, probably will not exceed a width of about 1 Å (possibly except for the relatively large lattice steps round the (110) face in a b.c.c. lattice). It can therefore be assumed that most if not all of the potential difference between "hills" and "valleys" has levelled out at a distance of about 4 Å. This means that in the coordinate system used here the critical distance x_c (cf. eq. (23)) will be approximately the same for ionization above the ion cores and above the gaps between cores.

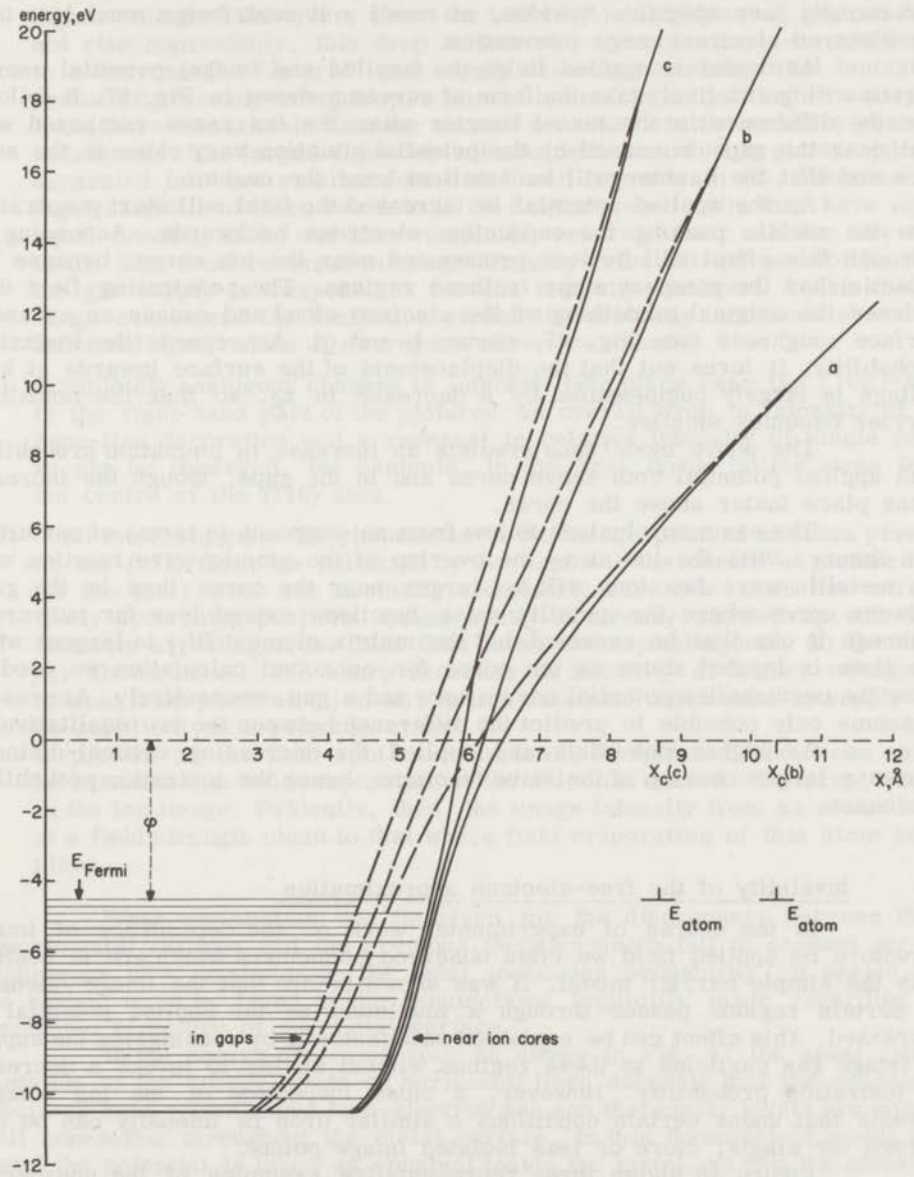

Figure 47

Energy diagram showing the potential energy for an electron near an ion core and near the gap between ion cores in the presence of an applied field.

Curves a, b and c represent the situation at increasing strength of the applied voltage, x_c the critical distance for ionization, E_{atom} and E_{Fermi} the total energy of the electron when in the helium atom and in the metal, respectively, and φ the work function of the metal

An evaluation of the total "image" potential should also include the electron-ion image interaction. We can, however, expect the latter to be structurally less specific. Besides, at small x it contributes much less than the electron-electron image interaction.

At moderate applied fields the (applied and image) potential energy curves will qualitatively take the form of curves a shown in Fig. 47. It follows that the difference in the tunnel barrier near the ion cores compared with that near the gaps is caused by the potential situation very close to the surface and that the barrier will be smallest near the cores.

As the applied potential is increased the field will start penetrating into the metal, pushing the conduction electrons backwards. According to Brandon this effect will be less pronounced near the ion cores, because the potential has the steepest slope in these regions. The penetrating field thus reduces the original smoothing of the electron cloud and causes an enhanced surface roughness (see Fig. 47, curves b and c). As regards the ionization probability, it turns out that the displacement of the surface inwards at high voltage is largely compensated by a decrease in x_c, so that the tunnelling barrier becomes smaller.

The above model thus predicts an increase in ionization probability with applied potential both above cores and in the gaps, though the increase takes place faster above the cores.

The same conclusions follow from an approach in terms of perturbation theory. With the ion at x_c the overlap of the atomic wave function with the metallic wave functions will be larger near the cores than in the gaps between cores where the metallic wave functions extend less far outwards. Although it can thus be assumed that the matrix element H'_{if} is largest when the atom is located above an ion core, for an actual calculation we need to know the perturbation potential near a core and a gap, respectively. At present it seems only possible to predict the difference between the two qualitatively.

As higher potentials are applied the decreasing critical distance allows a larger overlap of the wave functions, hence the ionization probability increases.

(c) Invalidity of the free-electron approximation

In the course of experimental work on the dependence of image structure on applied field we often observed phenomena which are in conflict with the simple barrier model. It was shown before that the image intensity in certain regions passes through a maximum as the applied potential is increased. This effect can be explained satisfactorily by considering the supply of image gas particles to these regions without having to invoke a decrease in ionization probability. However, a close inspection of the ion images reveals that under certain conditions a similar drop in intensity can be observed for single, more or less isolated image points.

Figure 48 shows three representative examples of the unexpected phenomena. The areas of interest are indicated in picture 48(a), which has been taken at 8.0 kV and 20 °K after cleaning of the tungsten tip by field evaporation at 10.7 kV and 77 °K. Pictures (b) to (f) show the effect of increasing the applied voltage in steps of 0.2 kV. All other experimental conditions, including photographic procedures, were kept unchanged.

(i) In the region on the extreme left we observe that in the row of bright dots directed to the (110) face (four atoms in (a)) the intensity drops at higher voltages. However, since the intensity in neighbouring regions does not rise appreciably, this drop in intensity cannot simply be attributed to a decrease in "lateral" gas supply assuming the integrated ionization probability already to be unity in (a) and to remain unity at higher voltages. Even more remarkable than the overall decrease are the relative changes in intensity. The large bright dot indicated with an arrow in picture (a) has separated into two smaller dots with lower intensity in (d). Whereas the right-hand one of these two dots is the brighter one in (d), they have about equal intensity in (e) and have completely reversed their relative intensity in (f). This local reversal in image intensity rules out the possibility that the gas supply is responsible for the intensity changes. In the voltage range considered the ionization probability evidently increases above the left-hand spot, while it decreases above the other.

(ii) Completely analogous changes in intensity take place near the [100]-zone in the right-hand part of the pictures: an overall drop in intensity of the zone-line decoration and a reversal in relative intensity of single dots, as can be observed, for example, in the first three lattice steps from the centre of the (110) face.

(iii) Most interesting are the phenomena at the image point of an atom present on the (211) face, as indicated by the arrow in the centre of picture (a). As the (211) faces are normally completely bare this atom has a relatively protruding position. Consequently it already showed up with high intensity at voltages far less than those corresponding with (a) (pictures not shown here). The sharp decrease in intensity at higher voltages is evident from pictures (a) to (d). In this case also a decrease in supply can be ruled out as a possible cause.
In picture (e) the faint spot has completely disappeared and it can safely be assumed that field evaporation of the atom has caused this abrupt change in the ion image. Evidently, then, the image intensity from an atom drops at a field strength close to that where field evaporation of this atom takes place.

What explanation can be given for the discrepancy between these experimental findings and the previous theories which fail to account for the occurrence of a maximum in the local ionization probability? It seems that the reason is to be found in the assumptions implicitly made regarding the electronic structure of the metal surface.

In the energy diagrams such as shown in Fig. 47 the usual representation of the energy levels as horizontal lines suggests that the conduction electrons form a continuous free-electron sea and that empty levels are equally well accessible throughout the metal surface. In this Sommerfeld model of a metal the potential is taken as constant inside the metal, so that the discreteness of the positive charge distribution due to the ion cores is neglected. Such an approach, however, is unrealistic when an explanation is sought for a phenomenon which in fact probes the surface on an atomic scale, being so sensitive that it "feels" the difference between protruding atoms and the gaps between atoms.

If, contrary to conventional usage, we tentatively assume that the ion cores themselves form regions in the crystal surface where few, if any, empty conduction levels are available, we can very schematically set up the modified energy diagrams as presented in Fig. 49. Here the upper diagram gives a cross-sectional view through the protruding atoms, while the lower one represents a cross-section through the gaps of the surface structure shown at the right. Although we realize that these diagrams are of a very simplified character, they might serve to illustrate the argument.

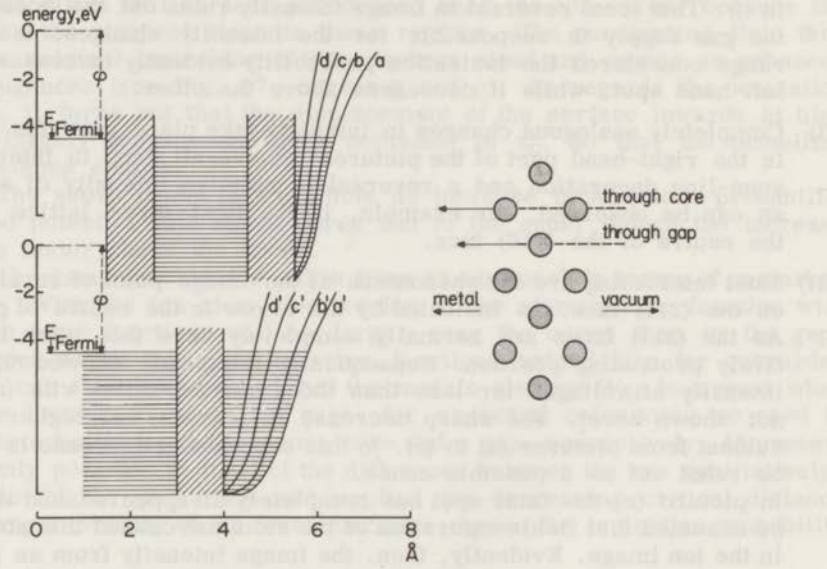

Figure 49

Modified tunnel-barrier model of Fig. 47.
The upper diagram represents the potential energy situation along normal through an ion core, the lower diagram along normal through a gap between cores of the surface structure shown at the right. Curves a to d and a' to d' schematically show the effect of increasing applied voltage. Cross-hatched areas represent the ion core regions, which have been assumed to measure one third of the interatomic distance

The effect of the cores is to create "pools" of conduction electrons near the surface and one can easily understand that these pools are wider in the gaps than before the cores. The depth of the pool might be considered a measure of the conduction-electron charge density.

When relatively low voltages are applied (see curve a in Fig. 49) the potential close to a core will not appreciably change compared with the

field-free situation. Initially, therefore, the ionization probability increases with applied potential because the width of the barrier is reduced.

Once the applied potential is so high that the field starts penetrating into the metal, thereby raising the conduction levels in the pool, the electrons drain out of the surface region (curve c) until at a still higher voltage an almost completely denuded core is exposed (curve d). It is conceivable that in this situation, which incidentally must be close to the point where the ion is torn off by the field, tunnelling into an empty state beyond the core is largely prohibited by an increased barrier width. In that case the ionization probability would indeed pass through a maximum prior to the field evaporation of the surface metal atom.

A much better description than is possible with the rather inadequate terminology of the tunnel barrier model, though again only qualitative, is provided by the formalism of perturbation theory. Instead of taking for the electronic states plane waves inside the metal and decaying functions outside, we now require wave functions which reflect the presence of the singularities in the potential due to the ion cores. Such functions can be found by using the orthogonalized-plane-wave method applied in band calculations[37]. In this method the wave functions for the conduction states must satisfy the condition that they are orthogonal to all core states. Inside the cores the wave functions therefore rapidly oscillate with low maximum amplitude, resembling the wave function for the atomic state above the shells which make up the core. For this reason it is not to be expected that the core region can make an appreciable contribution to the matrix element for the electronic transition. For not too small a core diameter the occurrence of a maximum in the ionization probability can then be understood as follows.

As a result of field penetration and the concomitant decrease in electron density in the outer surface region, the metallic wave functions become perturbed and extend less far outwards than if no field penetration takes place. This circumstance alone would have resulted in a decrease in overlap of metallic and atomic wave functions, but initially the simultaneous decrease in the critical distance allows for a compensation, so that the ionization probability increases.

When, however, the field penetration becomes stronger the point might be reached where the polarized wave functions of states lying at the Fermi surface have such small values near the core that the decrease in critical distance, which itself becomes less pronounced at stronger field penetration, no longer prevents a decrease in overlap. Consequently, the ionization probability starts decreasing.

Obviously the question arises how a core has to be defined and how an estimate of the magnitude of its diameter can be given. This is especially difficult for the transition metals, since it is not yet clear whether the d-electrons should be included in the core or not. Supposing, for instance, that for tungsten the latter is true (the 5d-states show a fairly large overlap), a low estimate of the width of the core region as meant above might be obtained by putting the core diameter equal to twice the radius of maximum radial charge density of the 5p-states. Using the functions calculated by Basch and Gray[38] in this way we find a value of about 1 Å, which indeed seems large enough to bring about the decrease in the ionization probability according to the explanation proposed above.

Viewed in a different way, the phenomenon can be understood by realizing that increasing the applied potential has two opposing effects. On the one hand the separation of the gaseous atom into an electron and an ion becomes easier, but on the other hand the same is true for the metal atom at the surface. The latter means that with increasing field penetration the metal atom less readily wants to "accept" the electron from the gaseous atom.

In the gaps between the cores the ionization probability steadily increases with the applied potential because the effect of field penetration will be compensated by a decrease in the critical distance. The moment the cores are torn off by the field the situation is similar to the one discussed above. For, what was initially called a gap region has now changed into a core region.

According to the above picture the image contrast must also pass through a maximum, instead of continuously increasing with applied potential. At a voltage probably not far removed from the evaporation voltage the ionization probability above the cores will be about equal to that above the gaps and the image contrast will have completely disappeared. Experimentally a loss in contrast is indeed observed at very high voltage, but this has always been attributed[3] to a saturation of the integrated ionization probability, i.e. to a supply-limited ionization process. A strong argument against this view is provided by the experimental observation that field evaporation is enhanced by the presence of image gas, which proves that a fairly large fraction of the image particles can pass through the ionization zone without being ionized[14].

A further consequence for the interpretation of ion images is that an image point which shows up very weakly can be due either to an atom in a less protruding position or, in complete contrast, to an atom being close to field evaporation. A decision between these two possibilities might be made by measuring the variation of the intensity of the spot with applied potential.

The question could be posed whether a decrease in ionization probability has not already occurred for atomically smooth areas even at best-image voltage. This would, for example, account for the remarkable fact that the image intensity in the (111) areas of a tungsten tip at best-image voltage equals that at a voltage about half as high. So far this phenomenon has been attributed solely to a decrease in gas supply to these areas when at higher voltage other areas also start emitting (cf. the discussion in section V-3(a)).

The problem raised here is closely related to that of the possible dependence of the ionization probability on crystallographic direction. Compared with the conventional barrier model, the perturbation treatment offers the great advantage that it emphasizes the importance of the electronic structure of the metal surface. It thus becomes readily understandable that the field ionization of the same gas can vary markedly for different metals[5]. However, the electronic configuration does not depend on the type of metal only. Certainly it will also be different for the various crystallographic directions in one and the same metal. Indications of a crystallographic specificity in field ionization probability are afforded by the highly symmetrical intensity patterns in the ion images of various metals, particularly in that of platinum[1,2], inasmuch as these cannot be attributed to differences in local field or gas supply alone. This assumption is, however, difficult to verify experimentally since the image intensity is determined by the interplay of various effects,

each of which alone cannot easily be controlled. Nevertheless the process of field ionization in principle furnishes a unique experimental tool to study the electronic differences on an atomic scale.

An explanation of structural effects clearly also requires a more advanced model of the metal surface than the free-electron approximation provides for. A qualitative insight into the different behaviour of various metals and possibly even into that for the various crystal faces of one metal might be gained by modern band calculations, e.g. by using computed values[37] of the electron-charge distribution in the bulk. But an adequate, more quantitative treatment can only be obtained when the presence of the surface is taken into account in the calculations. As matters stand, this seems a very difficult task to achieve.

V-6. THE PROBABILITY OF FIELD IONIZATION AT A COVERED SURFACE

Under normal helium image conditions most adsorbates are removed from the surface by (promoted) field desorption. However, in Chapter IV it was shown that when adsorption of nitrogen and carbon monoxide on tungsten causes a rearrangement of the surface atoms, a small part of the adsorbate is left on the surface after imaging. For the interpretation of the ion images of these partially covered surfaces it is of prime importance to know how the ionization probability is affected by the presence of a chemisorption complex.

So far the problem has been given little attention, probably on the assumption that an adsorbed atom or molecule forms a more or less distinct protuberance on the surface and so, again by analogy with macroscopic electrostatics, gives rise to local field enhancement and causes the ionization probability to increase[39,40,41]. This, however, is an unwarranted simplification; whilst electrostatics are not applicable to phenomena on an atomic scale, they certainly are not where a non-metallic adsorbate is concerned.

Two limiting cases may be distinguished, according to the type of bonding between metal and adsorbate. In the first case the bonding is completely localized and the metal surface atoms might be regarded as "demetallized", being incorporated in a surface complex which strongly resembles an ordinary inorganic compound or coordination complex. No free electrons or closely spaced empty energy levels are available in the surface layer to prevent the high field from penetrating into it. The surface layer will thus behave like a dielectric rather than like a metal. A tunnelling electron then can only be accommodated in an energy state extending in the metal, there being no empty levels of the right energy in the surface layer. The problem, considered in the barrier model, consists in estimating the difference in the potential barrier before and after adsorption while the applied potential is kept constant.

Field penetration involves the occurrence of two effects. Firstly the surface of the metal, being defined as located at the edge of the Fermi sea, is shifted inwards. Secondly field penetration causes the potential just outside the surface layer to be somewhat higher than it was in the clean state at the same place. The overall effect will be that the whole barrier is shifted towards the metal, but the potential gradient becomes smaller. (The situation

resembles the one discussed previously for the potential above the gaps between cores compared with that above the cores.) Consequently, the potential barrier has become larger after adsorption. We have here neglected the effect of a possible change in work function induced by adsorption, because in most cases this will modify the effective potential barrier only slightly.

The above qualitative reasoning thus predicts a decrease in ionization probability for the case of complete field penetration through the outer surface layer(s). Apart from an intrinsic decrease in ionization probability upon chemisorption, it also seems possible that the width of the demetallized layer and/or the dimension of the adsorbed species prevent an image-gas particle from approaching the surface up to the critical distance.

The demetallization considered here will probably also give rise to a loss in potential "contrast" in the surface. Consequently the adsorbate will cause the image contrast to decrease.

The extreme opposite of the first case, above, is presented by self-adsorption with delocalized bonding. Here the metallic surface is extended outwardly, i.e. closely spaced electron levels become available outside the original surface. The potential gradient above the adsorbed metal atom protruding from the surface relative to its immediate surroundings will be rather large as was shown before. In consequence, the ionization probability at the site in question increases.

For adsorption systems with intermediate bond type no general predictions can be made. The barrier model then no longer seems very useful, while on the other hand application of the perturbation theory requires a detailed knowledge of the electronic structure.

As regards the bonds formed upon chemisorption of gases like hydrogen, carbon monoxide, nitrogen and oxygen, they most likely belong to the first type discussed above. Results obtained by applying various techniques, like the measurement of the change in resistance[42], in magnetization[43] and in Hall voltage[44], all lead to the interpretation in terms of a demetallization of the metal surface atoms upon formation of the chemisorption complex. Field penetration over such a complex, if not causing its desorption, will then lower the ionization probability locally, making it rather unlikely that the adsorbed species of these gases can show up individually as bright dots as has often been assumed.

Of course the act of adsorption might induce such changes in the steric configuration at the surface, e.g. by the formation of small clusters, that the ionization probability is locally increased compared with the situation at the initially smooth surface, even if some adsorbate remains present. However, the purely electronic effect of chemisorption seems to be one of lowering the ionization probability, although it must be kept in mind that exceptions cannot strictly be ruled out as long as the details of the electronic configuration of the surface complexes are unknown.

Concluding we may state that these theoretical considerations confirm the interpretation of the ion images obtained after adsorption as proposed in Chapter IV.

Having discussed the dependence of the local ionization probability on the applied voltage and the effects induced by adsorbates, we have reached a point where we can examine more closely the changes in the ion images of a covered surface at field strengths below the best-image field for the clean

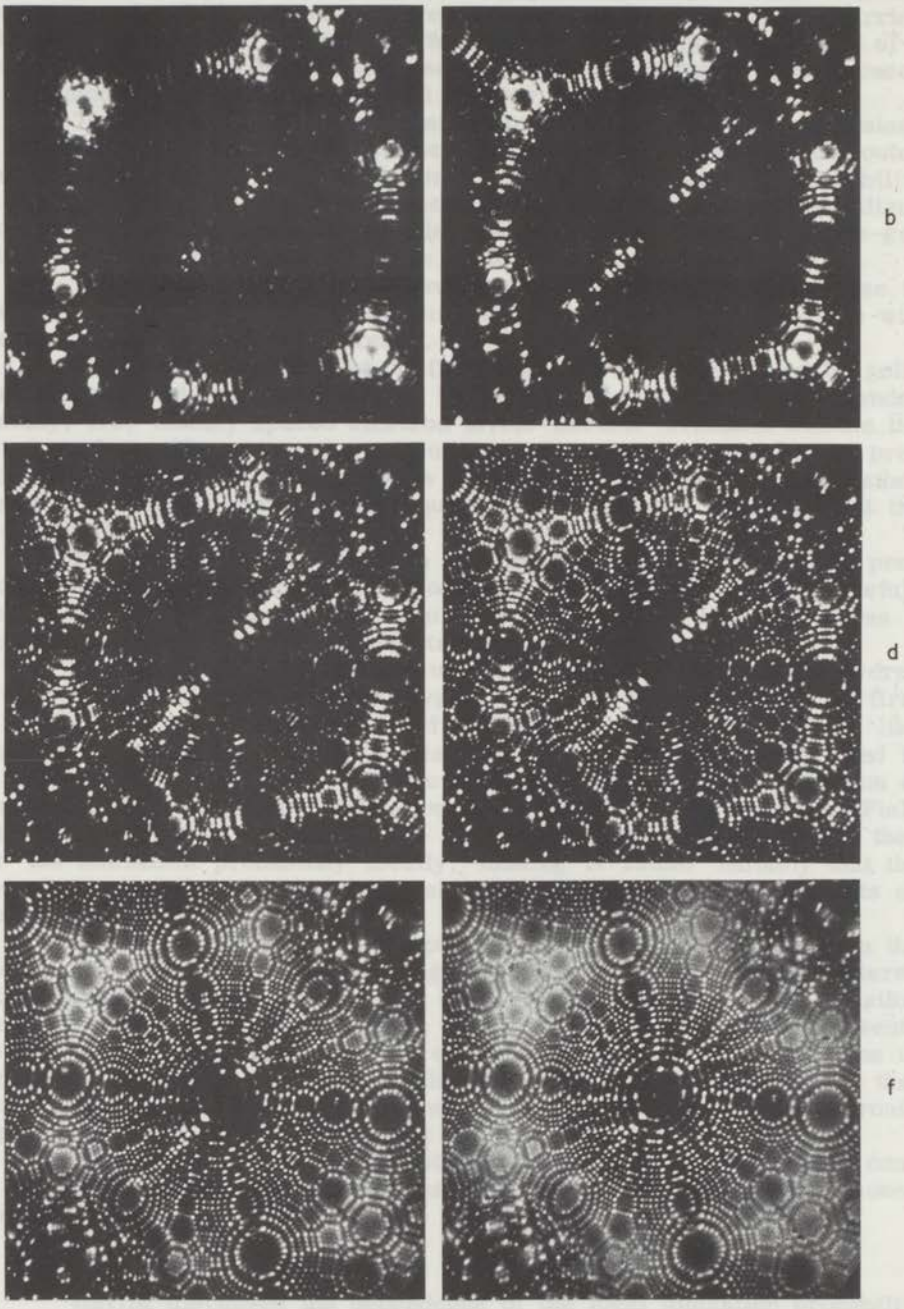

Figure 42

Ion images of a clean tungsten surface field-evaporated at 77 °K and 10.7 kV; images at 20 °K and (a) 6.4, (b) 7.0, (c) 7.6, (d) 8.0, (e) 8.6, (f) 9.0 kV

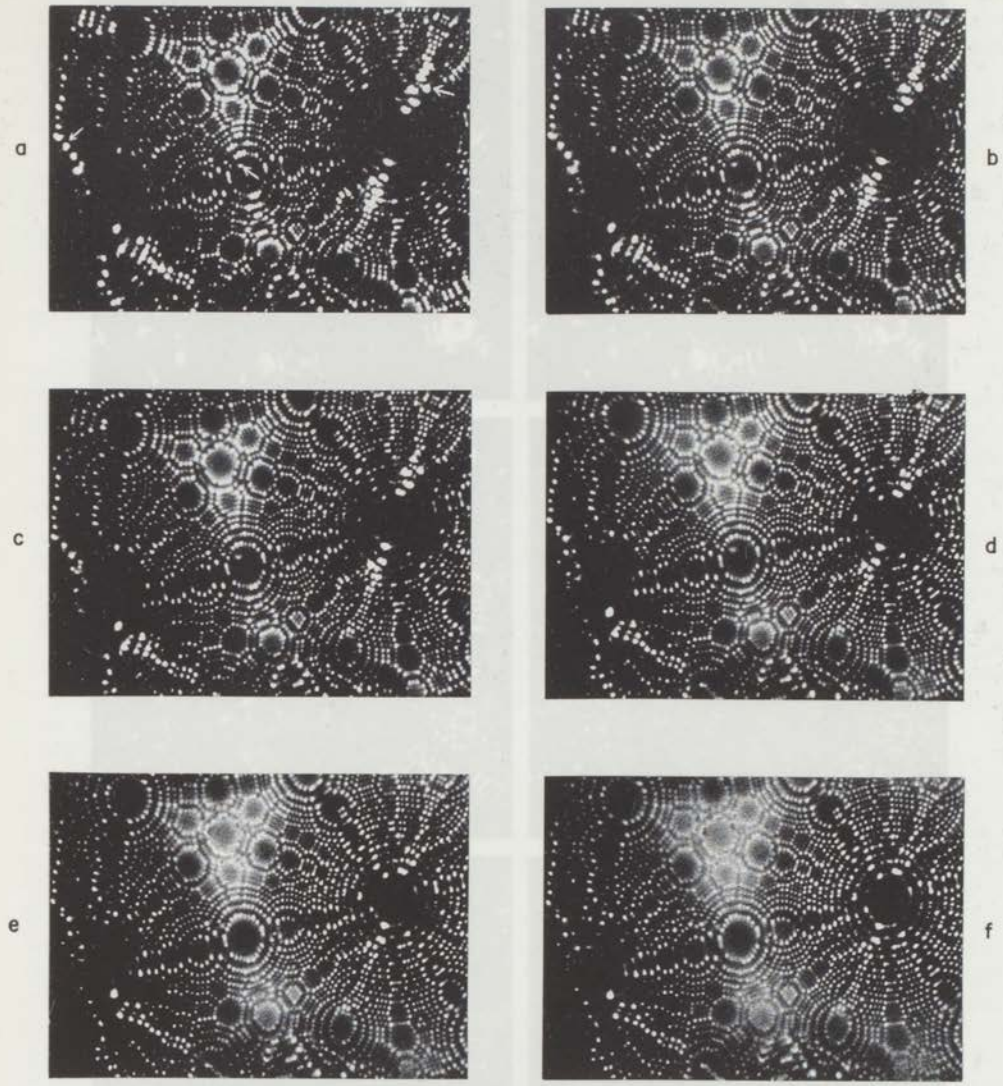

Figure 48

Ion images of the same part of a clean tungsten surface field-evaporated at 77 °K and 10.7 kV; images at 20 °K and (a) 8.0, (b) 8.2, (c) 8.4, (d) 8.6, (e) 8.8, (f) 9.0 kV

Arrows point to areas where image points lose intensity as the applied voltage is increased

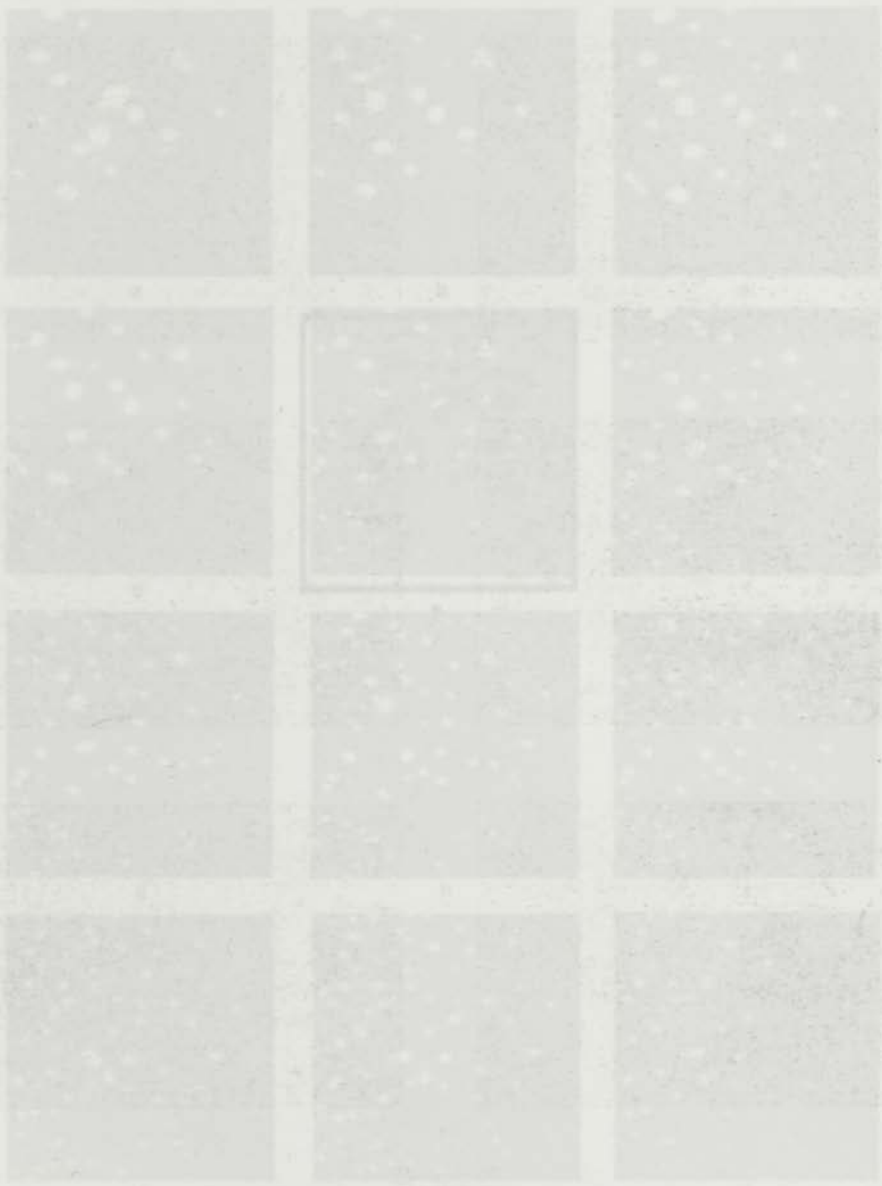

e

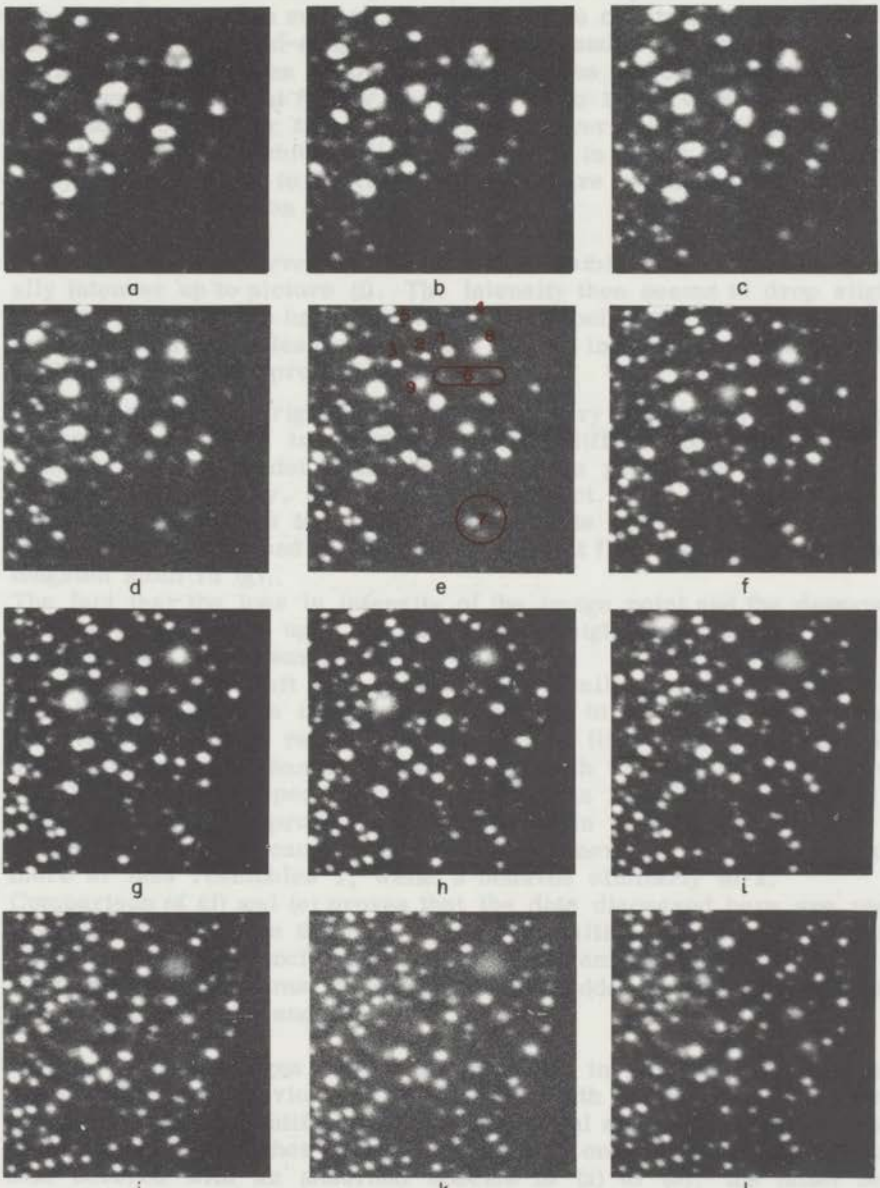

Figure 50

Ion images of the same part of a tungsten surface after nitrogen adsorption at 20 °K; the initially clean surface was field-evaporated at 77 °K and 13.4 kV; images at 20 °K and (a) 8.5, (b) 8.7, (c) 8.9, (d) 9.1, (e) 9.3, (f) 9.5, (g) 9.7, (h) 9.9, (i) 10.1, (j) 10.3, (k) 10.5, (l) 10.7 kV

surface (cf. section IV-4.2.). Fig. 50 presents a sequence of ion images of the same part of a tungsten surface after adsorption of nitrogen at 20 °K. The tungsten tip was first field-evaporated at 77 °K and 13.4 kV. After cooling down to 20 °K and nitrogen adsorption ion pictures were taken at increasing applied voltage, starting at 8.5 kV and going up to 10.7 kV, which was about the best-image voltage for the clean surface. Several interesting phenomena can be noted, some of which will be discussed in more detail. The areas where they occur lie close to the (111) region and are numbered in picture (e). The following interpretation is proposed:

(i) In area 1 it is observed that the faint dot visible in (a) becomes gradually intenser up to picture (f). The intensity then seems to drop slightly until in (k) the image has disappeared. This behaviour closely resembles that observed at a clean surface and the dot in question might therefore be identified with a protruding metal atom.

(ii) The appearance of bright dot 2 proceeds very differently. While up to picture (d) the area in question remains diffuse and has a very low intensity, a bright dot suddenly appears in picture (e). In (f) it has already lost intensity, and in (g) it is extinct. The most plausible explanation here seems to be that adsorbate is present in (a) to (d) and that it is field-desorbed in (e) with subsequent field desorption of a bare tungsten atom in (g).
The fact that the loss in intensity of the image point and the desorption follows immediately upon its appearance might indicate that the atom stands proud of the surface.
Bright dot 3 to the left of 2 appears in a similar abrupt manner in (d). The intensity of this image point rises up to (h) and then decreases. However, the image remains visible up to (l), which suggests a less protruding position than 2. In agreement with this no image at all was visible before the appearance in (d), whereas 2 had faintly showed its presence before its pronounced appearance in (e).
Both types of change can be observed quite generally; for instance, dot 4 more or less resembles 1, while 5 behaves similarly to 2.
Comparison of (d) and (e) proves that the dots discussed here are really new ones created "on the spot", for the positions of all image points visible in (d) are unchanged in (e). The removal of adsorbate in the first stages also seems evident from the sudden appearance of dots in area 6 (pictures (e) and (f)).

(iii) In area 7 three images can be distinguished in picture (e). All of them show a different behaviour as the field strength is increased. The upper left one might be identified with a clean metal atom, its intensity gradually changing at higher fields. The lower one probably represents a site covered with an adsorbed species in (a) to (e), the latter being removed at (f). The diffuse image on the right does not develop into a bright dot but is removed at an early stage. This can be explained satisfactorily by assuming field desorption of a whole chemisorption complex, i.e. the adsorbate together with one or more metal atoms, which originally acted as the (diffuse) ionization centre. In that case no bare protruding metal atoms are locally exposed, in contrast with the cases discussed above where presumably only the adsorbate was removed.

(iv) The development of image 8 is less easily interpreted. At very low voltage the image point (picture (a)) shows a peculiar shape with a triangular symmetry, being less bright in the centre. Such triangles together with similar but less symmetrical image structures are observed all over the ion image, but never on a clean surface. The changes in these triangular image structures are also remarkable, being completely different from the other ones. First the triangle gradually changes into a circular dot at (e), which then loses intensity and becomes more and more diffuse going from (f) to (k). In (l) the diffuse spot has disappeared, while a relatively bright dot with two or three of minor intensity has appeared at the same place.
A completely similar behaviour is shown by image 9 which after a large drop in intensity in (h) also splits up into three fairly sharp dots.
It is surprising that the image 8 which shows up so brightly already in (a) is only removed near best-image voltage. This suggests a protruding position of a cluster-like ionization region accompanied by a strong bond between adsorbate and metal. The images 8 and 9 could then tentatively be attributed to structures in which a nitrogen atom is embedded in the locally protruding surface. Polarization by the penetrating field perhaps increases the binding energy in the same way as the [100]-zone line decoration on a clean surface is assumed to be stabilized. It seems to be mainly this type of nitrogen which at best-image voltage remains adsorbed at the surface and can be detected by measuring the electron emission characteristic after pumping off the image gas. A more definite description seems impossible at this stage.

The present results provide additional evidence for the conclusion we arrived at in section IV-4.2. that chemisorption of nitrogen leads to a decrease in the ionization probability and in the image contrast. But what is even more important here, they show that the intricacy of image formation in the presence of adsorbates can to a large extent be unravelled by studying the variations in the ion images as a function of applied voltage, particularly below best-image voltage. If by such investigations, which will undoubtedly profit much by image intensification (see section IV-5.1.), the theory of image formation can be advanced, we, conversely, may expect that field-ion microscopy will become a powerful tool for elucidating problems of surface chemistry.

REFERENCES

1. E.W. Müller, Advan. Electron. Electron Phys. 13, 83 (1960).

2. E.W. Müller, Science 149, 591 (1965).

3. R. Gomer, "Field Emission and Field Ionization", Harvard University Press, Cambridge, Massachusetts (1961).

4. D.G. Brandon, Brit. J. Appl. Phys. 14, 474 (1963).

5. M.J. Southon and D.G. Brandon, Phil. Mag. 8, 579 (1963).

6. R.J.W. LeFèvre, "Advances in Physical Organic Chemistry", ed. Gold, Vol. 3, Academic Press, London (1965).

7. M.J. Southon, quoted by D.G. Brandon, Brit. J. Appl. Phys. 14, 474 (1963).

8. U. Feldman and R. Gomer, J. Chem. Phys. 37, 2380 (1966).

9. E.W. Müller, J. Appl. Phys. 28, 1 (1957).

10. E.W. Müller and K. Bahadur, Phys. Rev. 102, 624 (1956).

11. B. McCarrol and G. Ehrlich, "Condensation and Evaporation of Solids", Proceedings of the International Symposium held at Dayton, Sept. 1962, ed. E. Rutner, P. Goldfinger and J.P. Hirth, New York, Gordon and Breach.

12. T.T. Tsong and E.W. Müller, J. Chem. Phys. 41, 3279 (1964).

13. E.W. Müller, J. Appl. Phys. 27, 474 (1956).

14. O. Nishikawa and E.W. Müller, J. Appl. Phys. 35, 2806 (1964).

15. H.D. Beckey, Z. Naturforsch. 14a, 712 (1959).

16. M.G. Inghram and R. Gomer, Z. Naturforsch. 10a, 863 (1955).

17. M. Drechsler and G. Pankow, Proceedings of the International Conference on Electron Microscopy, London (1954), p. 405.

18. M. Drechsler and P. Wolf, 4th International Congress on Electron Microscopy, Berlin (1958), Band I, p. 835.

19. E.W. Müller, S. Nakamuru, O. Nishikawa and S.B. McLane, J. Appl. Phys. 36, 2496 (1965).

20. Z. Knor, Chem. Listy 59, 1277 (1965).

21. S.A. Schaafs, Handbuch der Physik, Vol. 8, ed. S. Flügger, Springer, Berlin (1963).

22. J.K. Roberts, Proc. Roy. Soc. (London) A129, 146 (1930); A135, 192 (1932); A142, 518 (1933).

23. G. Ehrlich and F.G. Hudda, Phil. Mag. 8, 1587 (1963).

24. T.T. Tsong and E.W. Müller, J. Appl. Phys. 37, 3065 (1966).

25. T.C. Clemens and E.W. Müller, J. Chem. Phys. 37, 2684 (1962).

26. A.J. Jason, R.P. Burns and M.C. Inghram, J. Chem. Phys. 43, 3762 (1965).

27. T.R. Hogness and E.C. Lunn, Phys. Rev. 26, 44 (1925).

28. H.H. Michels, J. Chem. Phys. 44, 3834 (1966).

29. F.E. Harris, J. Chem. Phys. 44, 3636 (1966).

30. G.A. Gallup and M.S. McKnight, J. Chem. Phys. 45, 364 (1966).

31. L. Pauling and E.B. Wilson, "Introduction to Quantum Mechanics", McGraw Hill, New York (1935).

32. A.S. Davydov, Quantum Mechanics, Pergamon Press Oxford (1965), Chapter IX.

33. R. Gomer and L. Swanson, J. Chem. Phys. 38, 1613 (1963).

34. D.S. Boudreaux and P.H. Cutler, Surface Science 5, 230 (1966).

35. J.C. Davis and P.H. Cutler, Surface Science 1, 194 (1964).

36. D.G. Brandon, Phil. Mag. 7, 1003 (1962).

37. W.A. Harrison, "Pseudopotentials in the Theory of Metals", Benjamin Inc., New York (1966).

38. H. Basch and H.B. Gray, Theor. Chim. Acta 4, 367 (1966).

39. G. Ehrlich and F.G. Hudda, J. Chem. Phys. 36, 3233 (1962).

40. G. Ehrlich, Advan. Catalysis 14, 255 (1963).

41. J.F. Mulson and E.W. Müller, J. Chem. Phys. 38, 2615 (1963).

42. W.M.H. Sachtler and G.J.H. Dorgelo, Z. Physik. Chem. (Frankfurt) 25, 69 (1960).

43. J.W. Geus and A.P.P. Nobel, J. Catalysis 6, 108 (1966).

44. N. Hansen and W. Littman, Ber. der Bunsengesellsch. f. phys. Chemie 67, 970 (1963).

APPENDICES

1. MICROSCOPE SCREENS

The most widely used method to render the screen of a microscope tube conducting is the conducting glass method[1], which imparts an optically transparent coating with a resistance of a few thousand ohms. We found the following procedure to give good results. All parts of the tube that have to be non-conducting are covered with Aquadag, whereupon the tube is heated to about 475 °C (preferably in an oven). The coating is then applied by blowing the vapour of stannic chloride into the tube by means of a stream of air. Here, the use of a washing bottle is very convenient. If desired, the coating can be removed by hydrofluoric acid or reduction with hydrogen.

For the preparation of fluorescent screens many methods have been described[1,2,3]. Particularly important points for ion microscopy are that the screen should be fine-grained and have a high yield of light. Moreover, the fluorescent powder should be applied in a very thin homogeneous layer, because pictures are taken from the back of the screen. Although zinc sulfide has the highest efficiency, willemite, a zinc silicate, is in most cases preferable, being less subject to deterioration by heating and ion bombardment.

The following procedure results in very uniform and thin fluorescent screens. Into the thoroughly cleaned tube, taken with the conducting screen down in horizontal position, small glass spheres (about 0.2-0.3 cm in diameter) are introduced, so that 2 to 3 layers are formed. Five drops (for a screen of about 10 cm in diameter) of a glycerine-ethanol (1 : 10) mixture are added and spread by shaking the tube with a continuous movement for 30 to 60 seconds. The glass spheres are then removed and an evenly spread layer is obtained. The fine-grained phosphor is now poured onto the glass plate in excess amount (a few grams) and spread by turning the tube and tapping the walls. The excess amount has the effect of polishing the phosphor layer; it is removed when the layer has become uniform. This can easily be checked by holding the tube towards a window. The layer has the correct thickness when the window frames are faintly discernible. After the walls of the tube have been wiped clean the screen is heated at 400 °C.

The absence of a binder from the fluorescent layer with this method has a favourable effect on the light yield; moreover, whenever the screen becomes damaged, it is easily replaced by a new one.

2. THE PREPARATION OF METAL TIPS

The tip and the heating loop on which it is spot-welded were both made of tungsten wire (purity 99.99%) of 0.015 cm in diameter. The assembly was mounted on the tungsten rods by means of the closely fitting spiral ends of the loop. The arrangement and the approximate dimensions are shown in Fig. 19.

The actual tip was made by electrolytic etching. Various methods have been described[2,4] also for metals other than tungsten. In practice every experimentalist has to work out the details of a procedure himself, as the making of a tip is more or less an art which cannot exactly be described.

We used a freshly prepared 5% aqueous solution of caustic soda into which the tip wire was vertically inserted up to about 0.3 cm below the weld. The other electrode was a platinum wire. When an ac voltage (about 6 V) was applied the tungsten wire was etched away at the meniscus of the fluid. At the moment the lower part broke off, the voltage was switched off and then turned on again for just a second or even less. After carefully rinsing of the Dewar and the tip assembly with water and acetone, the tip was inspected under the optical microscope at 500 x magnification. When the tip showed a slender taper and was unresolvable at the end it was considered to be useful. The radius actually obtained can only be determined by the microscope experiment itself. After replacement of the stainless steel cylinder the Dewar was sealed to the tube.

The whole procedure of a tip renewal did not take more than one hour.

3. PHOTOGRAPHIC PROCEDURES

The very low intensities in the ion microscope require the use of large-aperture objectives and fast films for recording the ion images. Müller[2] recommends Kodak spectroscopic Film 103 a - G, but this film was not easily available, as it has to be stored at low temperature. Polaroid films with speeds of 10,000 and 3000 ASA (the latter is used by Ehrlich[5]), are rather contrasty and also have the disadvantage that only a positive image is obtained.

Following the Cambridge group[6], we used Gevaert Scopix-G (increased speed, 35 mm) which does not require extreme care during transport and storage. Before being inserted in the camera (a Nikon F with f/1.4 lens), the film was uniformly pre-exposed to ensure that the threshold value had just been exceeded, so that after developing a slight fog became visible. Besides increasing the film speed, this procedure also resulted in a favourable decrease of contrast. The pre-exposure took place in the dark room under standardized conditions.

The film was developed with Gevaert G-150 (1 : 6) during two minutes at 20 °C with continuous stirring. The slight fog on the developed film did not diminish the quality of the pictures.

REFERENCES

1. R. Gomer, "Field Emission and Field Ionization", Harvard University Press, Cambridge, Massachusetts (1961).

2. E.W. Müller, Advan. Electron. Electron Phys. 13, 83 (1960).

3. W. Espe, "Werkstoffkunde der Hochvacuumtechnik", Band III, Deutscher Verlag der Wissenschaften, Berlin (1959).

4. D.G. Brandon and M. Wald, Phil. Mag. 6, 1035 (1961).

5. G. Ehrlich and F.G. Hudda, J. Chem. Phys. 33, 1253 (1960) and 36, 3233 (1962).

6. D.G. Brandon, Brit. J. Appl. Phys. 14, 474 (1963).

SUMMARY

Chemisorption, even of simple diatomic gases, generally leads to the formation of a number of surface complexes or "states" with distinct physicochemical properties. The enlargement of the insight into their origin and nature constitutes the prime objective of research into chemisorption.

The first part of this thesis deals with the investigation of two systems, viz. the carbon monoxide-tungsten and the nitrogen-tungsten system, which show the complex adsorption behaviour most clearly. Since, in our view, any improvement of the understanding of these systems requires (i) the study of the adsorption on surfaces with a well-defined structure and (ii) the application of techniques which provide information about what happens on an atomic scale, we have set out to study them by combining field-emission and field-ion microscope techniques. The theoretical basis of these experimental methods is extensively discussed in Chapter II, while Chapter III gives a detailed description of the apparatus used and the procedures followed in the experiments.

For the present work the conventional field-emission microscope technique was modified such that measurements could be carried out on each of the exposed crystal faces separately. Moreover, by utilizing the phenomenon of field evaporation perfectly ordered surfaces were prepared.

Under optimum operating conditions the resolution of the field-ion microscope is so high (≈ 2 Å) that individual surface atoms are imaged. Thus the ion microscope permitted a complete characterization of the surface prior to adsorption, while a comparison of images taken before and after adsorption furnished significant information about the atomic processes taking place.

The experimental results are reported and discussed in Chapter IV. The adsorption of both carbon monoxide and nitrogen on tungsten causes a rearrangement of surface atoms even at temperatures below 300 °K. The activation energy required decreases with increasing coverage. This has been attributed to a weakening of the intermetallic bonds upon chemisorption. The activation energy proves to be smallest for the less densely packed crystal faces.

In the carbon monoxide-tungsten system at 77 °K the rearrangement is very limited in extent. Two adsorption layers can be distinguished: a chemi-adsorption layer and a physisorbed layer on top. At 300 °K, however, there is a complete surface corrosion, involving the formation of the most strongly bound species, i.e. the β-states. On top of this corrosive chemisorption layer additional carbon monoxide may be weakly adsorbed.

Adsorption of hydrogen at 300 °K does not cause any rearrangement of a tungsten surface, but carbon monoxide on a surface precovered with hydrogen again induces a rearrangement, proving that the hydrogen is replaced.

In the nitrogen-tungsten system a pronounced surface reconstruction is observed also at low temperature above a certain minimum coverage. There are strong indications that at these temperatures surface rearrangements take place to a less extent according as the rate of adsorption is higher.

Measurements at individual crystal faces, both thermally annealed and ideally ordered ones, demonstrate the existence of a very marked crystal-

lographic specificity as regards the change in work function induced by the adsorption. Some faces show an increase in work function, others a decrease. Besides, it is found that the values obtained at 77 and 300 °K depend on whether or not preadsorption has taken place at 300 and 77 °K, respectively.

Results for the (110) face of tungsten indicate that nitrogen adsorption on this face is feasible at 300 °K. Previous reported evidence, obtained by field-ion microscopy, that no adsorption takes place is proved to be invalid.

Experiments using very sharp tungsten tips surprisingly showed the possibility of detecting single surface events such as the adsorption of an individual molecule.

The present findings demonstrate that for carbon monoxide and nitrogen on tungsten, adsorption models presupposing a fixed configuration of the metal surface are incorrect. The novel interpretations advanced in this study satisfactorily explain the simultaneous occurrence of different adsorbed states, their stabilities and surface potentials.

Thus the most stable species of nitrogen, identified as nitrogen atoms incorporated into the surface, is linked with a positive surface potential. Nitrogen chemisorbed on the surface, either as atoms or in a molecular form, appears to have a negative surface potential. Field desorption experiments confirmed these ideas.

As a final point of interest, the present study proves that the greater part of the adsorbate is removed from the surface upon imaging in the helium-ion microscope, when operated at the usual conditions. Those atoms or molecules which remain on the surface do not show up as bright dots as had previously been assumed, but instead they lower the ionization probability and the image contrast. Imaging at low fields, where much less desorption takes place, has revealed remarkable ordered structures in the case of nitrogen adsorption.

The second part of this thesis treats of several aspects of image formation in the ion microscope. With regard to the supply of image gas particles to the ionization region near the tip surface some corrections are made to kinetic descriptions given previously. The concept of an "average hopping height" is found to be of little use in any discussion of the temperature dependence of the ionization rate.

For an explanation of the phenomena at very low temperatures and low ionization rates great importance attaches to the formation of liquid films. As is shown this can lead to a decrease in the ionization rate owing to steric effects.

With the aid of a kinetic model for the gas supply and taking into account the non-uniformity of the tip surface, an analysis is given of the i-V characteristics of a helium-ion microscope at different temperatures. Various possible interactions of image gas particles with gas-covered surfaces are discussed. Some objections are raised against explanations recently given for the improved image formation of a mixed $He-H_2$ ion microscope; it is suggested that the improvement might be due to the formation of HeH^+ ions.

Evidence has been obtained that the ionization probability above a protruding metal atom passes through a maximum when the applied voltage is increased to the evaporation voltage. The phenomenon can be explained

qualitatively in terms of time-dependent perturbation theory by adopting functions which are orthogonal to the core states for the wave functions of the conduction states. The loss in image contrast for a clean surface at high fields is attributed to the ionization probability becoming approximately the same above protruding atoms and above the gaps between them.

The presence of an adsorbed complex modifies the ionization probability locally, depending on the type of bond formed. It is made plausible that chemisorption which "demetallizes" the outer surface atoms causes a decrease in the ionization probability and in the image contrast. This conclusion agrees with the experimental results reported in Chapter IV.

Finally it is pointed out that for solving the problems connected with the image formation of covered surfaces it may be advantageous to study the variations in the images with applied field, particularly in the range of fields below the best-image field for a clean surface.

SAMENVATTING

Chemisorptie, zelfs van eenvoudige twee-atomige gassen, leidt in het algemeen tot de vorming van een aantal oppervlaktecomplexen of "toestanden" met verschillende fysisch-chemische eigenschappen. Het verkrijgen van meer inzicht in het ontstaan en de aard van dergelijke complexen vormt de belangrijkste doelstelling van de research op het gebied van chemisorptieverschijnselen.

Het eerste deel van dit proefschrift beschrijft een onderzoek van een tweetal systemen, namelijk het koolmonoxide-wolfraam en het stikstof-wolfraam systeem, welke het voornoemde ingewikkelde adsorptiegedrag bij uitstek vertonen.

Om deze systemen beter te leren begrijpen is het ons inziens noodzakelijk, (i) de adsorptie te bestuderen aan oppervlakken met een goed gedefinieerde structuur en (ii) technieken aan te wenden die inlichtingen verschaffen over hetgeen zich op atomaire schaal aan het oppervlak afspeelt. Op grond van deze overwegingen hebben we ons ten doel gesteld, de systemen te bestuderen door het in combinatie toepassen van veldemissie- en veldionenmicroscopie. De theoretische achtergronden van deze experimentele methodieken worden uitgebreid behandeld in Hoofdstuk II, terwijl Hoofdstuk III een gedetailleerde beschrijving geeft van de gebruikte apparatuur alsmede van de wijze van experimenteren.

In ons onderzoek werd de algemeen gangbare veldemissietechniek zodanig gewijzigd dat metingen konden worden verricht aan afzonderlijke kristalvlakken. Bovendien werd door gebruikmaking van z.g. veldverdamping een volledig ideale ordening van de schone wolfraamoppervlakken bereikt.

Onder optimale werkingscondities is het oplossend vermogen van de veldionenmicroscoop zo groot (ca. 2 Å) dat individuele oppervlakte-atomen worden afgebeeld. Hierdoor bood de veldionenmicroscoop de mogelijkheid om vóór de adsorptie de structuur van het metaaloppervlak volledig vast te leggen, terwijl een vergelijking van de ionenbeelden vóór en ná adsorptie belangrijke informatie verschafte omtrent de zich aan het oppervlak voltrekkende atomaire processen.

De experimentele resultaten worden in Hoofdstuk IV besproken. De adsorptie van zowel koolmonoxide als stikstof veroorzaakt een herrangschikking van oppervlakte-atomen, zelfs bij temperaturen beneden 300 °K. De hiervoor vereiste activeringsenergie daalt naarmate de bedekking van het oppervlak toeneemt. Dit wordt toegeschreven aan een verzwakking van de intermetallische bindingen door de chemisorptie. De activeringsenergie is het laagst voor de minst dicht gestapelde kristalvlakken.

In het systeem koolmonoxide-wolfraam is de herrangschikking bij 77 °K zeer gering. Twee adsorptielagen kunnen bij deze temperatuur worden onderscheiden: een chemi-adsorptielaag met daarop een fysisch geadsorbeerde laag. Bij 300 °K daarentegen vindt een volledige oppervlaktecorrosie plaats, die gepaard gaat met de vorming van de meest stabiele toestand, de z.g. β-koolmonoxide. Bovenop deze corrosieve chemisorptielaag kan nog weer koolmonoxide worden geadsorbeerd, zij het in een minder stabiele bindingstoestand.

Waterstofadsorptie bij 300 ^{o}K brengt geen herrangschikking van een wolfraamoppervlak teweeg, maar koolmonoxide op een met waterstof voorbedekt oppervlak wél, hetgeen bewijst dat de waterstof wordt verdrongen.

In het systeem stikstof-wolfraam is een aanzienlijke herrangschikking van het oppervlak ook bij lage temperaturen waargenomen boven een bepaalde minimum bedekking. Er bestaan duidelijke aanwijzingen dat bij deze temperaturen herrangschikking minder sterk optreedt naarmate de adsorptiesnelheid hoger is.

Metingen aan afzonderlijke kristalvlakken, zowel thermisch gegloeide als ideaal geordende, wijzen uit dat er sprake is van een duidelijke kristallografische specificiteit met betrekking tot de verandering in uittreepotentiaal na chemisorptie. Van sommige vlakken wordt de uittreepotentiaal verhoogd, van andere daarentegen verlaagd. Daarbij is verder geconstateerd dat de waarden die men bij 77 en 300 ^{o}K verkrijgt afhangen van de omstandigheid of al of niet voorbedekking heeft plaatsgevonden bij 300 ^{o}K, respectievelijk 77 ^{o}K.

De resultaten voor het (110)-vlak van wolfraam tonen aan dat adsorptie van stikstof op dit vlak ook optreedt bij 300 ^{o}K. In het verleden naar voren gebrachte bewijzen, gebaseerd op experimenten met de veldionenmicroscoop als zou geen adsorptie optreden, zijn ongeldig bevonden.

Experimenten waarbij gebruik gemaakt werd van zeer scherpe wolfraampunten boden verrassenderwijs de mogelijkheid één enkele gebeurtenis, zoals de adsorptie van een stikstofmolecuul, te observeren.

De in deze studie verkregen resultaten leiden tot de conclusie dat elk adsorptiemodel, dat voor de hier onderzochte systemen een onveranderde configuratie van het oppervlak vooronderstelt, tot een onjuiste beschrijving voert. De nieuwe door ons naar voren gebrachte interpretaties verklaren op bevredigende wijze de aanwezigheid van verschillende adsorptietoestanden, hun stabiliteiten en oppervlaktepotentialen. Zo wordt de meest stabiele vorm van geadsorbeerde stikstof vereenzelvigd met in het oppervlak ingebouwde stikstofatomen; deze toestand geeft aanleiding tot een verlaging van de uittreepotentiaal. Stikstof die gechemisorbeerd is op het oppervlak, hetzij in atomaire vorm hetzij in een moleculaire vorm, verhoogt daarentegen de uittreepotentiaal. Een nadere bevestiging van deze opvattingen is verkregen door middel van velddesorptie-experimenten.

Tenslotte is van belang op te merken dat dit onderzoek aantoont dat tijdens het maken van een heliumionenbeeld onder de gebruikelijke condities het grootste deel van het adsorbaat van het oppervlak wordt verwijderd. Atomen of moleculen die achterblijven op het oppervlak worden niet afgebeeld als heldere stippen, maar geven daarentegen aanleiding tot een verlaging van de ionisatiewaarschijnlijkheid en van het beeldcontrast, dit in tegenstelling tot hetgeen andere auteurs hebben verondersteld. Ionenopnamen die verkregen werden bij lage veldsterkte, waarbij aanzienlijk minder velddesorptie optreedt, gaven opmerkelijk geordende structuren te zien na stikstofadsorptie.

Het tweede deel van dit proefschrift handelt over een aantal aspecten van de beeldvorming in de ionenmicroscoop. Met betrekking tot de toevoer van beeldgasdeeltjes naar het ionisatiegebied nabij het metaaloppervlak zijn enige correcties aangebracht op eerder in de litteratuur gegeven beschrijvingen. Het blijkt dat bij het beschouwen van de temperatuurafhankelijkheid van

de ionisatiesnelheid het begrip "average hopping height" van weinig betekenis is.

Voor een verklaring van de verschijnselen die bij zeer lage temperaturen en lage ionisatiesnelheden optreden is de vorming van vloeistoflagen een zeer belangrijke factor. Aangetoond wordt dat dergelijke lagen een daling in de ionisatiesnelheid kunnen teweegbrengen als gevolg van het optreden van sterische effecten.

Met gebruikmaking van een kinetisch model voor de gastoevoer en in aanmerking nemende dat het oppervlak van de metaalpunt niet uniform is, wordt een analyse gegeven van de stroomspanningskarakteristieken van een heliumionenmicroscoop bij verschillende temperaturen. Voorts worden de mogelijke interacties van de beeldgasdeeltjes met door gas bedekte oppervlakken besproken. Tegen recente verklaringen voor de verbeterde beeldvorming in een He-H_2-ionenmicroscoop zijn een aantal bezwaren aan te voeren; de veronderstelling wordt geopperd dat hier wellicht de vorming van HeH^+-ionen een rol speelt.

Experimenten tonen aan dat de ionisatiewaarschijnlijkheid boven een vooruitstekend metaalatoom door een maximum gaat wanneer de aangelegde spanning opgevoerd wordt tot de veldverdampingsspanning. Een kwalitatieve verklaring voor dit verschijnsel is mogelijk in termen van de tijdsafhankelijke storingsrekening wanneer men voor de golffuncties van de geleidingselektronen functies kiest die orthogonaal zijn ten opzichte van de golffuncties van de niet-geleidingselektronen. De verlaging in beeldcontrast voor een schoon oppervlak bij hoge veldsterkte wordt toegeschreven aan het feit dat de ionisatiewaarschijnlijkheid een uniforme waarde aanneemt boven het oppervlak.

De aanwezigheid van een adsorptiecomplex brengt een verandering teweeg in de ionisatiewaarschijnlijkheid ter plaatse, afhankelijk van het bindingstype. Het is aannemelijk dat chemisorptie die de atomen in de buitenste lagen "demetalliseert" zowel ionisatiewaarschijnlijkheid als beeldcontrast verlaagt. Deze conclusie is in overeenstemming met de experimentele resultaten vermeld in Hoofdstuk IV.

Tenslotte wordt er op gewezen dat het voor het oplossen van de problemen die verband houden met de beeldvorming van bedekte oppervlakken nuttig kan zijn, de variaties in de ionenbeelden als functie van de aangelegde veldsterkte te bestuderen, en meer speciaal bij veldsterktes lager dan die, welke nodig is voor een optimaal beeld van een schoon oppervlak.

ACKNOWLEDGEMENTS

The author is much indebted to the management of the Koninklijke/Shell-Laboratorium for the opportunity to perform the work described in this thesis and the facilities granted for its publication.

He wishes to express his gratitude to Mr. J. Moolhuysen for his capable assistance in carrying out the experiments, to Mr. A. M. van den Broek for the skilful performance of all the glass-blowing work, and to many colleagues with whom he had enlightening discussions.

The pleasant cooperation with the administrative and technical staff of the laboratory during the preparation of the manuscript is gratefully acknowledged.

STELLINGEN

1. Tegen de beschrijving, welke Gomer geeft van het veldionisatieproces in aanwezigheid van een vloeistoflaag aan het metaaloppervlak, zijn overwegende bezwaren aan te voeren.

R. Gomer, Field Emission and Field Ionization, Harvard University Press, Cambridge, Massachusetts (1961), p. 82.

2. De door Tsong en Müller aangevoerde bewijzen voor hun verklaring van de verbetering van de beeldkwaliteit, welke wordt verkregen door toevoeging van enkele procenten waterstof aan het helium in een veldionenmicroscoop, zijn niet overtuigend.

T.T. Tsong en E.W. Müller, J. Appl. Phys. 37, 3065 (1966).

3. Van Oostrom's conclusie, dat in het systeem stikstof-wolfraam bij kamertemperatuur geen herrangschikking van het metaaloppervlak optreedt, vindt geen rechtvaardiging in de door hem gepubliceerde resultaten voor dit systeem.

A.G.J. van Oostrom, Phys. Letters 22, 137 (1966) en proefschrift, Amsterdam (1965).

4. De opvatting van Schwab en Volkmar, als zou de chemisorptie van ammoniak aan wolfraam endotherm verlopen, berust op een foutieve interpretatie van hun meetresultaten.

G.M. Schwab en L. Volkmar, Z. phys. Chem. N.F. 43, 38 (1964).

5. Het gebruik door Schmidt e.a. van het gemiddelde van de dilatometrische glasovergangstemperaturen bepaald in afkoel- en opwarmgedrag als "de" glasovergangstemperatuur, is te verwerpen.

R.J. Schmidt, R.F. Boynton en L.E. Santucci, Preprint Am. Chem. Soc. (Div. Petr. Chem.) 10, 17 (1965).

6. De verandering van het n.m.r.-spectrum van $Zr(C_3H_5)_4$ bij temperatuursverhoging van -66 tot -20 °C wordt door Becconsall e.a. toegeschreven aan het optreden van interne rotatie van de CH_2-groepen. Een plaatswisselingsmechanisme via σ-gebonden C_3H_5-groepen verdient echter de voorkeur.

J.K. Becconsall, B.E. Job en S. O'Brien, J. Chem. Soc. (A), 423 (1967).

7. Bij de reactie tussen buteen-1 en palladiumacetaat in azijnzuur is door Bryant e.a. een andere produktverdeling gevonden dan die, welke door Kitching e.a. is gerapporteerd. Het is mogelijk hiervoor een verklaring te geven door de (temperatuurafhankelijke) associatie van palladiumacetaat in aanmerking te nemen.

D.R. Bryant, J.E. McKeon en P.S. Starcher, Abstracts Second International Symposium on Organometallic Chemistry, Madison (Wisc.) Aug. 1965, p. 94.
W. Kitching, Z. Rappoport, S. Winstein en W.G. Young, J. Am. Chem. Soc. 88, 2054 (1966).
T.A. Stephenson, S.M. Morehouse, A.R. Powell, J.P. Heffer en G. Wilkinson, J. Chem. Soc. 3632 (1965).

8. Het door Cotton e.a. voorgestelde mechanisme voor de isomerisatie van triphenylphosphine-methallylpalladiumchloride is niet in overeenstemming met de experimenteel waargenomen kinetiek van deze omzetting.

F.A. Cotton, J.W. Faller en A. Musco, Inorg. Chem. 6, 179 (1967).
K. Vrieze, C.MacLean, P. Cossee en C.W. Hilbers, Rec. trav. chim. 85, 1077 (1966).

9. In tegenstelling tot hetgeen Maire e.a. concluderen, sluiten hun experimentele resultaten met betrekking tot de hydrogenolyse van cyclo-alkanen over platinafilms en over platina/alumina katalisatoren geenszins uit dat de drager van invloed is op het mechanisme van de ringopening.

G. Maire, G. Plouidy, J.C. Prudhomme en F.G. Gault, J. Catalysis 4, 556 (1965).

10. De berechting van militairen, die een overtreding of misdrijf hebben begaan buiten de specifiek militaire sfeer, dient niet door de militaire maar door de commune rechter te geschieden.

11. De geringe aandacht, welke regering en parlement besteden aan het bevolkingsvraagstuk in Nederland, laat zich slechts karakteriseren door het woord "struisvogelpolitiek". Een duidelijke bevolkingspolitiek, waarbij ondermeer gestreefd wordt naar een geleidelijke afschaffing van de kinderbijslag, is dringend gewenst.

Leiden, 31 mei 1967

A.A. Holscher